Since January 2020 Elsevier has created a COVID-19 resource centre with free information in English and Mandarin on the novel coronavirus COVID-19. The COVID-19 resource centre is hosted on Elsevier Connect, the company's public news and information website.

Ceramics International 47 (2021) 2917–2948

Contents lists available at ScienceDirect

Ceramics International

journal homepage: www.elsevier.com/locate/ceramint

Review article

Mixed oxide nanotubes in nanomedicine: A dead-end or a bridge to the future?

Masoud Sarraf [a,b,**], Bahman Nasiri-Tabrizi [c,d,*], Chai Hong Yeong [e], Hamid Reza Madaah Hosseini [b], Saeed Saber-Samandari [d], Wan Jefrey Basirun [f], Takuya Tsuzuki [g]

[a] Centre of Advanced Materials, Department of Mechanical Engineering, Faculty of Engineering, University of Malaya, Kuala Lumpur, Malaysia
[b] Materials Science and Engineering Department, Sharif University of Technology, P.O. Box 11155-9466, Azadi Avenue, Tehran, Iran
[c] School of Biosciences, Faculty of Health and Medical Sciences, Taylor's University, Subang Jaya, Malaysia
[d] New Technologies Research Center, Amirkabir University of Technology, Tehran, Iran
[e] School of Medicine, Faculty of Health and Medical Sciences, Taylor's University, Subang Jaya, Malaysia
[f] Department of Chemistry, Faculty of Science, University of Malaya, 50603, Kuala Lumpur, Malaysia
[g] Research School of Electrical Energy and Materials Engineering, College of Engineering and Computer Science, Australian National University, Canberra, 2601, Australia

ARTICLE INFO

Keywords:
Mixed oxide nanotubes
Anodization
Electrochemistry
Nanomedicine
Bioassays

ABSTRACT

Nanomedicine has seen a significant rise in the development of new research tools and clinically functional devices. In this regard, significant advances and new commercial applications are expected in the pharmaceutical and orthopedic industries. For advanced orthopedic implant technologies, appropriate nanoscale surface modifications are highly effective strategies and are widely studied in the literature for improving implant performance. It is well-established that implants with nanotubular surfaces show a drastic improvement in new bone creation and gene expression compared to implants without nanotopography. Nevertheless, the scientific and clinical understanding of mixed oxide nanotubes (MONs) and their potential applications, especially in biomedical applications are still in the early stages of development. This review aims to establish a credible platform for the current and future roles of MONs in nanomedicine, particularly in advanced orthopedic implants. We first introduce the concept of MONs and then discuss the preparation strategies. This is followed by a review of the recent advancement of MONs in biomedical applications, including mineralization abilities, biocompatibility, antibacterial activity, cell culture, and animal testing, as well as clinical possibilities. To conclude, we propose that the combination of nanotubular surface modification with incorporating sensor allows clinicians to precisely record patient data as a critical contributor to evidence-based medicine.

Abbreviations: MONs, Mixed Oxide Nanotubes; TiO2 NTs, Titanium Dioxide Nanotubes; HA, Hydroxyapatite; PVD, Physical Vapor Deposition; Fe3O4, Magnetite; Fe^{2+}, Ferrous Ion; Fe^{3+}, Ferric Ion; XPS, X-ray Photoelectron Spectroscopy; EG, Ethylene Glycol; DMSO, Dimethyl Sulfoxide; FA, Formamide; DMF, Dimethylformamide; NMF, N-methylformamide; ZrO2 NTs, Zirconium Dioxide Nanotubes; HfO2 NTs, Hafnium Oxide Nanotubes; IMCs, Intermetallic Compounds; V2O5, Vanadium Pentoxide; RF, Radio-Frequency; SBF, Simulated Body Fluid; GEP, Gene Expression Programming; MOPSO, Multi-Objective Particle Swarm Optimization; AgNPs, Silver Nanoparticles; GO, Graphene Oxide; HObs, Human Osteoblasts; ECs, Endothelial Cells; VSMCs, Vascular Smooth Muscle Cells; MSCs, Mesenchymal Stem Cells; OPC1, Osteo-Precursor Cell Line; ALP, Alkaline Phosphatase; S. aureus, Staphylococcus Aureus; S. epidermidis, Staphylococcus Epidermidis; E. Coli, Escherichia Coli; Ag2O NPs, Silver Oxide Nanoparticles; ROS, Radical Oxygen Species; hASCs, Human Adipose-Derived Stem Cells; BIC, Bone-Implant Contact; APH, Anodization-Cyclic Precalcification-Heat Treatment; DRI, Drug-Releasing Implants; CAGR, Compound Annual Growth Rate; PSIs, Patient-Specific Implants; CT, Computed Tomography; LEDs, Light emitting diodes; MEMS, Microelectromechanical Systems.

* Corresponding author. New Technologies Research Center, Amirkabir University of Technology, Tehran, Iran.
** Corresponding author. Centre of Advanced Materials, Department of Mechanical Engineering, Faculty of Engineering, University of Malaya, Kuala Lumpur, Malaysia.
E-mail addresses: masoudsarraf@um.edu.my (M. Sarraf), b.nasiritabrizi@gmail.com (B. Nasiri-Tabrizi).

https://doi.org/10.1016/j.ceramint.2020.09.177
Received 5 September 2020; Received in revised form 16 September 2020; Accepted 18 September 2020
Available online 24 September 2020

1. Introduction

In the recent decade, there has been a great increase in patients requiring artificial implants as replacements for damaged tissues such as hip joints and teeth due to the increase of the elderly population [1]. Thus, many efforts have been directed toward identifying appropriate biomaterials for the production of durable medical implants. Among the different kinds of biomaterials, metallic-based materials are the most common replacement compounds for bone treating [1]. Pure titanium (Ti) and its biomedical-grade alloys have been extensively used as medical implants owing to their high biocompatibility, fatigue life, corrosion resistance, and lower Young's modulus, compared to other medical implants, e.g., cobalt alloys and stainless steel [2–4].

Despite the inherent benefits of Ti alloys, supplementary exploration is necessitated to attain developed clinical achievements. As this category of alloys is employed in the manufacturing of medical implants, due to insufficient physiological adaptation, increases the risk of implant failure [5–7]. This also causes the detrimental accumulation of wear debris and ions discharge into the biological media [8]. To overwhelmed these weaknesses, different types of surface reformations are proposed. For instance, surface coating of implants is a useful method to develop the biological performance of the medical implants, in which the coating layers commonly perform as defensive armors to minimize wear and corrosion, whereby diminishes the risk of implant failure [9–13].

Electrochemical anodization is a process that produces a durable and corrosion-resistant anodic oxide layer on a metal surface that protects the inner bulk metal [14]. Nanotube coatings by anodization have received increased attention recently, for the manufacturing of orthopedic and dental implants [15–41]. Numerous researchers have found that the coating morphology has a great impact on the biocompatibility of metallic implants [15,42–44]. In particular, the nanotube morphology enhances the physical interlocking of the osteoblast cells on the surface of the implant. Also, the formation of nanotubular arrays improves osseointegration through the development of a bone-like apatite layer [45,46]. For instance, a substantial increase in the cell adhesion was detected on titanium dioxide nanotubes (TiO_2 NTs) possibly due to an improved interlocking of the hydroxyapatite (HA) layer with the nanotubes [47]. Accordingly, it seems that the combination of physical vapor deposition (PVD) and anodization, could produce well-adherent coating layers with high mechanical and tribological performance, in addition to the presence of porosity to improve the implant biomechanical performance [47]. On the other hand, the implantable materials should possess adequate antibacterial behavior to inhibit the development of bacterial agglomeration [48–50]. One particular approach to boost the antibacterial activity of biomaterials is with the integration of antimicrobial agents such as copper (Cu), silver (Ag), and zinc (Zn) [51]. However, the fast release of metal ions into the human body is inevitable, causing temporary antibacterial behavior and amplified cytotoxicity. This concern thus obliges an antibacterial compound with greater cytocompatibility and the restrained release of ions.

Based on the descriptions above, much attention has been focused on the design and fabrication of advanced implants to improve patient well-being [52]. The main advantages of advanced implants compared to the traditional products are that the patients experience less discomfort and have a lower risk of infections. Following the vast popularity of this approach, deeper questions emerge, the most important of which is whether this strategy leads the blind into a pit or a horizon with a huge outlook? There are still several challenges that need to be addressed, on the safety and performance of the nanostructured implants prior to commercial use [53]. The present review focuses on the recent fabrication approaches of the MONs and their parameters, which control the tubular geometry, self-ordering degree, and crystal configuration. The review also includes the scientific aspects and clinical perceptions on MONs, also on their potential applications in nanomedicine, especially in advanced orthopedic implants. The final part sums up the central points of the review and presents some viewpoints for future consideration.

2. Concept of mixed oxide nanotubes

Fig. 1 shows a schematic side view of various configurations of MONs. In chemistry, a mixed oxide is an oxide with cations of a single element in different oxidation states (Type I) or cations of more than one element (Type II) [54]. These oxide structures are usually produced by the template method. The magnetite (Fe_3O_4) that includes the Fe^{2+} (ferrous ion) and Fe^{3+} (ferric ion) cations in a 1:2 ratio, as well as perovskite compounds i.e. ABX_3 (A and B are two cations of very different sizes, and X is an anion that bonded to both), are well-known as typically mixed oxides [55]. During the last decades, the preparation of mixed oxides has been developed as they have several significant properties such as superconductivity, magnetism, ferroelectricity, catalytic activity, and ionic conductivity [55–57]. It must be noted the nanotechnology has led to more efficient mass production, and as expected has become an important industry [58]. Accordingly, numerous attempts have been made to employ nanotechnology in various sectors, for instance in electronics, environmental protection, and biomedical applications [59]. The main reason why nanotechnology has received great attention is that the physiochemical behavior of nanostructured materials is different from those of the bulk materials [60]. Thus, by utilizing these nanostructures, solutions to the problems and limitations associated with the traditional ways can be obtained. From this viewpoint, the preparation and applications of MONs are challenging yet exciting research fields.

On the other hand, an additional definition of MONs can be given by a mixture of different oxides, rather than a mixed M1–M2 oxide (Type III). This type of MONs is commonly produced by electrochemical anodization, where nanotubes with electrochemically tunable morphologies can be produced. For instance, high-resolution X-ray photoelectron spectroscopy (XPS) revealed that the nanotubes developed on the β-Ti-45Nb alloy are composed of TiO2 and Nb2O5, rather than a mixed Ti–Nb oxide [61]. For this purpose, anodization or electrochemical oxidation is a well-known method to prepare the protective layers and self-organized mono- and mixed oxide nanotubes. In view of the fact that the self-organized mono- and mixed oxide nanotubes can be formed on Ti and other valve metals, these unique nanotubular surface modifications have attracted increasing interest for the fabrication of more effective implantable apparatus for biomedical applications [62–64]. In this review, the main focus is not only to provide a comprehensive comparison of the current preparation and characterization of Type III MONs and generate a list of potentially suitable platforms but also to discuss the disadvantages and possible improvements in the fabrication process.

3. 3. comparison between mono and mixed oxide nanotubes

In the past decades, electrochemical anodization for the growth of thick and homogeneous oxide coatings, as well as the development of self-organized nanotubes on different valve metals have received much attention in the literature [65–71]. The electrochemical oxidation is initiated at the interface of metal-oxide followed by the outwards migration of metallic ions under the application of an external electric field. Simultaneously, oxygen ions migrate to the metal-oxide junction and react with cations and materialize into a dense metal-oxide layer. The oxide layer propagates on the condition that the electric field is sufficient to allow ion transmission throughout the oxide, but the procedure eventually ceases, leading to a finite thickness of the oxide layer. In addition to the development of self-assembled nanoporous and nanotube coatings, porous oxide films could also occur under controlled experimental conditions [72]. So far numerous findings have reported the formation of mono- and MONs coatings, with some of their outstanding achievements, are summarized in the following section.

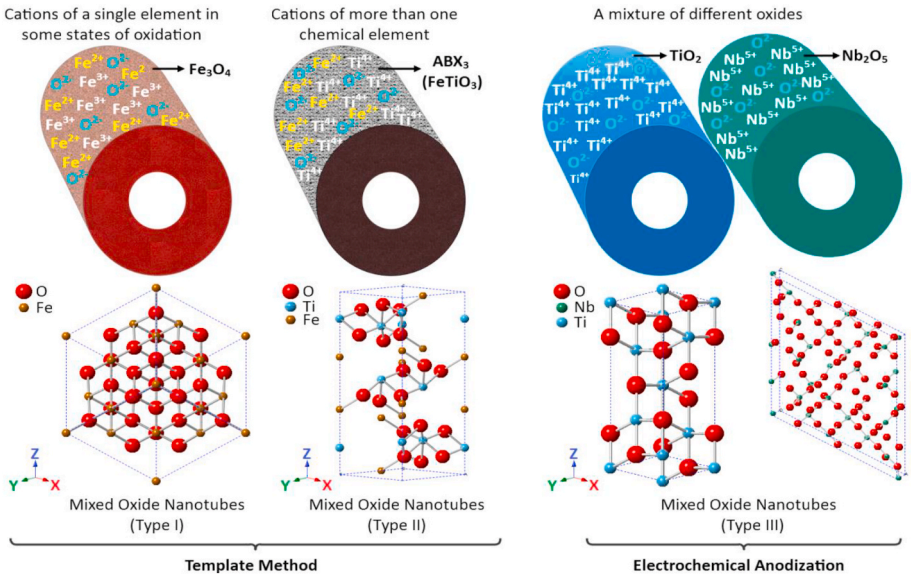

Fig. 1. A schematic side view of various configurations of MONs; type I (like Fe_3O_4), type II (like $FeTiO_3$), and type III (like TiO_2–Nb_2O_5).

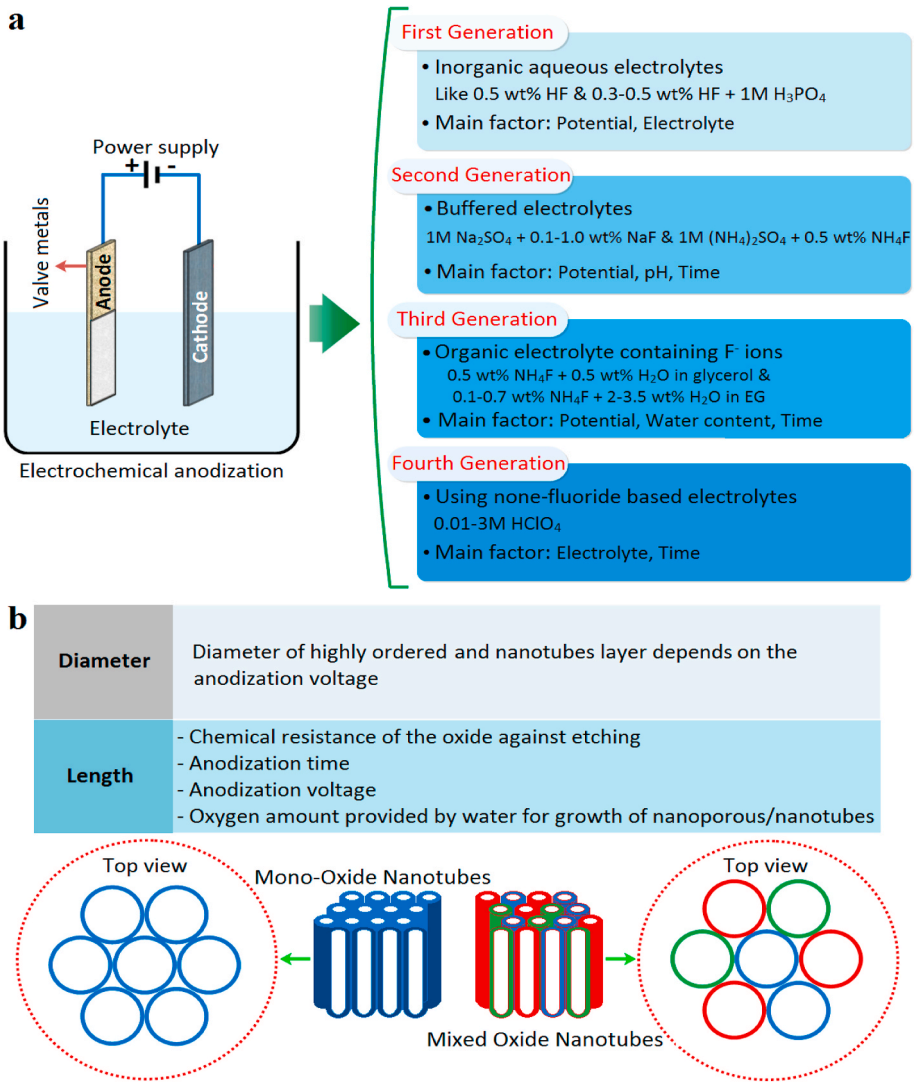

Fig. 2. (a) A schematic view of electrochemical anodization and different generations of TiO_2 NTs synthesis via the anodization technique, and (b) key factors for the generation of mono- and mixed oxide nanotubes on different valve metals and their alloys.

3.1. Mono-oxide nanotubes

The first report on the preparation of a self-organized nanoporous oxide film by anodization was performed on Al in an C2H2O4 electrolyte under specific circumstances [73]. The results of this work initiated a new pathway for the anodization of different types of valve metals and triggered thousands of papers for the preparation and application of nanoporous structures. The anodized nanoporous Al_2O_3 was utilized as photonic crystals and template for the fabrication of various nanostructures, thus several models have been proposed to describe the growth mechanisms of the self-ordered nanoporous alumina [72]. The proposed mechanisms of the self-ordering nanoporous Al_2O_3 could also be applied in the development of self-organizing nanostructured coatings on various valve metals, e.g. Ti, Zr, Hf, V, Nb, Fe, and Ta [72,74–80]. Nevertheless, contrary to Al, anodization in an acidic solution causes the formation of a compact oxide coating. Therefore these conditions are inadequate to produce self-organizing nanoporous oxide layers of these metals [72]. To overcome this issue, the presence of fluoride anions is required for the development of self-organizing nanostructured coatings. The main advantage of fluoride is its potential to produce water-soluble metal-fluoride compounds, which prevents the development of metal-oxide layer at the tubular bottom, by a mild but steady chemical dissolution of the metal-oxide layer. The size of the anions is also a vital issue, where the smaller F^- ions have a higher migration rate through the oxide lattice compared to the O^{2-} ions. This causes the development of a fluoride-rich film at the metal-oxide interface which is the basis of the nanostructured coating development. Some outstanding books and reviews have described the growth mechanism of mono-oxide nanotube arrays by the anodizing method. In the following section, a summary of the development of some mono-oxide nanotubes under different experimental circumstances has been described [72,81–85].

One specific tactic to decrease the depreciation in body fluids and to improve the wear and corrosion resistance is to generate a homogeneous TiO_2 layer on the surface of the Ti implants. In particular, the development of anodic TiO_2 NTs has recently received much interest in the modification of metal implants owing to their outstanding biocompatibility and resistance to bio-corrosion. Fig. 2a displays a schematic view of electrochemical anodization, as well as the different generations of TiO_2 NTs synthesized via the anodization technique. The rapid oxide dissolution was the chief restriction of the primary generation of nanotube synthesis, leading to nanotubes with less than 1 μm length. Hence, in the second generation, HF was exchanged with KF or NaF to achieve a higher pH and expand the nanotube length up to ~5 μm. Nanotubes with a length of 6 μm could be formed in 0.1 M KF, 1.0 M H_2SO_4, and 0.2 M C6H8O7 aqueous electrolyte (25 V and 20 h) as the pH was kept to 5 [86,87]. The third generation of synthesis gave more amendments in the NTs length through non-aqueous electrolytes or organic polar solvents, for instance, ethylene glycol (EG), dimethyl sulfoxide (DMSO), formamide (FA), dimethylformamide (DMF), and N-methylformamide (NMF) mixed with HF, NH_4F or KF [88–92]. Finally, the fourth generation of nanotube synthesis involves the use of non-fluoride electrolytes [93].

All self-ordering nanotubes produced by electrochemical anodization in various electrolytes on various valve metals and their alloys appear to pursue the same growth principles and the key factors for the generation of nanotubes as shown in Fig. 2b. It is well-known that the diameter of the nanotube is controlled through the anodization voltage; while the length of nanotubes is governed by the oxide resistance against electrolyte solutions, which also attributes to the voltage of anodization, anodization time, and the oxygen amount delivered by water for the growth of nanotube arrays. As mentioned above, dependent upon the anodizing circumstances, self-organized nanostructured coatings can also be formed on various valve metals and their alloys, where the examination and optimization of processing parameters are favorable for obtaining nanotubes with high-aspect-ratio. Thick and smooth zirconium dioxide nanotubes (ZrO_2 NTs) could be achieved using organic and mixed electrolytes at a potential of 40 and 20 V, respectively [94–98]. Irregular ZrO_2 NTs were produced using a one-pot anodization process without any pretreatment, even in the presence of contaminations as well as surface heterogeneity. To attain highly ordered nanotube arrays, pretreatments on Zr were also proposed to boost the self-organizing process. Electropolishing, dip-etching, and two-step anodizing were carried out on Zr substrates to attain highly self-organized nanotubular arrays. In the same way, hafnium oxide nanotubes (HfO_2 NTs) with a high aspect ratio can be fabricated under a broad range of anodization circumstances [99].

With regards to tantalum, certain conditions must be met to achieve the nanoporous and nanotube arrays which are extremely corrosion resistant in the acidic media [100–108]. Based on the literature, Ta_2O_5 nanotube arrays were grown under an anodization voltage range of 10–20 V after 5–120 s in a mixed H_2SO_4 and HF electrolyte with 1 wt% H_2O. However, prolonged anodization causes the destruction of the nanotubes and the presence of dimples which is most likely due to the development of a thin fluoride-containing layer at the interface of metal-oxide. Similarly, well-aligned anodic nanotubes have been obtained on other valve metals such as niobium (Nb) and tungsten (W) [109,110].

3.2. Mixed oxide nanotubes

Nanotubular coatings can be fabricated by controlling the anodization conditions, where they can generate not only mono-oxide nanostructures but also MONs. However, the preparation of MONs by electrochemical anodization is not entirely understood because the formation mechanisms are complex, where a wide range of MONs can be produced depending on the type of metal and anodization conditions [55]. The formation of MONs have been observed on binary, ternary, quaternary systems as well on more complex alloy systems such as Ti-Al [111,112], Ti-Mo [113,114], Ti-Nb [61,115–117], Ti-Ta [116,118,119], Ti-Zr [75,116,120–122], Ti-Mn [123], Ti–6Al–7Nb [124–132], Ti–6Al–4V [132–142], Ti–35Nb–5Zr [143], Ti–28Zr–8Nb [132,144], and Ti–29Nb–13Ta-4.6Zr [145–147]. The presence of various elements in Ti alloys significantly influences the electrochemical behavior and morphology, as well as the composition of the resultant oxide nanotube arrays. In the presence of different elements, the composition of the as-anodized layer is closely related to the metallic ratio of the alloy. For example, the nanotubes formed on the Ti–Al alloy system consist mainly of titania and alumina, and it is closely related to the ratio of Ti and Al in the base alloy. In some cases, it is not possible to identify the MONs due to the low phase fraction of other oxides relative to the dominant phase (TiO2) [131]. In such cases, it is necessary to perform XPS to distinguish a mixed oxide structure from a mono structure and to measure the elemental composition, and chemical state of the elements in the MONs [61].

3.3. Mixed oxide nanotubes on Ti alloys

Resembling the development of titania nanotubes on pure Ti, the formation of MONs on Ti-based alloys relies on the processing factors, such as pH, anodization time, anodic potential, and fluoride ion concentration. Nonetheless, the morphological features of nanotubular coatings on the Ti alloys are somewhat dissimilar compared to the formation on pure Ti owing to the selective dissolution of the oxide layer in fluoride electrolytes and the solubility of metal fluorides during the anodization process. For ternary systems, both the α and β phases are present with the addition of the other element, where organized nanotube coatings are formed in the α phase, while a combination of nanotubes and nanopores is observed in the two-phase (α + β) component. In the following section, the development of MONs on different Ti alloys is presented [61,85].

3.4. Binary alloys

3.4.1. Ti–Al alloys

Because of the dissimilar oxide morphologies that could be formed on Al and Ti, it is very interesting to assess the electrochemical feature of different compositions of the Ti–Al alloys prepared in an F−-comprising electrolyte and to appraise the critical circumstances which control the evolution of one type of morphology to the other. Besides that, the length scale of the self-organization procedure is important, where the well-organized oxide configurations on Al and Ti surface by anodization could be voltage regulated [148,149], but the total self-organizing length is dissimilar for the two substrates. In this regard, the self-organizing properties of anodic oxides on refractory metals are studied in detail [150,151], which has two dissimilar morphologies, the highly organized parallel aligned porous oxide configurations, and the organized arrays of nanotubes. The top-view SEM micrographs of oxide-layers grown on Al, $TiAl_3$, TiAl, Ti_3Al, and Ti in 1 M H_2SO_4 comprising 0.15 wt% HF at potentials of 10, 20, and 40 V are shown in Fig. 3, where the evolution from porous to tubular configuration is detected [150].

As shown in the figure, the self-ordered oxides could be generated over an extensive potential range. The very regular porous configuration is formed on Al, comprising of some hexagonal nanopores with the mean interpore distance ranging from 30 nm at 10 V to 55 nm at 40 V. In contrast, the pores are partly enclosed by bundles of oxide needles owing to the non-uniform etching of the pore walls throughout prolonged anodization in F−-comprising electrolytes at lower potentials [152]. It is reported that the morphological features in the self-ordered configurations depend on the anodization voltage and the alloy's composition, where the tubular division is attributed to the augmented stress due to the rising volume expansion, as changing the composition from Al to Ti [150,151].

3.4.2. Ti–Mo alloys

Previous results on emerging Ti–Mo alloys showed that these alloys are promising as medical implants due to the low elastic modulus, electrochemical constancy in biological media, and high corrosion resistance [153–155]. However, the formation of MONs on Ti–Mo alloy is not free from challenges. For instance, it was suggested that a multi-purpose optimization of the electrolyte solution, especially the F^- concentration and water quantity, at 150 V for 20 h, could lead to the development of self-organized MONs on Ti–7Mo alloy. However, the results showed that only porous oxide layers with higher Mo concentration were formed using the proposed approach [156,157]. Given the possible nanotubes generation on binary Ti–Mo alloys and to overcome the challenges, Oliveira et al. [114] studied the formation of self-organized nanotubes on biomedical Ti–Mo alloys (Ti–6Mo and Ti–15Mo) using the electrolyte solution proposed by Ji et al. [158] for pure Ti, to ensure that the matrix configuration is attained at the nanotubes, where the α phase is only formed on the Ti–6Mo, while the β phase is only formed on the Ti–15Mo [159].

From the SEM images as shown in Fig. 4a–e, the nanopores were formed after 2 h, which are transformed into nanotubes following 4 h, and eventually well-defined, homogeneously distributed MONs with a mean diameter of 90 nm are developed on the Ti–Mo alloy after 6 h. The electrochemical assessments revealed that the MONs formation on the Ti–Mo alloys gave better protective features than the oxide films instinctively developed on the respective alloys [114] (Fig. 4f).

3.4.3. Ti–Nb alloys

Based on previous studies, the titania layer developed on the Ti-14.6Nb alloy showed excellent photocatalytic activity [113]. Besides that, Nb is an alloying element for Ti alloys that are widely utilized for biomedical applications, for instance, the Ti–29Nb–13Ta-4.6Zr alloy [160]. Accordingly, the findings on MONs formed on Ti–Nb alloys provide some essential information for employing MONs coatings on the Ti-based implants for different orthopedic applications [117,161,162]. Also, it is reported that a TiO_2–Nb_2O_5 mixture possesses a higher photocatalytic activity compared to the pure TiO_2 [163] and also found that this MONs structure possesses metallic behavior [164], making them potential conducting transparent materials.

In electrochemical anodization, it is vital to reach an equilibrium between the oxide growth and local oxide dissolution, where the equilibrium is sensitive to the F^- concentration, as the chemical dissolution of oxide is accompanied by the release of the soluble $[TiF_6]^{2-}$ complexes [61]. The different valve-metal oxides undergo dissimilar dissolution kinetics in F^--comprising solutions [165]. From the electrochemical data, the dissolution rate of Nb_2O_5 is only 1 nm min^{-1}, compared to the dissolution of TiO_2 which is 20 nm min^{-1} [166]. This shows that the formation of Nb_2O_5 at the anode is more resistant to F^- ions compared to TiO_2 in 1 M NaH_2PO_4 with 0.5 wt% HF (pH 4.5) [61]. Thus the TiO_2 dissolution rate in an F^--comprising electrolyte is of crucial importance to the length of the developed nanotubes [167], likely, the growth of the anodic oxides on Ti–Nb alloys differs drastically from the pure Ti. In this context, Ghicov et al. [61] explored the formation of MONs in a binary Ti–45Nb alloy. They reported that the shape and dimensions of TiO_2 NTs reinforced with Nb_2O_5 could be controlled within a wide parameter range. The Nb_2O_5 undergoes a much lower chemical dissolution rate compared to the TiO_2 in the F^- solution, thus the nanotube corrosion is hindered upon the formation, which results in the development of longer MONs (Fig. 5a–g). This feature enables the tuning of the TiO_2 NTs for particular applications, such as photon absorption and insertion of microbiological species. Furthermore, the MONs possess higher thermal resistance compared to the pure TiO_2 NTs, which enables thermal treatment at much higher temperatures.

In this regard, ultrafast MONs development on the Ti–Nb alloy by

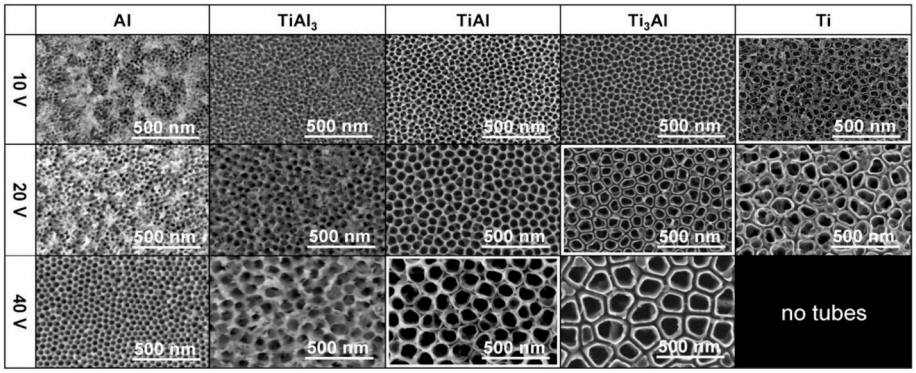

Fig. 3. An overview of the morphologies formed on the different Ti–Al alloys at different anodization voltages grown in 1 M H_2SO_4 containing 0.15 wt% HF (Reproduced with permission from Ref. [150]).

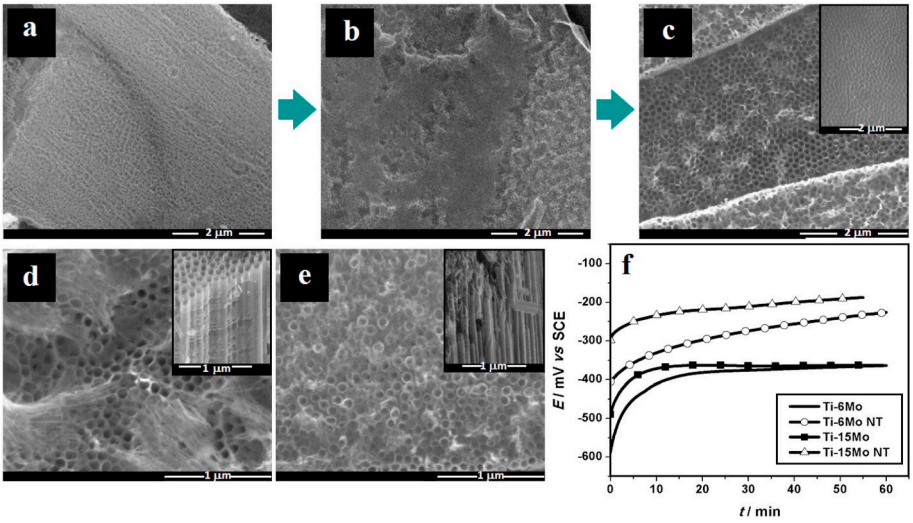

Fig. 4. SEM images of Ti–6Mo alloy anodized at 40 V for (a) 2, (b) 4, and (c) 6 h (Insert: bottom view of the MONs) as well as (d) pure Ti, and (e) Ti–15Mo alloy anodized at 40 V for 6 h (Inserts: a cross-sectional view of the fractured area of the respective specimens); (f) open-circuit potential against time in Ringer solution for Ti–Mo alloys before and after the development of MONs (Reproduced with permission from Ref. [114]).

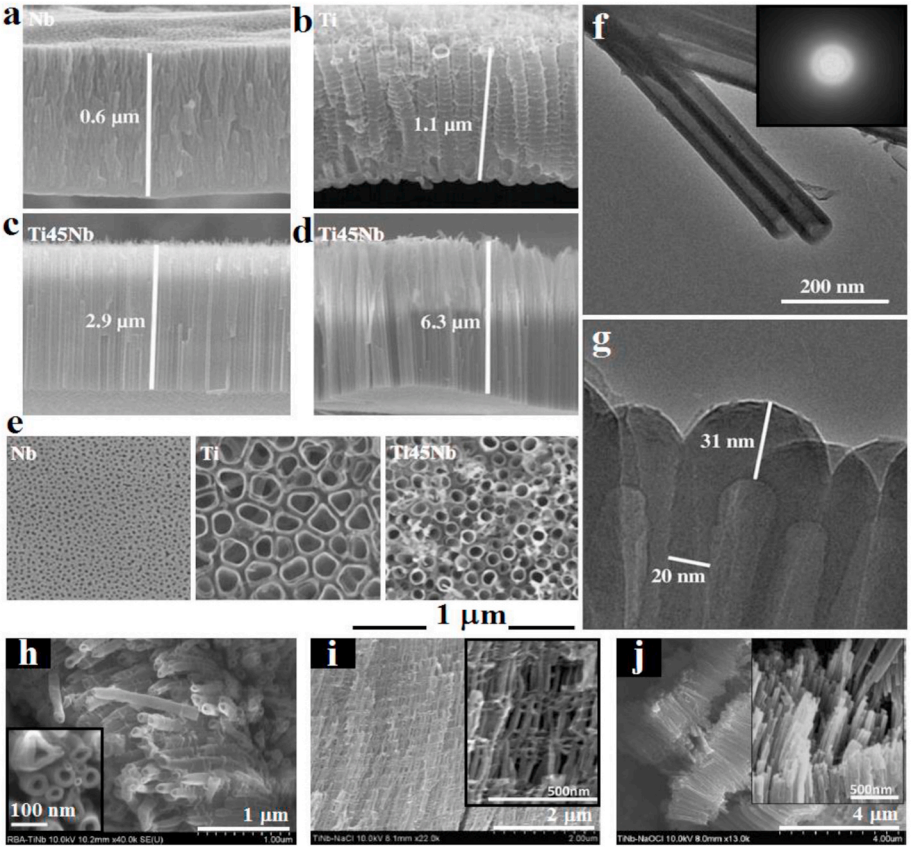

Fig. 5. Cross-section SEM micrographs of (a) Nb, (b) Ti, and (c) Ti–45Nb alloy from the anodization at 20 V for 2 h in a 1 M NaH_2PO_4 with 0.5 wt% HF, and of (d) the Ti–45Nb alloy after 20 h at 20 V; (e) Top-view SEM micrographs of Nb, Ti, and Ti45–Nb; (f) TEM (inset: corresponding SAED pattern) and (g) HRTEM images of MONs (TiO_2–Nb_2O_5 NTs) formed at 20 V for 2 h (Reproduced with permission from Ref. [61]); (h) FE-SEM images of MONs on Ti–Nb alloy following anodization in (h) NaCl–$NaClO_4$ mixed solution buffered, (i) NaCl, and (j) $NaClO_4$ solutions at pH 4 (Reproduced with permission from Ref. [116]).

quick breakdown anodization in NaCl–$NaClO_4$ mixed electrolyte, NaCl, and $NaClO_4$ solutions at pH 4 was also examined by Jha et al. [116], as shown in Fig. 5h–j. They found that the intense evolution of hydrogen at the Pt cathode took place instantaneously upon anodization. The surface of Ti–Nb alloy is covered with white spots that are distributed very quickly over the surface upon 30 s of anodization. These white spots are the oxide nanotube bundles that form densely around a pit.

The results show the formation of two types of morphologies, which are the net-like and free-tubular configurations, were formed using quick breakdown anodization. For the net-like configurations, the MONs show a relatively homogeneous size (30–40 nm in diameter and several tens of micrometers in length), while in the case of free-tubular configuration, the diameter of the nanotubes varies significantly from 20 nm to more than 100 nm (Fig. 5h). In addition to the mixed electrolyte, Fig. 5i and j displays SEM micrographs of nanotubes anodized in NaCl and $NaClO_4$ solutions, respectively. In NaCl solution, the anodized surface was covered with loosely packed nanotube bundles with net-like morphology (Fig. 5i). On the contrary, the $NaClO_4$ solution led to the

more uniform coating but the nanotubes are segmented into packets of around 2 μm length (Fig. 5j). Contrary to the NaCl electrolyte, the nanotubes generated in $NaClO_4$ solution had smooth walls without ripples, thus it can be deduced that the net-like nanotubes are attributed to the presence of Cl^-, while the stacks of smooth-walled nanotubes are ascribed to the presence of ClO_4^-. This suggests that the mixed electrolyte possesses the advantage of attaining a large surface coating with a high adhesion strength, which is very important in modern implantology [168,169].

3.4.4. Ti–Ta alloys

Apart from the optimization in structural features of nanotubes (geometry and functionality), another noteworthy aspect of the β-type Ti-based alloys is the bimodal self-assembly. In this arrangement, the nanotubes consist of ordered tubes with different diameter sizes i.e. larger tubes that are surrounded by smaller tubes. In this regard, Tsuchiya et al. [118] explored the development of MONs on the Ti–Ta alloys such as Ti–13Ta, Ti–25Ta, Ti–50Ta, and Ti–80Ta, and examined possible formation mechanism of the bimodal self-organization on these alloys.

They found that the nanotube layers until 50% Ta are composed of tubular configurations underneath the top porous layers, as illustrated in Fig. 6a–i. This type of formation is due to a composition-dependent evolution from nanopores to nanotubes as proposed by Berger et al. [150] for the Ti–Al alloys. The anodization of binary Ti alloys leads to a highly non-uniform surface owing to the selective dissolution of the unstable phases and/or diverse reaction rates on various phases in the alloys. In the case of binary Ti–Ta alloy, there are somewhat large two-phase zones in the phase diagram. Accordingly, the anodized Ti–13Ta, Ti–25Ta and Ti–50Ta alloys exhibit some inhomogeneous surfaces, which can be ascribed to the alloys' microstructures, where the oxide coatings on Ti–13Ta and Ti–25Ta show a Widmanstätten-type microstructure and the tube diameters on Ti–13Ta and Ti–25Ta consist of random distributions (Fig. 6a–f). In the case of Ti–50Ta alloy, the oxide layer is composed of two zones, (i) black zones, consist of typical nanotubular structures, and (ii) white zones consist of nanoporous structures. From the bottom-view, the anodized Ti–50Ta alloy is composed of two distinct diameter tubes, where the larger tubes are surrounded by smaller tubes (Fig. 6g and h). This shows that an appropriate level of alloying elements is requisite for the nanotube development on two-size scales. Besides that, the Ta concentration significantly affects the nanotube diameter in such assemblies, as shown in Fig. 6i [118].

Fig. 6j-m shows the growth steps of MONs on the Ti–50Ta alloy. As demonstrated in Fig. 6j, a nanoporous layer is initially generated on the alloy surface, followed by the generation of a nanotubular layer developed underneath the nanoporous layer (Fig. 6k). In this step, the nanotube growth occurs at different rates, i.e. the faster tube growth occurs further in lateral directions and consequently, the growth of slower tubes will be stopped. The growth on two alloy phases (α or β) is different, thus the attainable bimodal tube diameters vary in the two phases. Moreover, the chemical compositions of the outermost nanoporous layers depend on the substrate phase that causes a disparity in the nanoporous dissolution rate in diverse zones, leading to an alteration evident in the top-view morphology. The underneath nanotube layers become apparent (Fig. 6l) owing to the dissolution of the nanoporous, which is followed by the drastic etching of the tubes which leads to the nanotube wall thinning and the nanotube surface roughening caused by the preferential etching of the tubes (Fig. 6m) [118]. It is therefore

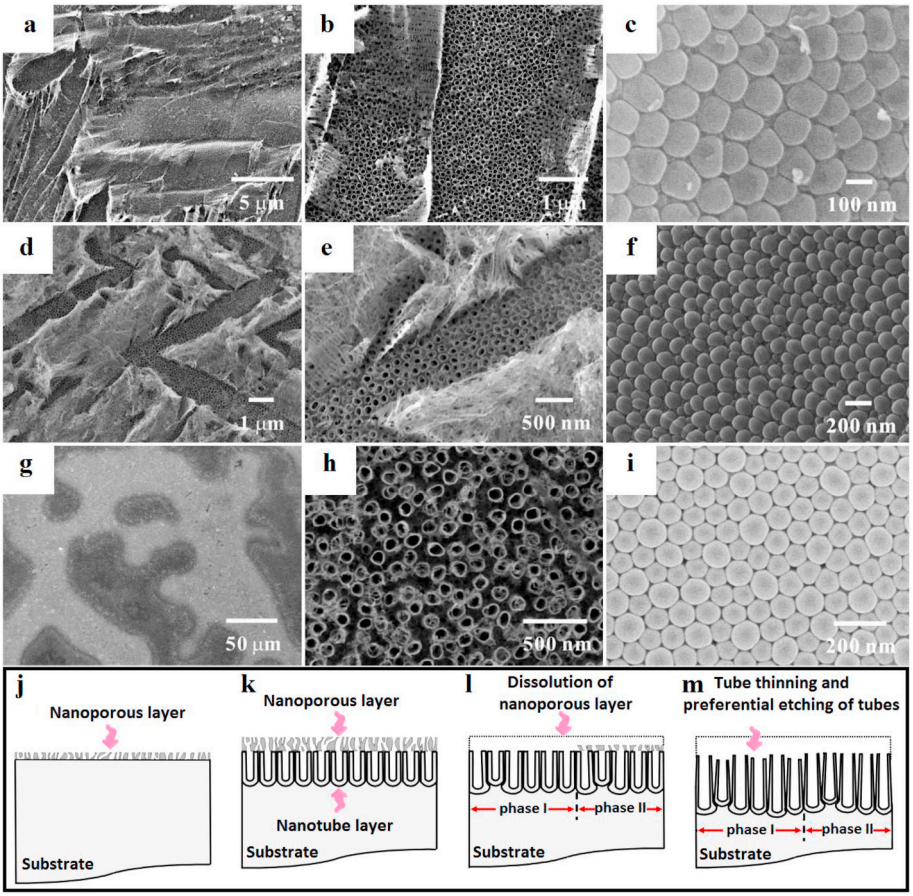

Fig. 6. Top- and bottom-view SEM micrographs of oxide layers developed on (a–c) Ti–13Ta; (d–f) Ti–25Ta; (g–i) Ti–50Ta by anodization at 20 V for 12,000 s in a mixed electrolyte (1 M H_2SO_4 + 0.15 wt% HF) as well as (j) schematic demonstration of the growth steps of self-organized MONs on Ti–50Ta alloy (Reproduced with permission from Refs. [118]).

suggested that homogenous MONs formation on a single-phase substrate can be attained if the specimen is timely detached from the electrolyte upon the nanoporous layer dissolution [118,170]. Following this study, Jha et al. [116] investigated ultrafast MONs formation on Ti–35Ta alloy by quick breakdown anodization in an electrolyte of 0.05 M $NaClO_4$ + 0.05 M NaCl in 50:50 vol% of H_2O: C_2H_5OH buffered at pH 4, at 40 V for 120 s, where pronounced localized flower-like nanotube structures are formed. They reported that the oxide nanotubes showed the least homogeneous configuration under the present anodization conditions.

3.4.5. Ti–Zr alloys

The development of nanotubes on the Ti–Zr alloys is widely studied due to the higher structural flexibility of zirconium titanate nanotubes compared to the pure TiO2 NTs [120,171]. In particular, an extended range of diameter and length of configurations can be formed by altering the anodization potential without loosening the highly ordered character of the substance. In this regard, comprehensive studies on the formation of multilayered oxide nanotubes on Ti–Zr alloys for modifying the configuration of a nanotubular valve metal system by electrochemical anodization are implemented by Yasuda et al. [75,120,122]. For this purpose, the first anodization was executed at 20 V for 15 min followed by a potential sweep from the OCP to 20 V at 20 V s-1, followed by a second anodization step at 20 V for 15 min after an opened circuit for 1 min.

Fig. 7a–f displays the SEM micrographs of the MONs on Ti–Zr alloy. As illustrated in Fig. 7a, a two-layer MONs structure is formed after a two-step anodization process, where the upper and lower layers were formed in the first and second anodization processes, respectively. There is a non-uniformity in the nanotube diameter in the zones, where the potential was switched off and on again. Besides that, the length of the nanotube for each layer is in harmony with the theoretical amount measured from the electric charge in each procedure [122]. The magnified SEM image in Fig. 7b shows that the generation of new nanotubular arrays in the bottom layer begins in the gaps between the present tubes in the top layer. By scraping the multilayer structure, fractures occur between the top (A) and bottom (B) layers, as shown in Fig. 7c. From Fig. 7d, the upper layer shows a tubular structure with a mean diameter and wall thickness of 90 and 10 nm, respectively, with a similar same morphology with the common single anodization. On the contrary, the top of the nanotubes in the bottom layer is composed of pores with a mean diameter of ~20 nm (Fig. 7e), where the remains of the tube bottoms from the nanotubular arrays of the top layer, as well as the development of many pores around them, are the dominant phenomena (Fig. 7f). It was proposed that these pores are the initial points of new tube growth at the bottom layer. Also, as schematically illustrated in Fig. 7g, the new tube growth begins in the gaps between the present tubes [75]. Given the development stages of the nanotubes at the underside, the possible choice for the rate-determining step of the tube expansion is either (i) diffusion of a metal cation or oxygen anion in the solid phase, (ii) charges for oxidation, (iii) chemical dissolution of oxide into the electrolyte, or (iv) diffusion of ions in the electrolyte [122]. Yasuda et al. [122] reported that the anodic current is progressively

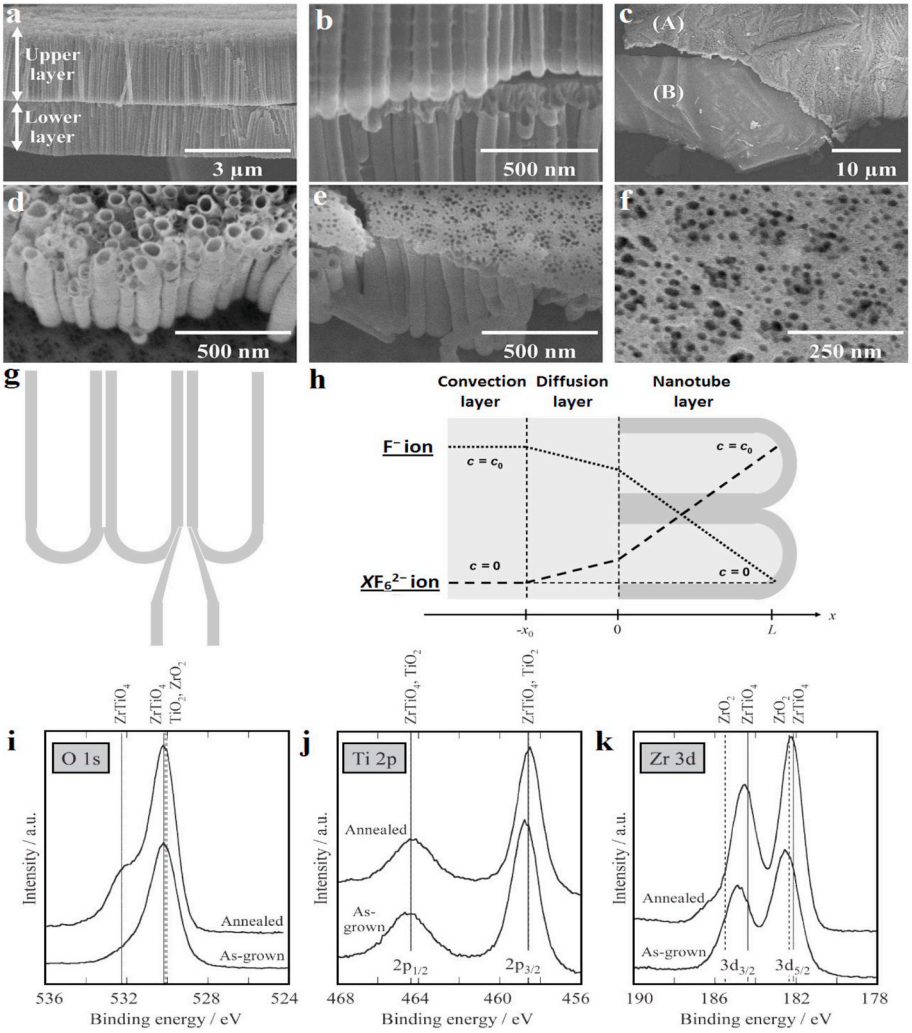

Fig. 7. (a,b) Cross-section and (c–f) surface SEM micrographs of the nanotubes formed by a two-step anodization process of Ti–Zr alloy at 20 V in 1 M $(NH_4)_2SO_4$ + 0.5 wt% NH_4F solution; (g) Schematic view of the development of new tubes between the gaps of the existing tubes as well as (Reproduced with permission from Ref. [75]) (h) the diffusion model for ionic species throughout the Ti–Zr alloy anodization (Reproduced with permission from Ref. [122]); XPS spectra of the 2 h anodized specimen after annealing at 450 °C for 3 h in the air (i) O1s, (j) Ti 2p, and (k) Zr 3 d (Reproduced with permission from Refs. [120]).

decreased with the generation of the nanotubes even at the end of the commencement phase. They assumed that the current decrease is due to the nanotube growth from the (iv) diffusion of ionic species, i.e. either F^-, TiF_6^{2-}, or ZrF_6^{2-}, and accordingly they proposed a diffusion-based model, as provided in Fig. 7h. In this model, the ions are consumed (F^-) or formed (TiF_6^{2-}, ZrF_6^{2-}) merely at the base of the nanotube, and the upper dissolution is insignificant, where it was hypothesized that the ions had a linear dispersion in the electrolyte along a concentration gradient between the tube bottom and the bulk electrolyte. It should be mentioned that the concentration of F^- and ionic species in the bulk electrolyte and at the bottom, respectively, is c_0, while the concentration of F^- and the ionic species at the bottom and the bulk electrolyte is zero [122].

The XPS peak positions were compared to the reference peaks [172,173] to assess whether the oxide tubes consist of a complex [$A_xB_yO_z$] oxides or consist of a mixture of two oxides [$A_xO_z + B_xO_z$]. According to the XPS data (Fig. 7i), the nanotubes are amorphous zirconium titanate with an excess of ZrO_2 and TiO_2, and these oxides are transformed into zirconium titanate upon thermal treatment. Other studies have shown that the anodic nanotubes grown on pure Ti had an amorphous structure [174–176], while the nanotubes formed on pure Zr had a crystalline structure [177,178]. Habasaki et al. examined the anodic coating formed onto Ti–Zr alloys [179], and realized that a homogeneous amorphous oxide layer was developed on the Ti–Zr alloy with the 50:50 wt% composition. This suggests that the crystallinity degree of the MONs could be altered using a base alloy with other compositions. Jha et al. [116] also studied ultrafast MONs development on Ti–Zr alloy, where nanotubes with uniform diameter are randomly oriented.

3.4.6. Ti–Mn alloys

It was predicted that the chemical diversity and dimensions of the MONs of the Ti-based alloys possess interesting electronic and physical characteristics, which can be modulated for a wide range of purposes [71,180]. From this viewpoint, organized arrays of MONs on Ti–Mn alloy with α + β microstructure can be a prospective material as both TiO2 and Mn2O3 are extensively employed in energy applications [181,182]. In addition to this type of approach, the microstructural properties, mechanical behavior, and biocompatibility of low-cost β-type Ti-(6–18)Mn alloys were examined after the solution treatment, where Ti–9Mn showed the best combination of tensile strength and elongation among the fabricated alloys, and comparable or superior to those of Ti–6Al–4V ELI, for every parameter evaluated. Moreover, the cell viability and metallic ion release ratios are similar to those of the pure Ti, making this alloy encouraging for orthopedic implants [183,184]. Mohapatra et al. [123] presented a comprehensive paper on the development of MONs on Ti–Mn alloy by anodization under ultrasonication in diluted EG comprising F^- ions, where the MONs with a diameter of 20–100 nm and length of 0.5–2.0 μm were formed depending on the processing parameters. The as-anodized nanotubes had a stoichiometry of (Ti, Mn)O2, while annealing at 500 °C in the oxygen atmosphere forms a mixture of anatase + rutile phases of TiO2 and Mn2O3. The Mn-doped TiO2 micro/nanostructure porous film was also fabricated by anodizing a Ti–Mn alloy, where the film heat-treated at 300 °C showed the utmost areal capacitance of 1451.3 mF cm-2 at a current density of 3 mA cm-2, employed as a high-performance supercapacitor electrode [185,186]. Fig. 8a–e shows the surface and cross-sectional SEM micrographs of nanotube arrays in the absence and presence of 3–10% Mn, where the diameter and length is ~110 nm and ~3.5 μm, respectively.

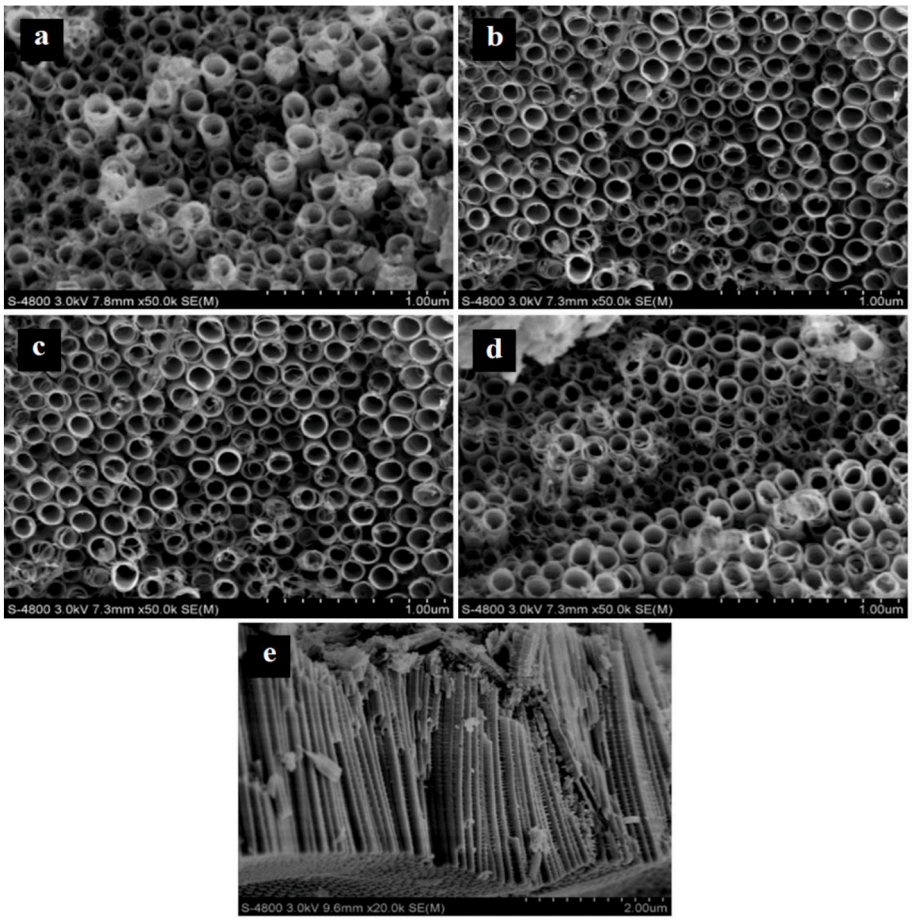

Fig. 8. Surface and cross-sectional SEM micrographs of nanotube arrays in the absence and presence of Mn; (a) TiO_2, (b,e) TiO_2–Mn (3%), (c) TiO_2–Mn (7%), (d) TiO_2–Mn (10%) (Reproduced with permission from Ref. [186]).

Vertically oriented, self-ordered MONs (TiO_2–MnO_2 NTs) were also prepared by single-step anodization process of Ti–Mn alloys in EG electrolyte [187]. From the microstructural assessments, the anodized specimens were composed of auto-aligned nanotubes over the surface of the Ti–Mn alloys, where the diameter, length and wall thickness of the MONs are in the range of 76–118 nm, 1.0–3.4 μm and 8–11 nm, respectively. The results showed that an increase in the applied potential caused an increased growth in the dimensions, whereas the increase in the Mn content in the alloy resulted in the growth of shorter nanotubes.

3.4.7. Ti–Hf alloys

Long-term experiences reveal that some of the Ti-based alloys suffer inadequate load transfer to the adjoining remodeling bone that may cause bone resorption and ultimate detachment of the prosthetic devices [188]. To solve these difficulties and to attain better performance in terms of mechanical behavior and biocompatibility, new Ti-based alloys comprising non-toxic and non-allergic secondary elements, e.g., Nb, Ta, Zr, Hf, Mo, and Sn have been developed [189]. With regards to Hf, this element is a member of the same group with Ti in the periodic table. This suggests that an alloy of Ti with Hf would be expected to show good physicochemical properties. Besides that, the Ti-*x*Hf alloy system does form any intermetallic compounds (IMCs) that are significant for excellent corrosion resistance [190,191]. On the other hand, electrochemical anodization is an effective approach for the surface amendment of bio-implants which can also be employed in this system. In this regard, Jeong et al. [192,193] presented comprehensive research works on the MONs development and morphological evolution, as well as apatite formability and corrosion behavior of the Ti–Hf binary alloys for metallic biomaterials utilization.

The homogeneous Ti–Hf alloys possess a needle-like microstructure of the α-phase, and nanotubes grown on the Ti-*x*Hf alloys are in the anatase phase after crystallization, as shown in Fig. 9a-h. They reported that homogeneous MONs with Hf contents up to 20 wt% could be grown. It was observed that the increase in the amount of Hf in the alloy resulted in the formation of MONs with a more narrow size, where the MONs had a length of ~1.7 μm and pore diameter of 80–120 nm. These results suggest that the MONs on the Ti–Hf alloys can be modified via changing the Hf content [192,193].

3.4.8. Ti–Co alloy

Based on the literature, a composite of Co3O4 and TiO2 NTs shows excellent performance in lithium-ion batteries [194], supercapacitor [195], wastewater treatment [196], and photoelectric conversion [197]. Furthermore, highly porous Ti–Co alloys are recently being developed for biomedical applications [198]. Two methods are proposed for the combination of cobalt (II, III) oxides with TiO2 NTs; (i) the anodization of Ti foils to create TiO2 NTs followed by the deposition of cobalt (II, III) oxides via different approaches, and (ii) melting the Co and Ti into alloys and the formation of the MONs by electrochemical anodization [199, 200]. In the first method, the cobalt (II, III) oxides were deposited onto the surface of TiO2, leading to agglomeration, shedding, and dissolution of the cobalt (II, III) oxides. On the contrary, the second approach allows the distribution of the cobalt (II, III) oxides in the interior of the TiO2 that would prevail over the above issue and enhance the composite material performance. More recently, Wang et al. [201] and Kobylański et al. [202] examined the fabrication and characterization of Co3O4-doped TiO2 NTs electrodes and TiO2-Co*x*O*y* composite NTs via a single-step electrochemical anodization process for visible-light-induced photocatalytic reaction, respectively. The diameter, and length of the MONs are almost unchanged with the increase of Co content, thus the diameter and length of the TiO2, TiO_2–3%Co, TiO_2–6%Co, and TiO_2–9% Co nanotubes are around 61.9 nm and 1.7 μm, 57.5 nm and 1.6 μm, 57.9 nm and 1.6 μm, and 55.0 nm and 1.6 μm, respectively [201]. Another recent work indicated that the increase of the water content in the electrolyte from 2 to 10% caused the development of TiO2-Co*x*O*y* composite NTs with larger diameters (88–125 nm for 2–10% H2O, respectively). Besides, the thickness of MONs layer has somewhat reduced from 2.3 to 2.0. This shows that higher H2O content leads to the development of MONs with a lower surface area and less photoactivity [202] (Fig. 10a-c). Since highly porous nanostructured Ti–Co alloy is promising a for biomedical applications, the formation of nanotubular arrays on the Ti–Co alloys open a new pathway for the development of MONs for various orthopedic applications.

3.4.9. Ti–V alloys

Vanadium (V) is a transition metal, ubiquitously scattered in the water, air, soil, crude oil and is present in biological organisms and is a natural constituent in most living beings. Moreover, there are groups of organisms that utilize V in their biological pathways. This element is a biological constituent, thus it is not surprising that V-based therapeutic drugs have been tested for the treatment of some diseases, especially for the treatment of diseases caused by parasites, diabetes, and cancer [203]. However, in biomedical implants, the presence of V may not give the same effect.

Allergy is an adverse effect on patients with an implanted orthopedic prosthesis. Although Ti is thought to be inert, the allergy towards Ti-based implants is still unknown. Recently, Engelhart and Segal [204] highlighted the case of a patient who experienced systemic dermatitis and implant failure after the surgical placement of a Ti-based alloy plate in the left foot. The prosthesis was detached and the eruption was cleared in the following weeks. Microstructural and electrochemical analyses reveal that the plate and screws suffered galvanic corrosion due to their dissimilar microstructures. This contributes to the *in vivo* release of vanadium. The patient was patch checked with some metals containing elements of the implant which gave a positive patch test reaction towards vanadium (III) chloride. This confirms the allergy towards V, thus clinicians should be aware of including vanadium as patch testing for patients with a suspected allergic reaction towards implants containing vanadium [204].

As mentioned earlier, self-organized nanotubes could be developed

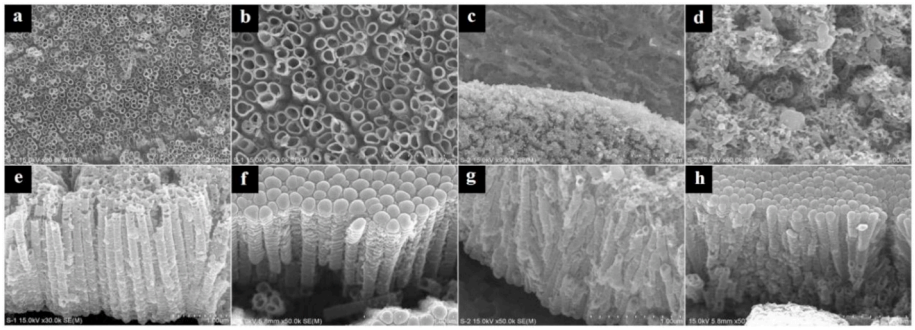

Fig. 9. SEM micrographs of MONs developed on Ti–Hf alloy following anodization for 2 h at 10 V in 1 M H_3PO_4 + 0.5 wt% NaF; top view, cross-sectional, and bottom of (a,b,e,f) Ti–20Hf, and (c,d,g,h) Ti–40Hf alloys (Reproduced with permission from Ref. [192]).

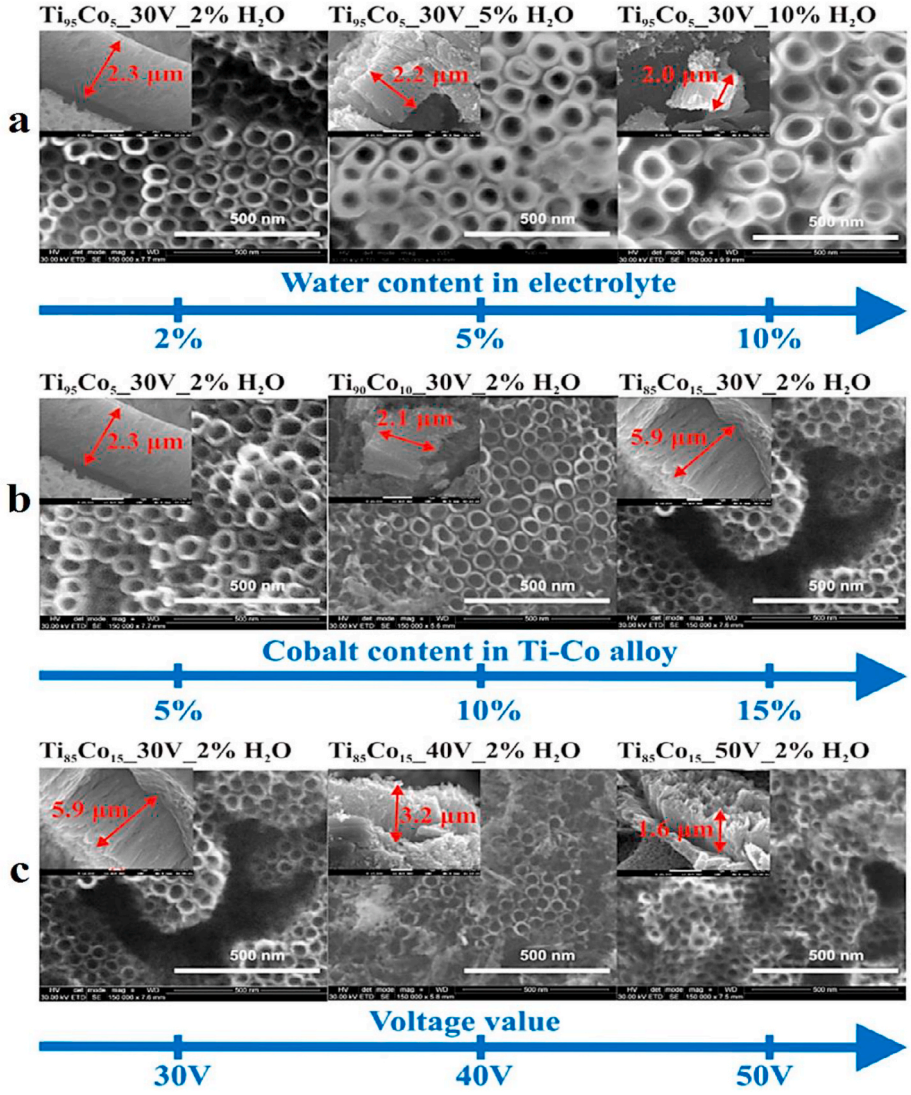

Fig. 10. The influence of (a) water content in the electrolyte, (b) content of Co in the alloy, and (c) applied voltage on the development of MONs (TiO_2-Co_xO_y) (Reproduced with permission from Refs. [202]).

successfully on a wide range of valve metals via optimized anodization processes. In some cases such as V, this approach is unsuccessful due to the increased solubility of oxides developed in common electrolytes. Thus, efforts to fabricate nanotubular arrays on Ti–V alloys are undertaken because V_2O_5 is one of the most favorable oxides for supercapacitor applications [205]. Yang et al. [206,207] found that highly ordered MONs of V2O5–TiO2 NTs can be developed on Ti–V alloys with a vanadium content of up to 18 at% via electrochemical anodization. In this case, V was electrochemically switchable, with a specific capacitance of 220 F g-1 and an energy density of 19.56 Wh kg-1, with perfect reversibility and long-term stability. This suggests that the MONs structure is an excellent material for supercapacitor applications. Nevárez-Martínez et al. [208] also studied the growth mechanism and photocatalytic behavior of hierarchical MONs of V2O5–TiO2 NTs on Ti–V alloys. Similar to previous studies, it was observed that the V content in the alloy possessed the strongest effect on the morphology, where the specimen with 5 wt% showed the best self-organization (length = 1 µm, diameter = 86 nm, and wall thickness = 11 nm). Besides that, the V2O5 species are responsible for the photoactivation of e− and h + under visible light, and a probable excitation mechanism was proposed. Recently, Han et al. [209] investigated the tribo-mechanical and corrosion properties of anodized Ti–V alloy in the NH4F/H3PO4 electrolyte annealed at different temperatures under different atmospheres. Highly crystalline MONs structures were developed followed by annealing from 200 to 600 °C. An improvement in the wear resistance of the Ti–V alloy was observed due to the high hardness and low coefficient of friction of the MONs structures. Furthermore, the corrosion analysis confirmed that the corrosion resistance of the sample annealed at 200 °C in air atmosphere was drastically higher than that of the bare substrate.

3.4.10. 4.1.10 other binary alloys

In addition to the above-mentioned systems, other binary alloys have also been studied to fabricate MONs structures for various applications. For instance, Liu et al. [210] studied the anodic formation of Ti–Ni–O nanotubes on shape memory alloys via pulse anodization in glycerol-based electrolytes. They examined the effects of anodization parameters and the annealing process on the microstructures and surface morphology of MONs and found that the type electrolyte significantly affected the development of nanotubes (Fig. 11a-c). This result could initiate focused research on the development of shape memory alloys for medical and non-medical applications.

Recently substantial efforts have been concentrated on the investigation of photoactive nanostructured substances, which can be employed as anodes in water photoelectrolytic cells. In this context, Zhang et al. [211] developed a novel hierarchical 3D Ti–Fe–O

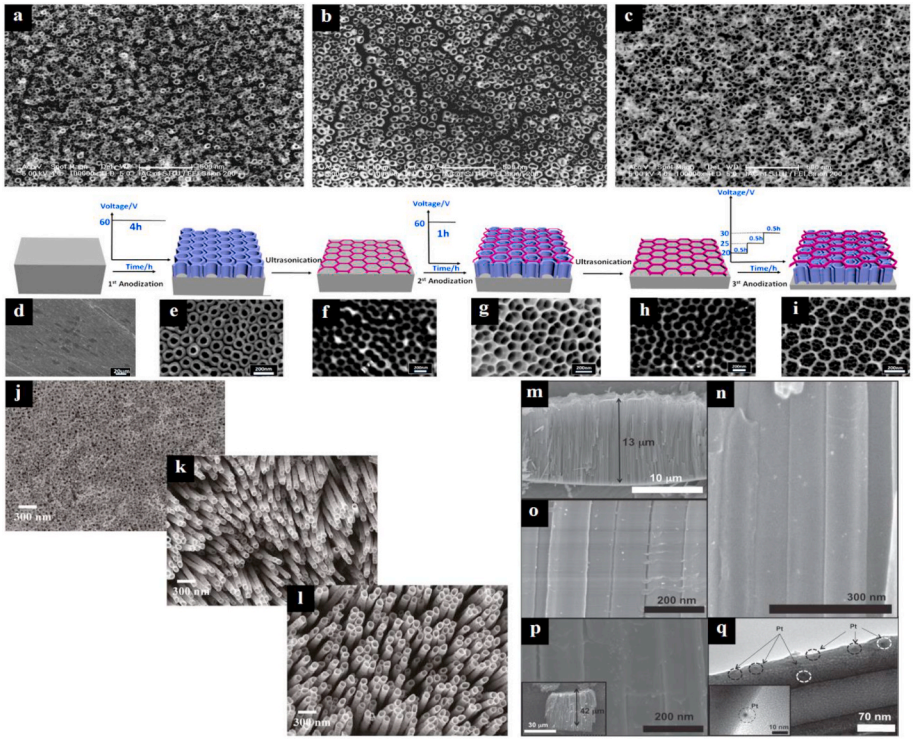

Fig. 11. Top view SEM micrographs of as-anodized Ti–Ni–O nanostructures fabricated at different pulse voltages in a non-aqueous electrolyte of 5% EG/glycerol containing 0.30 M $(NH_4)_2SO_4$ and 0.2 M NH_4F, (a) 30, (b) 40, (c) 50 V (Reproduced with permission from Ref. [210]); The development of Ti–Fe–O nanorings/nanotube configuration (d) Ti–Fe sheet, (e–g) the first, second and third-step of anodization, and (h,i) nanoimprints after ultrasonication (Reproduced with permission from Refs. [211]); FESEM top-view micrographs for Ti–Pd alloy anodized in FA electrolytes containing 0.2 M NH_4F and 0.1 M H_3PO_4 at 20 V for (j) 5, (k) 15, and (l) 24 h (Reproduced with permission from Refs. [212]); Cross-sectional SEM micrographs of Pt decorated TiO_2 NTs developed by anodization on 0.2 at% Pt containing Ti–Pt alloy for (m–o) 2, and (p) 4 h as well as (q) TEM image of decorated Pt on TiO_2 NTs (Reproduced with permission from Ref. [213]).

nanorings/nanotube configuration by three-step electrochemical anodization of Ti–6Fe (6 wt% Fe) alloy in an EG solution containing 0.3 wt% NH4F and 2 vol% H2O, as shown in Fig. 11d-i. The results showed an improved visible-light photoelectrochemical performance. Also, the heterojunction of the MONs (TiO2–Fe2O3) gave efficient charge separation. Allam et al. [212] also reported the growth of vertically oriented Ti–Pd mixed oxynitride nanotubes for enhanced photoelectrochemical water splitting. As illustrated in Fig. 11j-l, the morphological features rely on the anodization time and operating voltage. The MONs were utilized in solar-spectrum water photoelectrolysis, which showed a photocurrent density of 1.9 mA cm-2 and a ~5-fold rise in the photoconversion efficacy under AM 1.5 illumination (100 mW cm-2, 1.0 M KOH) compared to the pure TiO2 NTs prepared under the identical circumstances.

Besides that, Basahel et al. [213] studied the fabrication of self-ordered MONs anodized from Ti–Pt alloy with a low Pt content of 0.2 at% for photocatalytic hydrogen production. The MONs structure possessed a mean thickness of 13 μm which were composed of individual tube units with ~120 nm outer diameter. They have shown that prolonged anodization not only leads to the elongation of the nanotubes but also the increased particle density on the walls up to 250 μm-2 (Fig. 11m-q). This unique configuration resulted in a highly active photocatalyst for the production of H2 under UV or visible light radiation.

3.5. Ternary alloys

3.5.1. Ti–Al–V alloys

Ti possesses low density, great biocompatibility, and corrosion resistance owing to the inherent oxide film on the surface, which is a good choice for medical applications [214]. Nevertheless, the inertness of Ti, along with its suboptimal mechanical behavior restricts the life cycle of Ti implants [215]. To overcome these limitations, Ti-based alloys are designed as alternative implant materials that could be microstructurally classified as α, near-α, α + β, metastable β, and stable β [216]. Due to their non-heat-treatable character to maintain the α phase microstructure, the α and near-α Ti-based alloys have little influence on the mechanical behavior. In contrast, the β-based alloys attributable to the BCC crystal structure can be shaped even at low temperatures, which make it a proper option for multifaceted geometries. Merging the advantages of both phases, the α + β Ti-based alloys provide superior fracture toughness, tensile strength, wear-resistance, and heat treatable features enables the preparation of complex geometries for orthopedic purposes [217]. However, several studies have confirmed that the elastic behavior and load transfer from the implant device to the neighboring bone of the α + β type alloys are unsuitable for orthopedic applications [218] and could degrade after implantation [219]. In addition to modifying the chemical composition of the alloys, surface modification techniques such as physical deposition methods, thermochemical surface treatments, and electrochemical anodization have been investigated to modify the surface features of the Ti-based alloys [12,13,220]. In this section, the formation of MONs on ternary Ti–6Al–4V alloy is reviewed.

One of the pioneering efforts to utilize electrochemical anodization as an innovative approach for the surface modification of Ti-based alloys was performed by Dunn et al. [221,222], where porous surface coatings are formed by anodization and incorporating antibiotics onto the oxide surface. Zwilling et al. [223] also reported that anodization on Ti and Ti–6Al–4V alloys in the F^- ion solution is an effective approach to attain tunable tubular oxide layers under different anodization conditions [16,17,65,133,224–262]. Since the Ti–6Al–4V alloy is a dual-phase alloy, the development kinetics of nanotubes are dissimilar for the α and β phases [69]. Macak et al. [132] fabricated self-ordered porous oxide--nanotube layers on Ti–6Al–4V using an effortless electrochemical process in 1 M (NH4)2SO4 electrolytes comprising 0.5 wt% of NH4F. The results revealed that under certain circumstances, self-ordered porous oxide configurations were formed on the alloy surface, which is composed of nanotubes with a diameter and spacing of 100 and 150 nm, respectively. Besides that, the XPS spectra showed that the tubes are MONs with an almost stoichiometric oxide composition, with thicknesses of several hundreds of nanometers [132]. This research was a simple surface modification of Ti-based alloys that has a high potential for biomedical applications. In the same year, Yao et al. [18] tried to generate inimitable nanometer surface characteristics on Ti–6Al–4V

implants using a rapid and somewhat inexpensive electrochemical approach in 1.5 wt% HF and the direct-current voltage was set to 20 V for 10 s to 5 min. They reported that the surface characteristics were dependent on the time duration of the applied voltage. Following these findings, another research was conducted on the anodization of Ti–6Al–4V alloy by Narayanan et al. [6], where various coatings were formed by changing the period of deposition. Park et al. [263] also explored the development of oxide nanotubes on Ti–6Al–4V alloy in glycerol-comprising electrolytes. The treated surfaces exhibited a broad spreading of nanotubular diameters, in which nanotubular arrays with smaller sizes are distributed between the nanotubes with larger diameters. This study also highlighted that the diameters of the nanotubes can only be modified from 88.5 to 122.9 nm using various concentrations of electrolyte from 1 wt% NH4F + 20 wt% H2O to 1 wt% NH4F + 30 wt% H2O at 20 V, respectively [263]. Extensive research has been conducted in the field of nanotubes production on Ti-based alloys, especially the Ti–6Al–4V alloy in the last decade; whereby useful information is available on the impact of anodization on the features of MONs in this system [16,17,65,133,224–262]. One of the most comprehensive studies in this field was performed by Li et al. [254], where they explored the thermal constancy and *in vitro* bioactivity of nanostructured Ti–Al–V–O formed on Ti–6Al–4V. Following the anodization of the two-phase Ti–6Al–4V alloy, there were two different types of MONs on the surface of the alloy, which are the nanotubes formed in the α-phase area and the irregular nanopores expanded in the β-phase zone. They found that the Ti–Al–V–O nanotubes are stable at a high temperature of 675 °C in the air without collapse, whereas the irregular Ti–Al–V–O nanopores have lower thermal stability, which is in good agreement with our findings [133]. Recently, Atmani et al. [251] synthesized the MONs layer (~80–100 nm) on Ti–6Al–4V alloy using electrochemical anodization in fluoride containing alkaline solution and under different applied voltages (10, 20, and 30 V). Mansoorianfar et al. [247] also studied the fabrication and characterization of nanotube arrays on the Ti–6Al–4V surface for the enhancement of cell treatment in biomedical applications. More recently, a report on effects of the anodization on the morphology of NTs over Ti6Al4V in connection with hard tissue engineering application was presented by Poddar et al. [264], in which the anodization was carried at room temperature at different applied potential, i.e., 20, 25, and 30 V, as well as at a constant potential of 20 V at bath temperatures 30, 45, and 55 °C. As shown in Fig. 12a-f, the nanotube diameter and length increase with increasing the anodization voltage from 20 to 30 V. This suggests that longer NTs can be developed at higher voltages. Besides, dense NTs were formed as anodization was conducted at bath temperatures 45 and 55 °C (Fig. 12g-j). However, they believe that to recognize an exact growth mechanism at higher electrolyte temperature further studies is necessary.

3.5.2. 4.2.2 Ti–Al–Nb alloys

As mentioned above, among the Ti-based alloys, Ti–6Al–4V orthopedic implants are widely been used to substitute hard tissues and in bone fixation strategies due to the great strength, ductility as well as low density. Nevertheless, the main concern of using Ti–6Al–4V alloy in medical implants is the V content which could probably enhance the expressions of pro-inflammatory factors, provoke osteolysis, and have toxic effects in the body [204]. Research on the biological behavior of alloying elements shows that the chemical composition of alloys utilized in medical implants should be improved to reduce the adverse effects. Accordingly, alternative Ti-based alloys containing diverse alloying elements and concentrations are employed to improve the biocompatibility of the orthopedic implants. One such alloy is the Ti–6Al–7Nb [69] which possesses both the α and β phases, in which Al become constant the α phase while Nb as a substitute for V in the Ti–6Al–4V alloy becomes the stable β phase. This alloy is more ductile than Ti–6Al–4V, provides higher formability for making complex parts with excellent corrosion resistance compared to the Ti–6Al–4V alloy [265]. For this reason, this alloy has received significant attention as femoral components of hip prostheses. Even though the integration of alloying elements could improve the physicochemical properties of Ti-based alloys, the bioinert character and the incapability of Ti implants to bond with the bone is still a challenging task and is among the major failure of orthopedic implants. To improve osseointegration, surface modification of the orthopedic implants is vital because the surface-modified implants deliver an improved medium for bone cell purposes, leading to improved incorporation of the implant with the juxtaposed bone tissue [62,82]. To achieve this objective, various surface amendments are proposed to modify the physicochemical features of Ti-based alloys, such as sandblasting, hydrothermal process, sol-gel, physical as well as chemical vapor deposition [266]. Among them, the electrochemical anodization technique has attracted significant consideration owing to the effortlessness, lower cost, and capability of adjusting the surface properties in the nano regime [267].

Macak et al. [132,145] investigated the development of self-ordered nanotubes on Ti–6Al–7Nb via anodization in NH4F solutions, where under particular anodization circumstances the MONs configuration can be developed on the alloy surface. Based on the XPS analysis, the tubes are mixed oxides with an almost stoichiometric oxide composition, which can be grown with thicknesses of several hundreds of nanometers.

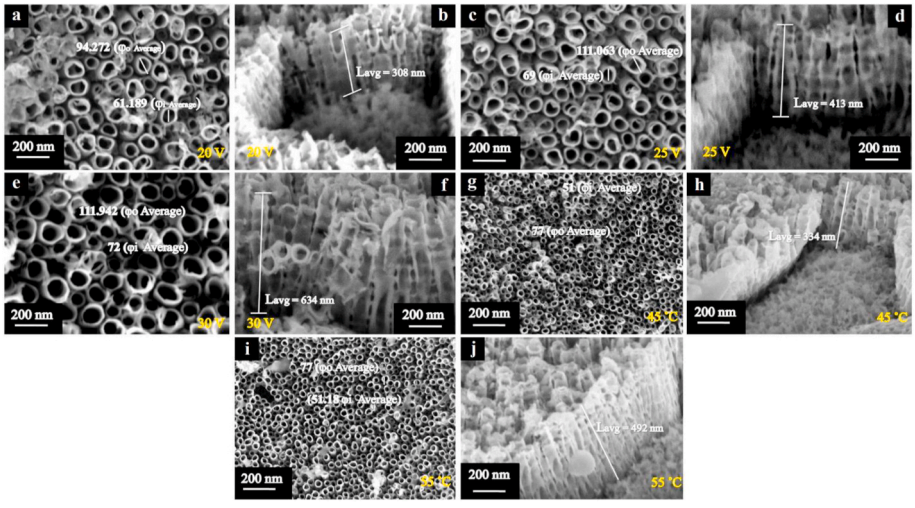

Fig. 12. FE-SEM micrographs of NTs diameter and length on Ti–6Al–4V at (a,b) 20 V, (c,d) 25 V, (e,f) 30 V at 30 °C, (g,h) 20 V at 45 °C, and (i,j) 20 V at 55 °C (Reproduced with permission from Refs. [264]).

Mazare et al. [268] also studied the development of nanotubes on the β phase contrasted with the α phase on Ti–6Al7–Nb alloy in an aqueous electrolyte (CH3COOH and 0.5 wt% HF) under 10 V potential. Rafieerad et al. [131] studied the development of MONs on Ti–6Al–7Nb alloy using different electrolytes, i.e. glycerol and EG. They reported that due to the inherent amorphous characteristic of the oxide layer, the diffraction peaks corresponding to MONs are not observed, while the MONs of anatase and rutile are detected following annealing in normal atmosphere at 600 °C for 2 h. The results of microstructural evolution showed that the mean length and diameter of the nanotubes ranged from 2.23 to 4.22 μm and 160–170 nm, respectively (Fig. 13a-l). They also found that the type of electrolyte and subsequent thermal treatment markedly influenced the surface wettability of the treated samples. In the same year, the electrochemical performance and the influence of thermal treatment on the microstructural features of MONs prepared on Ti–6Al–7Nb was comprehensively researched for medical purposes [269]. Recently, Ulfah et al. [140] also reported the formation of silver doped MONs with a mean diameter of 120 nm on Ti–6Al–7Nb alloy. These studies contribute significantly to the development of MONs for different biomedical applications such as medical implants, thanks to the microstructural features, photocatalytic mechanism, and antibacterial activity.

3.5.3. 4.2.3 Ti–Nb–Zr alloys

Ti and Ti-based alloys are the main metallic materials in biomedical appliances [218], and significant attempts are focused on the substitution of alloying elements (Al and V), presently with non-toxic elements such as Nb and Zr [270,271]. These substituting elements improve the mechanical behavior of the alloys because Nb is a β-stabilizer while Zr promotes the solid-solution hardening of the Ti–Nb–Zr alloys, which improves the mechanical performance of the alloys [272]. Given the biocompatibility of Ti–Nb–Zr alloys, Wang et al. [270] reported a higher cytocompatibility (L-929 fibroblasts) and hemocompatibility of the Ti–22Nb–4Zr alloy, where the substitution of Ti by Nb and Zr did not increase the cytotoxicity as compared to the commercially pure Ti. Moreover, Cremasco et al. [273] studied the cytotoxicity and fibroblast cell adhesion on pure Ti, Ti–6Al–4V, and Ti–25Nb–15Zr alloys, where both alloys exhibited lower toxicity effects after 24 h of cell cultivation. Regarding the surface modification of Ti–Nb–Zr alloys, numerous attempts were done to improve the physicochemical, mechanical, and biological performances. Allam et al. [274] studied the self-organized MONs on Ti–35Nb–5Zr alloy via anodization in aqueous and FA solutions containing NH4F at room temperature. The surface features were affected by the nature of the electrolyte and the applied voltage. The MONs structure exhibited a ~17.5% rise in the photoelectrochemical water oxidation efficiency compared to the pure TiO2 NTs (Fig. 14a-c). In the same year, Qin et al. [275] comprehensively examined the electrochemical anodization and crystallization behavior of Ti–35Nb-*x*Zr (*x* = 0, 5, 10, 15) alloys in 1 M (NH4)2SO4 containing 0.5 wt% NH4F electrolyte. They found that the Zr addition lowers the anodization voltage, decreases the nanotube diameter, increases the nanotube length, and improves the thermal stability of the alloys. It was also reported that Nb-doped TiO2 NTs possesses a room-temperature hydrogen sensing character, but the hydrogen sensitivity deteriorates with the subsequent introduction of Zr and caused instabilities in a highly concentrated hydrogen atmosphere. Jeong et al. [276] also examined the electrochemical behavior of HA/Ti films on the nanotubular Ti–35Nb–*x*Zr alloy, where the MONs layers were formed by anodization in 1 M H3PO4 electrolyte comprising 0.8 wt% NaF at room temperature. The results showed that the anodized Ti–35Nb-*x*Zr alloy surfaces possessed NT diameters ranging from around 60 to 220 nm and the lengths of NT ranging from around 2.9 μm in the case of Ti–35Nb–3Zr to around 3.6 μm for Ti–35Nb–10Zr. They also found that the Zr contents in the alloy had a great impact on the NT configuration, and two scales of the NT structure were developed as the Zr content increased (Fig. 14d-o). Similar research focused on the formation of MONs structures on different Ti–Nb–Zr alloys was also performed [143,277–280]. Accordingly, the Ti–Nb–Zr alloys appear as potential substitutes for the Ti–6Al–4V alloy in different biomedical devices and medical implants [281].

3.5.4. 4.2.4 other ternary alloys

In addition to the above-mentioned systems, there are several reports on the electrochemical anodization and the development of MONs on other ternary alloys. For instance, Kim et al. [282] investigated the morphology of hydroxyapatite nanotubes coated on the surface of Ti–35Nb-*x*Hf alloys as implant materials. For this purpose, different Ti–Nb-Hf alloys were produced by arc melting and heat-treated for 12 h at 1000 °C in an argon atmosphere followed by water quenching. Then, MONs development on these alloys was attained via anodization in H3PO4 electrolytes with 0.8 wt% NaF at room temperature. The hydroxyapatite was deposited onto the MONs by radio-frequency (RF) magnetron sputtering method. The morphology of the alloys was transformed from a needle-like to an equiaxed configuration with decreased Hf content and α″ phase, while the β phase was enhanced when the Hf content was increased. At lower Hf content, the tip of the nanotube with the β phase was coated with the HA film, while the α″ phase was free from the HA coating. Similar research by Park et al. also

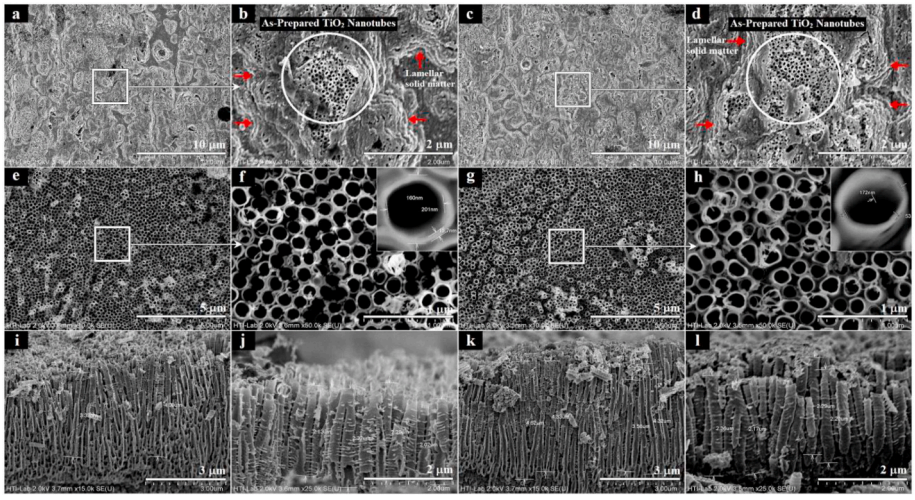

Fig. 13. Top and cross-sectional FESEM images of MONs developed on Ti–6Al–7Nb alloy using different anodization electrolytes, (a,b,e,f,i,k) EG and (c,d,g,h,j,l) glycerol, before and after heat treatment at 450 and 600 °C for 2 h (Reproduced with permission from Ref. [131]).

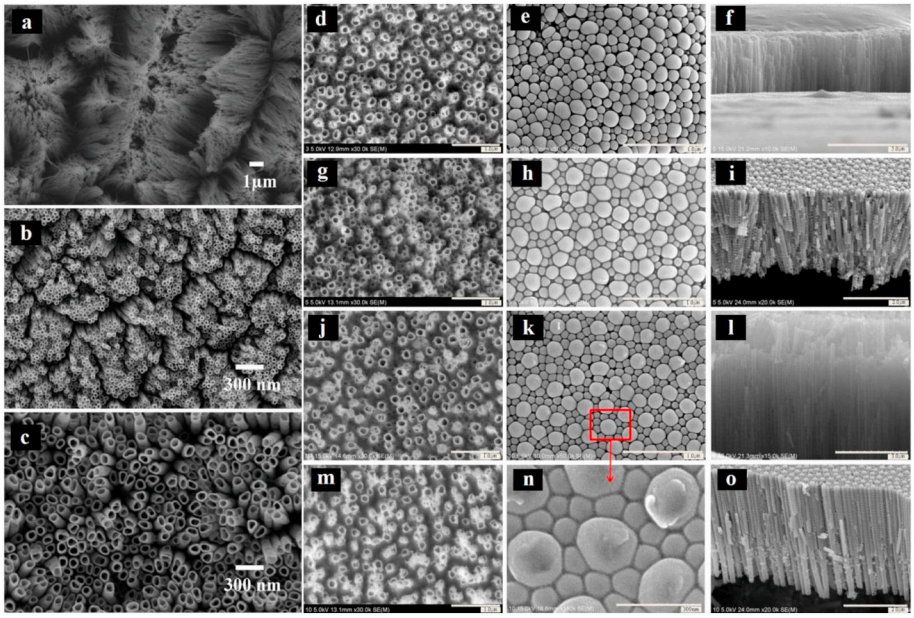

Fig. 14. FESEM top-view micrographs of the 20 h anodized Ti–35Nb–5Zr alloy in FA electrolytes containing 0.2 M NH_4F and 0.1 M H_3PO_4 at (a) 20, (b) 30, and (c) 40 V (Reproduced with permission from Ref. [274]), as well as top-, bottom-, and cross-sectional FE-SEM micrographs of NTs developed on Ti–35Nb-*x*Zr alloys by anodization in 1 M H_3PO_4 electrolyte comprising 0.8 wt% NaF at room temperature: (d–f) Ti–35Nb–3Zr, (g–i) Ti–35Nb–5Zr, (j-l and n) Ti–35Nb–7Zr, and (m,o) Ti–35Nb–10Zr (Reproduced with permission from Ref. [276]).

reported the formation of tubular structures on this alloy [283,284]. Other research groups examined the formation of MONs on Ti–30Nb-*x*Ta alloys via anodization in 1 M H3PO4 electrolyte with 0.8 wt% NaF [285]. The XRD analysis revealed that the phases in these alloys transformed from a duplex ($\alpha'' + \beta$) to solely β phase with the increase of Ta concentration. The as-anodized alloys possessed an amorphous structure and the SEM images showed that the mean diameters of the smaller and larger nanotubes in the absence of Ta are around 100 and 400 nm, respectively, while the smaller and larger MONs in the presence of Ta possessed diameters of around 85 nm and 300 nm, respectively. Besides that, as the Ta concentration increases from 0 to 15 wt%, the mean length of the MONs increases from 2 to 3.5 μm. The EDS results confirmed that the nanotubes consist of the Ti, Nb, Ta, O, and F elements. Fornell et al. [286] explored the development of self-ordered Ti(Nb, Sn) oxide nanotubes with a tunable aspect ratio and size distribution on the surface of Ti–21Nb–11Sn alloy via anodization in 0.31 M NaF + EG/water (50:50) electrolyte solution at voltages ranging from 5 to 50 V. These nanoarchitectures offer improved functionalities in extensive applications, such as biomedical, optoelectronic, photocatalysis, sensors, and electrochromic devices. In another study, Jeong et al. [287] investigated the effects of different applied potential in a two-step anodization process in a 1 M H3PO4 electrolyte and the solution of this electrolyte with 0.8 wt% NaF, to organize the morphological features of MONs on Ti–30Ta-*x*Zr alloys. The corrosion resistance was improved by increasing the Zr content in the Ti–Nb(Ta)–Zr alloy. The development of MONs on Ti–Al–Zr alloy was also assessed in organic electrolytes by anodization [288], where MONs with a length of around 6.13 μm, a pore diameter of 116 nm, and a wall thickness of 55 nm were formed at 50 V for 24 h in FA and glycerol mixtures (volume ratio 1:1) with 1.0 wt% NH4F. It was reported that the as-anodized nanotubes were amorphous and the crystallization occurred after thermal treatment in air at 400 and 600 °C for 3 h. Nanotubular films on Ti–2Al-1.5Mn alloy could be also formed via anodization in aqueous ammonium fluoride solutions at 20 V for 3 h [289]. These results show an improvement in the photo-absorption in the visible region and the photoelectrochemical response, thus could be used in solar applications.

3.6. 4.3 quaternary alloys

Quaternary β Ti-based alloys are receiving significant consideration as medical implant materials due to their very low Young's modulus analogous to human bone and outstanding biocompatibility [290]. The main objective of emerging such alloys is to reduce Young's modulus disparity between the bone (10–30 GPa) and the medical implant, which enhances the load sharing between them [291]. In this regard, different quaternary alloys such as Ti–Nb–Ta–Zr alloys (including Ti–4Nb–4Ta–15Zr [292], Ti–29Nb–13Ta-4.6Zr [293], and Ti–35Nb–5Ta–7Zr [294]) were investigated. Among them, the Ti–35Nb–5Ta–7Zr possesses a lower elastic modulus (55 GPa) and thus is considered as one of the best options for medical implants [290]. However, works on the physicochemical, mechanical, and biological features of the MONs on such quaternary alloys are restricted [295]. Anodic oxidation of the Ti–Nb–Ta–Zr alloys gives dissimilar formation rates owing to the dissimilar electrochemical oxidation rates of these elements in the alloy [146]. As a result, the dissolution was more selective, and homogenous self-ordered anodic nanotubes grow to different sizes, where tubes with a larger diameter are adjacent with eight tubes with a smaller diameter.

The nanotube growth initiates from two films – an outer nanoporous layer and a nanotube layer – from the potential sweep using a potentiostat. The outer nanoporous film dissolves in the electrolyte, thus prolonged anodization time is necessary to expand the nanotubes when the applied potential is low [147]. Recently Chiu et al. [295] presented a delicate anodizing process for the fabrication of quaternary Ti–Nb–Ta–Zr–O MONs which gave high-performance PEC water splitting. The MONs showed a higher photoactivity compared to the pristine TiO2 NTs. The higher photoactivity is because of the incorporation of alloying elements which improve the number of charge carriers, adjust the electronic configuration, and improve the hole injection kinetics for enhanced water splitting. They found that the anodization time could be tuned to attain the required nanotube length for different samples (Fig. 15a-d), which eliminates the effect of nanotube length on the PEC performance. Based on these findings, the MONs structures could be utilized for effective PEC water splitting for solar hydrogen production. The non-toxic and biocompatible features of this nanoarchitecture could achieve a distinct yet practically viable application in biotechnologically important fields, such as PEC biosensing and PEC biofuel reforming [295].

On the other hand, compared to the crystalline alloys, glass-forming amorphous Ti-based alloys possess superior features, e.g. higher strength and wear resistance, as well as and in part a lower elastic modulus and comparable corrosion resistance. In this context, some

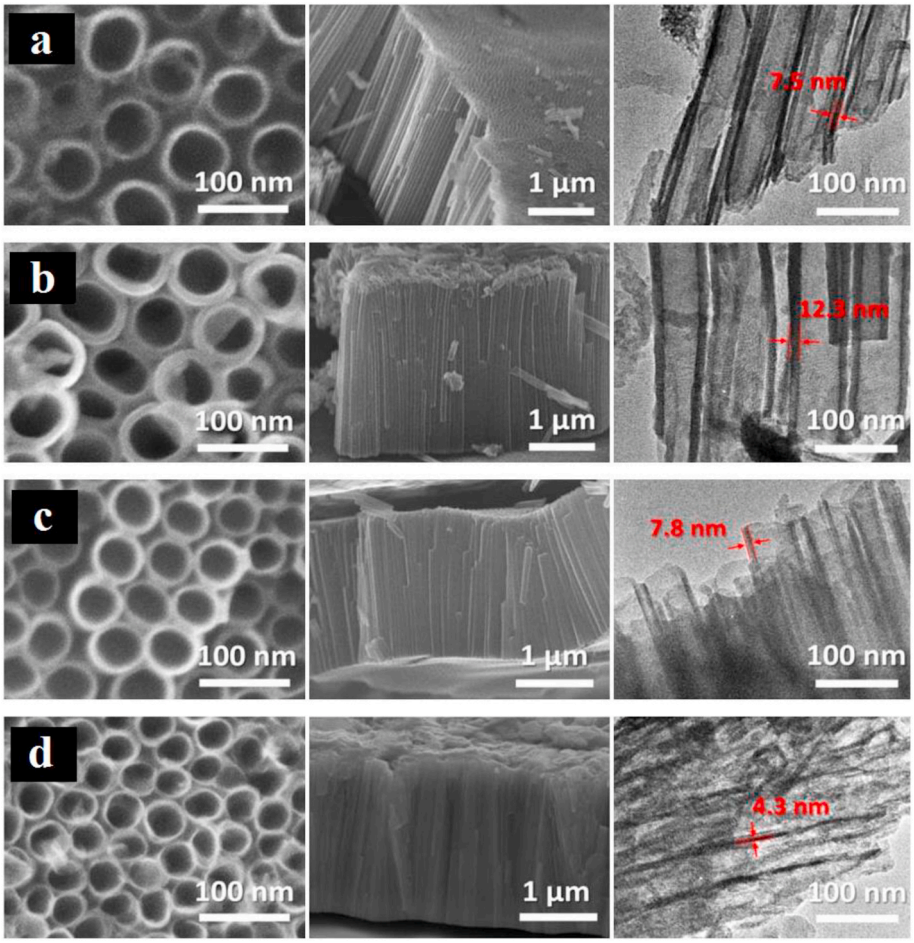

Fig. 15. Top and tilted-view SEM images and typical TEM images of (a) pristine TiO_2 NTs, Ti–Nb–Ta–Zr–O mixed-oxides formed in the presence of different H_2O contents in the electrolyte (b) 20, (c) 10, and (d) 0.9 vol% (Reproduced with permission from Refs. [295]).

glass-forming Ti-based alloys, such as the Ti60–Zr10–Si15–Nb15, are fabricated for implant purposes [296]. These alloys have very low corrosion rates in simulated body fluid (SBF) and sufficient apatite forming capability [297]. Also, an Nb comprising alloy possesses enhanced glass-forming capacity and mechanical behavior compared to the Ti75–Zr10–Si15 [298]. The anodization behavior of the glassy forms of Ti-based alloys is still in the preliminary stages of the investigation. For the first time, two glass-forming Ti-based alloys, the Ti75–Zr10–Si15 and Ti60–Zr10–Si15–Nb15 alloys were anodized in an EG-containing electrolyte to form nanotubes [299].

As these alloys are amorphous, they have no grain arrangement that is particularly interesting for the anodization of crystalline Ti, where the grain organization plays an important role in the consistency of the nanotubes [300]. As illustrated in Fig. 16a-h, the anodization of Ti75–Zr10–Si15 and Ti60–Zr10–Si15–Nb15 alloys in EG-based electrolytes produce highly ordered MONs. Smaller diameter nanotubes (~116 nm for Ti75–Zr10–Si15 and ~90 nm for Ti60–Zr10–Si15–Nb15) and shorter nanotubes (~11.5 µm for Ti75–Zr10–Si15 and ~6.5 µm for Ti60–Zr10–Si15–Nb15) could be formed on both amorphous alloys compared to TiO2 NTs grown on Ti foils under the same conditions. The TEM images in Fig. 16g and h shows a double-wall configuration of the as-anodized amorphous MONs with enriched Ti in the internal walls of the nanotubes, while Si is concentrated in the external walls, where the Zr and Nb are uniformly scattered. In addition to the glass-forming Ti-based alloys, the development of MONs on other quaternary alloys are also investigated for biomedical purposes, such as the Ti–Nb–Mo–Sn alloy. In this context, Mello et al. [301] explored the development of MONs with diverse morphological features on a Ti–30Nb–4Sn substrate with the gradual addition of Mo, wherein the impacts of anodization parameters, substrate roughness, and alloy composition were also examined. Although the martensitic phase was suppressed throughout with the rapid cooling owing to the Mo addition, all compositions exhibited a lower elastic modulus suitable for biomedical applications. The results revealed that the Mo addition increases the nanotube length and decreases the internal and external diameters. Also, the polished substrate favored the formation of uniform MONs layers. More recently, three different quaternary alloys, the Ti–6Al–4V-*x*Zr [302], Ti–24Nb–4Zr–8Sn [303], and Ti-*x*Nb-Ag-Pt [304], were investigated of their ability to form the MONs layer on these alloys. In the first case, Zhang et al. [302] investigated the formation of MONs on the Ti–6Al–4V-*x*Zr alloys ($x = 0, 20, 30, 40, 51$) via electrochemical anodization in the mixture of 98% EG + 2% deionized water + 0.2 mol.L-1 NH4F at 20 V from 5 to 300 min. They reported that the anodization was comparatively intense and the wear resistance was improved with the addition of Zr. In the second case, Majchrowicz et al. [303] fabricated self-organized MONs on a commercially pure α-phase Ti, single β-phase Ti–24Nb–4Zr–8Sn alloy and α + β-phase Ti–13Zr–13Nb alloy via electrochemical anodization in EG-based electrolyte with F- ions at a constant voltage of 20 V for 2 h. Despite employing the same processing factors in all specimens, the MONs formed on three different substrates showed different morphology: ribbed walls for the Ti and smooth walls for the Ti–24Nb–4Zr–8Sn and Ti–13Zr–13Nb alloys. In addition, the homogeneity and height of the MONs are controlled by the presence of alloying elements and the phase composition of both Ti alloys. Nanotubes of different heights were observed on the Ti–13Zr–13Nb, with a higher growth on the β phase but a lower growth on the α phase. They

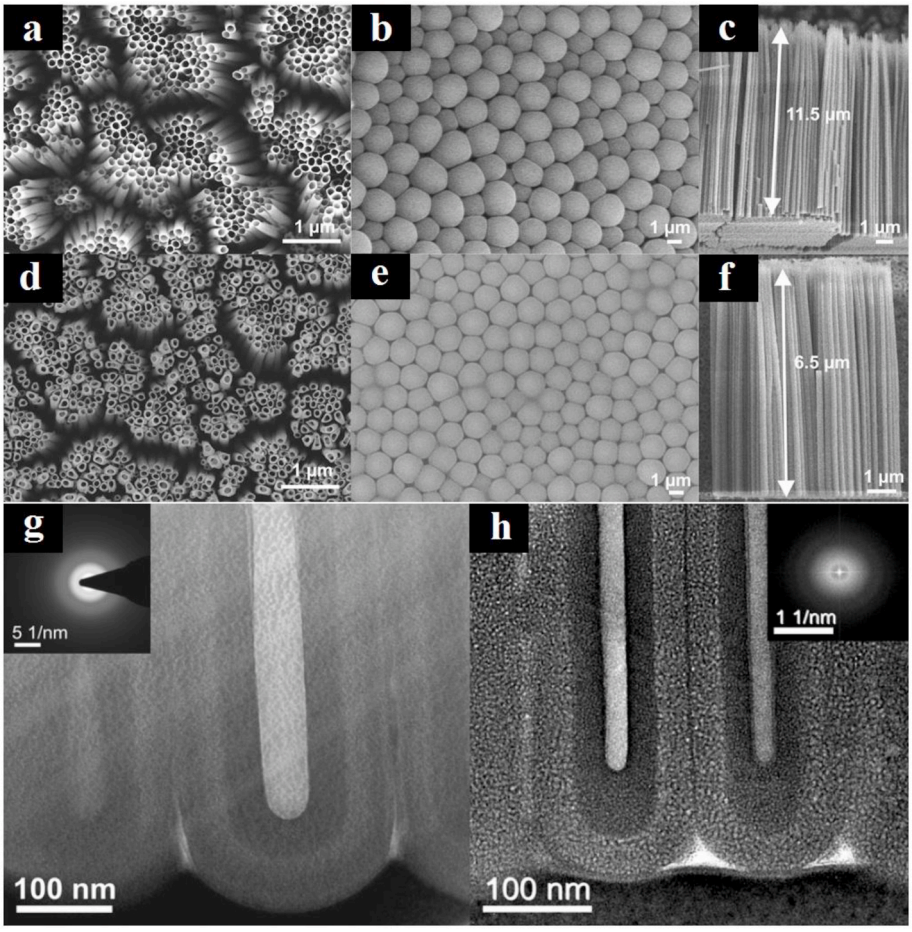

Fig. 16. (a,d) Top, (b,e) bottom, and (c,f) cross-sectional SEM view as well as (g,h) bright-field HR-TEM images and related SAED/FFT of the developed MONs on anodized Ti75–Zr10–Si15 and Ti60–Zr10–Si15–Nb15 alloys at 60 V for 6 h (Reproduced with permission from Ref. [299]).

concluded that the anodization of Ti-based alloys results in the formation of nanotubular arrays with a mixture of stoichiometric oxides – the TiO2, Nb2O5, ZrO2, and SnO2. In the third case, Kim et al. [304] studied the morphology changes of Ti-*x*Nb-Ag-Pt nanotube alloys with the Nb content via anodization at 30 V for 2 h in 1 M H3PO4 + 0.8 wt% NaF at 25 °C. The microstructural assessments showed that the needle-like configuration on α and α″ steadily vanishes with the increase of Nb, while the β-phase equilibrium structure appears with decreased particle size. In addition, the morphology of nanotubes could be altered depending on the Nb content. Consequently, as the Nb content increases, the highly ordered MONs degrades into irregular nanotubes, wherein the disparity in dissolution region at the bottom of the nanotubes was dependent on the Nb content.

3.7. 4.4 combined approaches

In addition to direct anodization of Ti alloys to develop MONs on the alloy surface, there are some different combined approaches, such as the PVD-assisted electrochemical anodization [74,127,129,136,166,253,305–309] and hydrothermal-assisted electrochemical anodization [310]. In an innovative approach, Rafieerad et al. [166] examined the optimization of TiO_2–Nb_2O_5–Al_2O_3 mixed oxide nanotubes on Ti–6Al–7Nb alloy substrate using the PVD technique. The Ti–6Al–7Nb substrate was sputtered by a niobium layer followed by the electrochemical anodization in EG/NH4F/ionized water (5 wt%) electrolyte, where the parametric optimization for higher mechanical strength was performed by the Taguchi method. For the first time, the same group also proposed a gene expression programming (GEP)-based model as a secure and precise approach to forecasting the mechanical strength of the PVD coated Nb, to form a combination of oxide nanotubes on the alloy surface. The results indicated that the values obtained from the GEP model are very close to the experimental design by the Taguchi method [307]. They recently proposed a multi-objective particle swarm optimization (MOPSO) algorithm as a precise approach to optimize the as-sputtered Nb parameters. The validated MOPSO experiments with maximized outputs corroborated the enhanced implant efficiency [129]. These results are effective for the optimization of nanostructured implants with different surface properties. In a similar work, the same group fabricated highly ordered ZrO_2–TiO_2–Nb_2O_5–Al_2O_3 nanotubes via PVD of a zirconium coating onto Ti–Nb alloy implant, followed by anodization at 60 V between 30 and 300 min [127]. More recently, they reported a novel approach for an optimized PVD deposition process, anodization, and spin coating, to improve the mechanical, tribocorrosion performance, anti-bacterial and osteoblast cytocompatibility behavior of the Ti–6Al–7Nb implant. In this regard, silver nanoparticles/graphene oxide (AgNPs/GO) decorations on combined nanotubular coating are also developed. This hybrid approach could be also utilized in the fabrication of various complex multifaceted nanotubes for a variety of orthopedic ailments [124].

4. *In vitro* studies for biomedical applications

The anodic mono-oxide nanotubes with outstanding properties have attracted much attention for various potential applications as anti-corrosion, self-cleaning thin films, and paints to sensors [311], electrocatalysis, and water photoelectrolysis [312], dye-sensitized and

solid-state bulk heterojunction solar cells [313], photocatalysis [314]. These nanostructures are also used in biomedical applications as biocompatible materials to enhance osseointegration, drug delivery systems, and advanced tissue engineering [43,315–318]. On the other hand, electrochemically developing MONs on various Ti-based alloys has been increasing in popularity as a chemical way to augment the existing and endow new properties to them. However, it is ambiguous whether this tactic can elicit properties strong enough to make MONs competitive for commercial purposes in medicine and elsewhere.

Fig. 17 shows some potential applications of MONs in various industries, for instance in orthopedic applications. In the following sections, we will provide an overview of current efforts toward MONs biomedical applications.

4.1. Mineralization abilities

In implant studies, bioactivity implies the development of bone-like HA on the implant as soaked in SBF. Recent research has reported that the HA creation kinetic as well as development in SBF is improved in the existence of a nanotubular configuration, probably due to the high specific surface area. As the NTs are developed on Ti, nearly all the osteoblast functions are preserved or amended, which could promote quicker bone regeneration around the implants without compromising the density. Also, the ordered nano configurations of the implant surface advance the osseointegration process via *in vivo* mechanical interlocking with the bone [136].

The HA formation onto anatase TiO_2 NTs is greater compared to other phases i.e. amorphous or rutile, possibly because of a closer lattice matching with the HA phase [319]. The anatase phase generates a solid and homogeneous apatite layer on the surface upon soaking in SBF for 30 h. The soaking of crystallized NTs in SBF for 14 days caused the development of a dense apatite layer on NTs, approving high bioactivity chiefly as a result of the formation of the anatase phase. The NTs could also be treated by NaOH to enhance the bioactivity and to stimulate HA formation. The as-formed TiO_2 NTs encourage the growth of bioactive sodium titanate with particularly fine nanofiber configuration on the NT edges. As soaking in the SBF, the sodium titanate nanofibers persuade nucleation and development of the nanostructured HA coating on the implant surface [320]. It was also reported that the MONs surface modification showed enhanced *in vitro* bioactivity, where a dense bone-like apatite film was developed on the mixed oxide nanotubes upon 10 days immersion in SBF from the MOPSO algorithm [129]. Similar behavior was also detected for the AgNPs/GO loaded TiO_2–Nb_2O_5–Al_2O_3 MONs, where remarkable improvements in the bioactivity of AgNPs/GO loaded MONs was observed compared to the bare substrate and MON coatings. This suggests that the surface modification enhances the hydrophilic behavior and bioactivity of metallic implants, and accordingly boosts the cell connection, enlargement, and dispersion. The surface modification could also improve the implant cytoskeletal organization [124]. It should be noted that lengthy nanotubular arrays with broader apertures increase the nucleation sites for the growth of calcium phosphates, leading to a homogeneous and dense apatite layer on the implant. Daihua et al. [321] studied the preparation of HA-MONs coating on Ti–6Al–4V via the hydrothermal-electrochemical method. The HA-MONs was directly formed onto the surface of Ti–6Al–4V as the applied voltage was between 110 and 140 V. They also provided the formation mechanism of the porous oxide film and HA. Characteristic apatite particles were also developed on the anodic MONs in Ti–15Mo, Ti–13Nb–13Zr, and Ti–6Al–7Nb alloys after alkali treatment which can be considered for dental implants [322]. These observations show that there are still many challenges to estimating MONs' biomineralization ability, especially in the case of binary, ternary, and quaternary Ti-based alloys.

4.2. Biocompatibility

The cell-implant interplay is a significant process for effective clinical implantation while the surface adaptation in the nano regime considerably alters the cellular response [43,68]. The impact of TiO_2 NTs on the cellular reaction was studied on different types of cells such as human osteoblasts (HObs), fibroblasts, chondrocytes, endothelial cells (ECs), vascular smooth muscle cells (VSMCs), epidermal keratinocytes and mesenchymal stem cells (MSCs) [323]. The reactions of ECs and VSMCs towards TiO_2 NTs indicate that the NT surface considerably enhances the EC proliferation, but decreases the VSMC proliferation. The reformed behavior of both EC and VSMC in the presence of NT arrays is advantageous for stent and other vascular applications [324]. Park et al. [325] examined the effect of highly-defined space variation between the TiO_2 NTs with six different diameters on the MSCs response and their differentiation into bone-forming cells. The experimental outcomes showed that apart from the chemistry of the surface, the nanoscale geometry also influences the cell response towards the biomimetic surface. The adhesion, propagation, relocation, and differentiation of the MSCs were maximized on the NTs with 15 nm tube diameter. The NTs with larger diameters resulted in decreased cell differentiation while the NTs with 100 nm diameter caused cell death. Das et al. [41] investigated the influence of anodic TiO_2 NTs on HObs via an osteo-precursor cell line (OPC1) from human foetal bone tissues. The TiO_2 NTs were formed via electrochemical anodization at 20 V for 2 and 4 h. The anodic NTs have a wall thickness of 39–51 nm, a length of 288–600 nm, and an inner diameter of 51–54 nm. In order to evaluate the bone cell-material interplay, the NTs grown in 4 h were employed owing to their homogeneous configuration and improved surface features. The NTs were treated by thermal annealing at 580 °C. The NTs exhibited improved cell growth and adhesion by forming filamentous arrangements with sufficient anchorage locations for filopodia

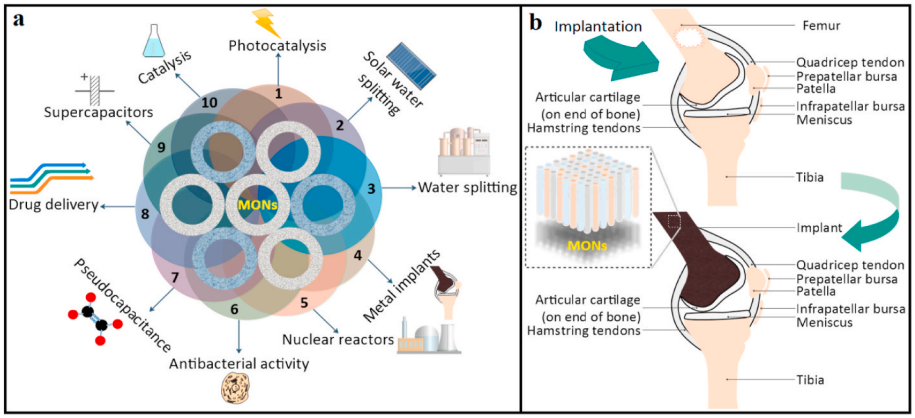

Fig. 17. Schematic representation of potential applications of MONs in various industries, for instance in orthopedic applications.

expansion. The nanostructures also showed early differentiation by intensified alkaline phosphatase (ALP) activity and considerable bone cell proliferation, from an MTT assay of a polished Ti control surface. These findings confirmed the developed osteoconductivity of TiO_2 NTs contrasted to typical polished Ti surface [320]. The biocompatibility analysis of MONs grafted on the surface of commercially pure Ti, Ti–6Al–4V and Ti–6Al–4V-ELI was conducted to present a novel platform for human pre-osteoblast cell (MC3T3) adhesion and proliferation [68]. The study shows that MC3T3 cells interact in a different way with MONs of dissimilar Ti alloys, where the adverse response to the pre-osteoblast cells was not observed. These findings suggest that osteoblast cell activity can be drastically improved through MONs surface engineering, and thus provide a suitable platform for orthopedic implants.

4.3. Antibacterial activity

Titania nanotubes have suitable biocompatibility seeing that they exhibit some antibacterial behavior, low cytotoxicity, appropriate firmness, and cytocompatibility [325,326]. Nevertheless, Ti-based materials possess inadequate antibacterial properties and many attempts have been conducted to improve their antibacterial activities, e.g. surface improvements of titania nanotubes using incorporation of AgNPs into the tubular structure for medical implants [51,327].

The implant infections ascribed to the adherence of antibiotic-resistant bacteria on the surfaces could not be healed through usual antibiotics and frequently result in implant exclusion to eliminate the infection. Hence, there is an increasing demand for complementary tactics for the healing of medical tool-related infections without the consumption of antibiotics. A surface amendment is particularly important to reduce the bacterial connection onto the surface of the implant. With regards to bacterial inactivation, TiO_2 NTs have some distinct advantages compared to other Ti–6Al–4V coatings. The bacterial reactions towards Ti–6Al–4V with dissimilar surface topographies exhibited a considerable reduction in the development of *Staphylococcus aureus* (*S. aureus*) and *Staphylococcus epidermidis* (*S. epidermidis*) on the TiO_2 NTs in contrast to the usual Ti surface. It is well-established that the level of bacterial development on the TiO_2 NTs intensely counts on the nanotube diameter so that the 20 nm diameter NTs possessed improved antibacterial behavior compared to the 80 nm diameter NTs. Also, rutile could present higher antibacterial efficiency relative to anatase [320, 328].

The NTs could be used for the encapsulation and identified transport of antibacterial agents. Popat et al. [11] employed TiO_2 NTs for the identified transport of gentamicin off-implants at the implantation zone. The liberation kinetics of gentamicin from these nano configurations and its impact on the bacterial adhesion were explored. The outputs of these assessments corroborated the superior capacity of the nano configurations for the antibiotic drug encapsulation, whereby the bacterial linkage on the NTs decreased drastically [11].

The antibacterial efficiency of the medical alloys covered with TiO_2 NTs could be boosted through the integration of other antibacterial mediators, e.g., AgNPs. In this context, Lai et al. [329] decorated AgNPs onto the TiO_2 NTs to enhance the implant confrontation against *Escherichia coli* (*E. Coli*) as a Gram-negative bacteria. Mei et al. [51] prepared TiO_2 NTs by integrating nanosized silver to enhance the antibacterial efficiency of dental implants against post-surgical bacterial infections. The amount of silver reserved the nanotubular morphology and effectively sterilized the oral pathogens. The results showed that the operation of inferior plasma voltages could give rise to an amassing of a high level of Ag on the surface, which notably compromised the biocompatibility of the sample. On the contrary, a low level of silver decoration was detected at high plasma voltages. The specimens produced at a high voltage are stated to possess continued antibacterial behavior owing to the adequate silver decoration in the right depths of nanotubes [328].

Sarraf et al. [74,328] recently prepared highly-ordered MONs decorated with Ag_2O nanoparticles for enhanced *in vitro* performance of Ti–6Al–4V (Fig. 18a and b). Compared to the uncoated sample (Ti–6Al–4V), the MONs have a bacteriostatic impact and restrained the enlargement of *E. coli* cells in 6 h of immersion, however, the cell regrowth commenced after 24 h of immersion. On the contrary, the Ag_2O NPs-decorated MONs decreased the quantity of viable *E. coli* cells and finally eradicated 100% of the bacteria during 2 h of immersion, without bacteria reexpansion following 24 h immersion. The antibacterial activity of this nanostructure is based on the synergistic impact of the TiO_2 NTs, straight interaction with silver oxide nanoparticles (Ag_2O NPs), and predominantly the liberation of silver ions. The results showed that the control (Ti-based alloy substance) and pure tantalum had no antimicrobial activity against *E. coli* propagation during 24 h of immersion, while the thermal-treated MONs and Ag_2O NPs-decorated MONs considerably diminished the *E. coli* activity during 2 h ($P < 0.001$) immersion without bacteria regrowth after 24 h immersion. The samples were treated and exposed to secondary sterile examinations to compare with the antibacterial performance of the nanostructured coatings. In contrast to the Ag_2O NPs-decorated MONs, the thermal-treated MONs nanotubes had decreased antibacterial activity after sterilization, confirming the effective function of Ag_2O NPs in attaining an enduring antibacterial behavior. The improved antibacterial activity of Ag_2O NPs-decorated MONs is due to the synergistic influence of Ta_2O_5 NTs, the liberated silver ions, and straight connection with the Ag_2O NPs. The Ag_2O NPs have a large surface-area-to-volume ratio, thus possess an active connection area with the bacteria. Ag_2O NPs possess a significant ability to disintegrate bacterial cells, by diffusion or adhesion of the silver ions on the membranes of the bacterial cell and eliminate the undesirable effects on the adjacent mammalian cells, compared to the pure nanoparticles. It is well established that the cell damage arising from Ag-based antibacterial materials is more prominent in the gram-negative bacteria compared to the gram-positive counterparts. Hence to realize the antibacterial behavior of Ag_2O NPs, *E. coli* cells were cultured as representative gram-negative bacteria. The size and morphology after adhesion with the nanotubular structure and Ag_2O NPs were investigated. From the FESEM observations, the bacteria culture on the MONs (Fig. 18c) shows the typical features of intact *E. coli* cells with a smooth surface without structural imperfections and rod-shaped morphology. On the contrary, the *E. coli* cells on the Ag_2O NPs decorated on the MONs surface (Fig. 18d) showed structural deficiencies, i.e. membrane disintegration (white arrows) and leakage of intracellular components (brown arrows). The antibacterial activity of Ag_2O NPs on *E. coli* cells is in agreement with the reports of Ag NPs and Ag^+ ions [328]. From the data, the disintegration of the cell membrane and the subsequent leakage of the intracellular substances is the most important disinfection mechanism of the Ag_2O NPs. The Ag^+ ions released from the Ag_2O NPs spread into the bacteria cells and release radical oxygen species (ROS). Concurrently, the Ag^+ ions interact directly with the phosphorus and sulfur compounds, such as DNA, RNA, and enzymes, which suppress the bacteria proliferation [328].

The antibacterial behavior of AgNPs/GO/MONs composite coatings was also explored as shown in Fig. 18e and f. This figure shows the factors of the *R*p and *R*a amounts versus the *E. coli* and *S. aureus* bacteria. As can be seen, there are great disparities between the antibacterial mediation of the Ti–6Al–7Nb implant and the modified samples. The similar-circumstance plate assay was done to investigate the antibacterial activity of the samples. The results showed that such favorable antibacterial efficiency could be attained using the 1:6 AgNPs/GO decorated MONs composite coating. Remarkably, the structural integrity of the metal oxide layer enhances the antibacterial efficiency. Because of this effect, the surface modification of NTs by GO resulted in modest antibacterial behavior [124].

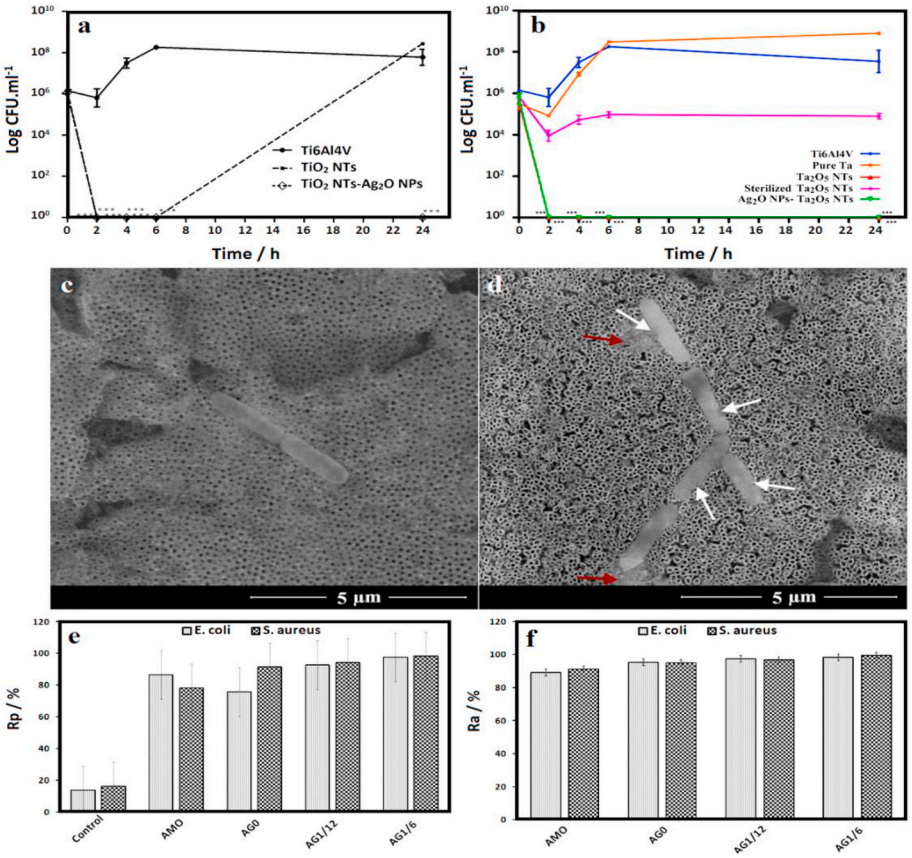

Fig. 18. Antibacterial activity of MONs compared to mono oxide nanotubes; (a) Ag_2O NPs-decorated MONs on Ti–6Al–4V opposed to *E. coli*, (b) Ag_2O NPs-decorated MONs on Ta/Ti–6Al–4V opposed to *E. coli*, (c) electron microscopy micrographs of *E. coli* cell culture on the mono-oxide Ta_2O_5 NTs and (d) Ag_2O NPs-decorated MONs for 2 h (where the white arrow show membrane disruption and the red arrow shows intracellular leakage); antibacterial activities opposed to *E. coli* and *S. aureus* bacteria in the (e) medium (*Rp*) and (f) on the samples (*Ra*); Ti–6Al–7Nb workpiece, thermal-treated TiO_2–Nb_2O_5–Al_2O_3 MONs (AMO), GO loaded TiO_2–Nb_2O_5–Al_2O_3 MONs (AG0), 1:12 AgNPs/GO loaded TiO_2–Nb_2O_5–Al_2O_3 MONs (AG1/12) and 1:6 AgNPs/GO loaded TiO_2–Nb_2O_5–Al_2O_3 MONs (AG1/6). One-way analysis of variance (ANOVA) followed by Tukey−Kramer post hoc test ($P < 0.05$) (Reproduced with permission from Ref. [74,124,328]).

4.4. Cell morphology, adhesion, viability and proliferation

Several assessments have provided evidence that MSCs, osteoclasts as well as osteoblasts exhibit size-selective responses as the dimension influences the cell interplay, in which the optimum diameter size for the cell linkage, propagation, enlargement, and differentiation fluctuates between 15 and 100 nm. It was specifically confirmed that the TiO_2 NTs arrays with 70 nm average diameter are the most favorable nanostructure for the osteogenic differentiation of human adipose-derived stem cells (hASCs). Smith et al. [330] found enhanced dermal fibroblasts and reduced epidermal keratinocyte linkage, propagation, and differentiation on nanostructured titania (diameter 70–90 nm, length 1–1.5 µm). It was also reported that the nanotubular configuration profitably encouraged cell propagation and functions in endothelial cells, but was diminished in vascular smooth muscle cells by determining the EdU (a Thymidine analog) which was integrated into the propagating cells [324]. Also, it was mentioned that the hydrophobicity/hydrophilicity of the titania nanotubular coatings is an important factor that supports the cell actions, which can be regulated by altering the diameter of the nanotube. Park et al. [331] cultured green fluorescent protein-labeled MSCs on TiO_2 NTs with various diameters to provide a deeper understanding of the influence of these nanoarchitectures on bone-forming cells and stem cells response, to induce cell activity which is responsive to the nanostructured coatings. The results gave maximum cell activity for nanotube diameters around 15–30 nm. Such lateral spacing precisely denotes the predicted lateral spacing of integrin receptors in focal contacts on the extracellular matrix, making the clustering of integrins into smaller spaces, resulting in the best possible integrin activation. When the diameter of tubes is larger than 50 nm, severe impairment of cell scattering and cell adhesion takes place, while a nanotube diameter of 100 nm resulted in cell apoptosis. The surface modification loaded with bioactive factors, in addition to the size of the nanotubes must be considered for optimized biomedical applications. The development of HA is very important for the osseointegration of bone implants. The superior adhesion of TiO_2 NT arrays on the electrodeposited HA is described by the adhesive tape examination and the live/dead cell staining assays, which is necessary for primary bone integration. These findings also demonstrate that the strongest adhesion of the HA surface with the nanotube arrays is at 560 nm. Moreover, the nanotubular arrays can certainly reinforce the collagen type I expression *in vivo* testing which takes into account the primary bone matrix protein in bone formation [82].

Several reports have compared the linkage and development of human cells on oxide nanotubes with various sizes and morphologies. Brammer et al. [332] revealed that the cell elongation significantly increases with the nanotube diameter to around 100 nm. Nonetheless, a larger nanotube diameter also influences the cell elongation. Also, increasing the diameters of nanotubes led to decreased cell linkage, due to the increased spacing between the tubes, though a greater gap could increase the dispersion of the cell. The results of the bioassay verified that outstanding cell adhesion was demonstrated by the TiO_2 nanotubes with diameter ˂ 100 nm. Park et al. [331] fabricated a nanostructured oxide layer (diameter 15–100 nm) and accomplished the *in vivo* analysis. The results revealed that the nanostructured oxide layer with a diameter of 15 nm leads to increased cell adhesion, propagation, and viability, compared to a smooth surface. The increase of the nanotube diameter to 15–50 nm led to a decrease in cell adhesion, cell proliferation, and cell viability. The cell adhesion, propagation, and viability decreased even further when the nanotube diameter was enlarged to 50–100 nm [333].

The HOb morphology and adhesion on the Ag_2O NPs-decorated MONs for 1–7 days of incubation are also examined by Sarraf et al. [74,328]. Even though no considerable cluster development was detected on the first day, the cells displayed dispersed morphology with enlarged cluster expansion and a distinctive osteoblastic morphology following three days of incubation. The continuous cell dispersion led to the development of finger-like protrusions and copious filopodial

behavior following seven days of incubation, demonstrating the positive impacts of nanotopography on the stimulation of distinctive phenotypic features and propagation of the HOb cells [74,328]. The confocal laser-scanning microscopy images also showed a homogeneous spreading of the HOb cells on the surface of the Ag_2O NPs decorated-MONs with increased cell numbers at the intervals. Fig. 19 shows the reflexes from the fix seeded osteoblasts on the unprocessed and processed Ti–6Al–7Nb alloy. From this figure, the cells are appropriately attached and proliferated through the samples with relevant bioactivity characteristics. As can be seen, the cells are alive and in good health, as verified through a distinctive polygonal osteoblastic cell morphology after the first day of cell culture. The cells are mostly flowing in a large part of the nanotubular arrays. The FESEM micrographs show that the cells are partly connected to the unprocessed Ti–6Al–7Nb after the first day of cultivation due to the inherent bioactivity of the substrate. However, the mutual action of metallic substrates with osteoblast in extended culturing times and implantation phase is an important issue that should be considered in developing nanostructured implants [124]. It is verified that the Ti with nanoporous structure encourages the ripening of focal linkages and the development of filopodia with specific nanoscale protrusions through the osteogenic cells [124]. In agreement with the MTT-ALP analysis, the microscopy observations in Fig. 19 demonstrate that the cells are still viable on the nanostructured surfaces following the first, third, and fifth days of cell culture. This figure clearly shows the bone cell populations on top of the nanostructured coatings. Confocal microscopy of hFOB cells seeded on different samples shows a typical lens-shaped feature of the live osteoblast cells with natural cell development dynamics. From the day-1 images, live cells are identified in nearly all the samples, where the quantity of discerned live cells suggests that MONs wrapped with GO (AG0) and MONs wrapped with 1:12 AgNPs/GO (AG1/12) present higher biocompatibility compared to other samples. From the day-3 images, a few sound cells are observed on the MONs wrapped with 1:6 AgNPs/GO (AG1/6) and annealed MONs. In contrast, a large number of cells are found on top of the AG0 and AG1/12. This suggests that the incorporation of GO into the nanotubular arrays improves the cytocompatibility behavior of the Ti–6Al–7Nb implant by forming a prospective bioactive platform. From the day-5 results, the seeded osteoblastic cells are more flowing and form intense islands with a similar trend. Thus, more osteoblast cells have wrapped the specimen surface after five days of growth compared to the day-3 growth [124].

5. *In vivo* studies

In general, there is insufficient *in vivo* data to recognize the reasons for the improved osseointegration and osteoconductivity of the nanostructured implants. However, some investigations of *in vivo* behavior on titania nanotube arrays with diverse properties are performed [44,316,334–339]. For instance, the electrochemical behavior, surface features and improved *in vivo* bone reaction of nanostructures titania on microstructured surfaces of blasted, screw-formed Ti-based implants has been studied by Sul et al. [316], where the surrounding implant had a well-settled trabecular architecture with some alterations in the newly created bone constructions in the periosteal and endosteal sections. In the periosteal area, active developments of woven bone were detected, where the alkaline phosphatase activity is known to be more pronounced than in the endosteal region. In the endosteal area, newly created bone is obviously recognized by the demarcation lines between dark and pale stained bone tissue on both basic fuchsin and toluidine blue-stained regions. Close bone/cell contact was monitored on both implant surfaces. Direct bone/cell contact is normally detected in a very thin rim of bone tissue in the marrow cavity area of the titania nanotube surfaces. In the direct bone/cell contact area defined by the LM observations, further high-resolution SEM micrographs often exhibit near interfacial contact distance or truly direct contact with the fluorinated titania nanotubular arrays but reveal no direct bone/cells contact with the blasted implant surfaces. These show some common histological features of the electrochemically modified implant surfaces compared to the non-bioactive surfaces [316]. Von Wilmowsky et al. [340] first investigated the *in vivo* behavior of the bioactivity of nanotube arrays. The *in vivo* results on adult pigs demonstrated that the Ti-based implants with a nanotubular configuration influence the bone development by improving the osteoblast function. Also, they found that a stronger implant-bone connection could be achieved if the implants are covered with nanotubes. One of the unexpected benefits of nanotubular coatings on the implant surface is that the nanostructured coating also endures

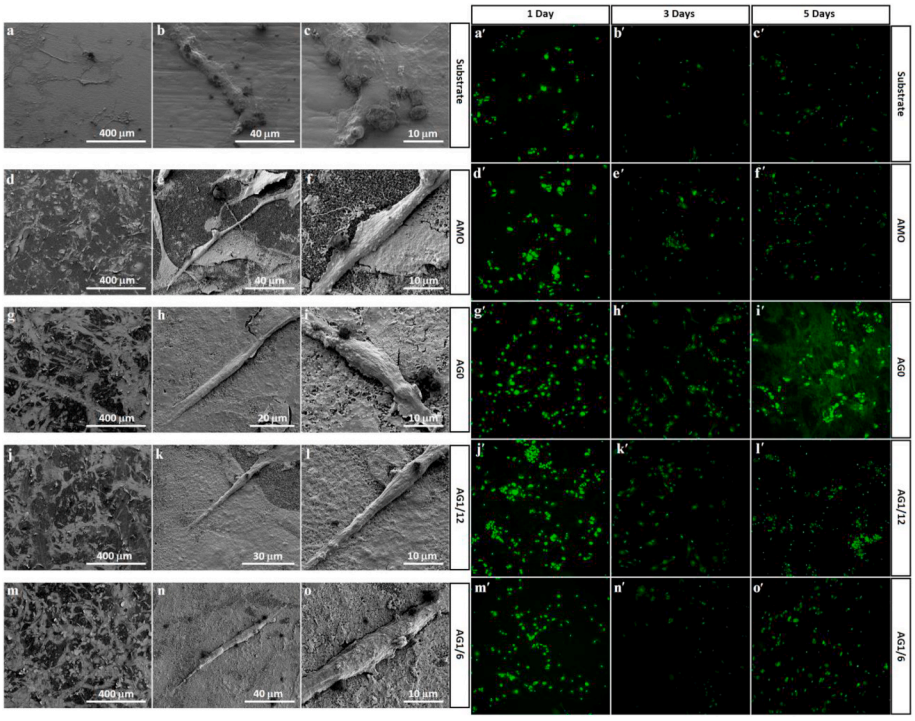

Fig. 19. FESEM images of hFOB cells after 24 h culturing and confocal laser-scanning microscopy observations (scale bars represent 100 μm) of adherent hFOB cells for 1, 3, and 5 days on (a–c and a'–c') Ti–6Al–7Nb substrate, (d–f and d'–f') crystallized TiO_2–Nb_2O_5–Al_2O_3 MONs (AMO), (g–i and g'–i') TiO_2–Nb_2O_5–Al_2O_3 MONs wrapped with GO (AG0), (j–l and j'–l') TiO_2–Nb_2O_5–Al_2O_3 MONs wrapped with 1:12 AgNPs/GO (AG1/12) and (m–o and j'–l') TiO_2–Nb_2O_5–Al_2O_3 MONs wrapped with 1:6 AgNPs/GO (AG1/6) (Reproduced with permission from Ref. [124]).

shear forces induced by the implant insertion. Nonetheless, with regards to the complex *in vivo* culture, the negative effects of the nanotubes towards cell growth could be established if the cell propagation is undesired.

The influence of different nanotube diameters (30, 70, and 100 nm) on the procedure of bone connection to the implant surface after 1–5 weeks of establishment, was also studied *in vivo*. The findings showed that the titania nanotubes control the bone creation at the interface of bone-implant to attain an appropriate osseointegration process. Besides, the dynamic bone deposition was detected in the chronological fluorescent labeling images. Contrary to the usual titanium implants, the bone-implant interaction and the level of gene expression are considerably enhanced in the implants with nanotubular coatings (especially the nanotubes with 70 nm diameter) [320]. Lv et al. [341] verified the substantial influence of nanotopography on the differentiation of hASCs in bioassays. They proved that a nanotubular structure with an average diameter of 70 nm at 20 V anodization is sufficient to supply the optimum conditions for osteogenic differentiation of the hASCs.

To approximate the osseointegration rate, Moon et al. [342] detached Ti implant screws from animal models following implantation and established that the interaction of an implant with the adjacent bone increased significantly following the development of the nanotubes. Jang et al. [338] investigated the impact of TiO_2 NTs on the osseointegration of orthodontic miniscrews. The miniscrews were inserted the New Zealand white rabbit legs for *in vivo* studies. The TiO_2 NTs were endowed with a rough surface while the miniscrew with TiO_2 NTs exhibited the highest BIC ratio of 52.8% with enhanced osseointegration. The results confirmed that the TiO_2 NTs on the thread valley of the Ti miniscrew are well preserved from the *in vivo* assessment. To assess the biomechanical behavior of Ti–6Al–4V miniscrews are also exposed to anodization-cyclic precalcification-heat treatment (APH), and their potential clinical applications are outlined [235].

This approach resulted in a MONs coating which covered with a dense apatite film, as shown in Fig. 20a–d. According to Fig. 20e–h, for the untreated samples, both after 3 and 6 weeks, the surface mainly exhibits interface fracture patterns between new bone and miniscrews. On the contrary, the surfaces of the APH sample display cohesive fracture patterns within newly shaped bone at both steps. The APH treated specimens exhibited better bioactivity and biocompatibility compared with untreated and anodized and heat-treated specimens. The *in vivo* results of APH-treated miniscrews possessed greater removal torque and bone-to-implant contact than did untreated miniscrews following both 3 and 6 weeks ($p < 0.05$). Besides, early accumulation of compactly mineralized bone surrounding APH-treated miniscrews was detected, indicating proper connecting to the treated surface [235], as illustrated in Fig. 20i–l.

The integrity during fixation and exploitation are two research topics related to the implants with a nanotubular oxide layer, in addition to the damage beginning and expansion stages. In numerous reports, damages of the nanotubes developed on the implant surface were detected by various techniques, e.g., micro scratch as well as nanoindentation. Shemtov-Yona et al. [343] explored the damage on the surface of nanostructured Ti and Ti–6Al–4V dental implants following elimination from the tissues. The results revealed that the anodized implant surfaces are free from damages. It was found that the nanotubes formed on Ti-based screws were devastated and detached at the screw edge, whereas the other segments of the implant screw reserved the tubular configuration with suitable incorporation with the animal tissue. Shivaram et al. [344] also reported that the nanotubes coating (length up to 1 μm) was free from damages following the implantation step. These findings show the significant progress in terms of improving and controlling bone-forming functionality for advanced orthopedic implant applications [72]. Recently, in a comprehensive study, Bose et al. [43] examined calcium phosphate coated 3D printed porous Ti with a nanoscale surface amendment for medical implant purposes, as schematically shown in Fig. 21. This figure displays the influences of the combination of doped calcium phosphate coating with nanoscale surface modification of porous Ti on early step osseointegration in a rat distal femur model. This nanoscale surface modification can also be employed on the stem zones of a total hip or knee arthroplasty to develop various MONs layers to commence early bone integration at the implant interface, which ultimately can result in enhanced healing [345].

6. Clinical trials

In general, the medical achievement of orthopedic implants is strongly connected to the early osseointegration stage, which depends on the implant surface properties. There are still numerous challenges to

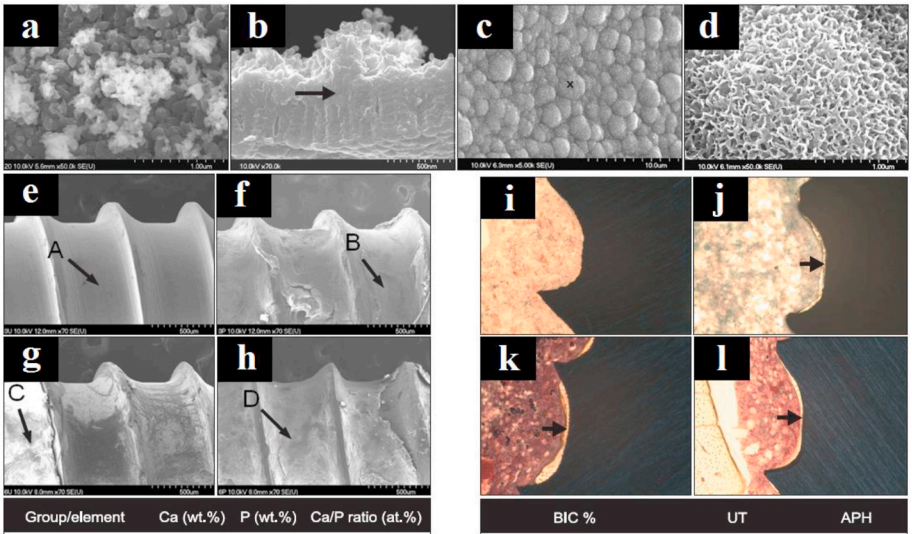

Group/element	Ca (wt.%)	P (wt.%)	Ca/P ratio (at.%)
UT 3 weeks (point A)	0.50	0.31	1.21
APH 3 weeks (point B)	3.44	3.68	0.72
UT 6 weeks (point C)	1.80	2.78	0.50
APH 6 weeks (point D)	11.10	5.94	1.45

BIC %	UT	APH
3 Weeks	8.25±6.67*‡	84.00±8.47*
6 Weeks	61.75±12.81††	91.50±3.58†

Fig. 20. Ca–P coated MONs developed on nanotubular Ti–6Al–4V miniscrews following the (a, b) APH treatment and (c, d) APH treatment and 3-day soaking in SBF, as well as morphology and histologic images (Villanueva staining, × 100) of the interface of bone-miniscrew for (e, g, i, k) untreated sample and (f, h, j, l) APH specimen in 3 and 6 weeks following insertion. The left table presents the chemical composition of the surface of extracted miniscrews, while the right table shows the percentage of BIC (%) measured on 5 threads of untreated and APH-treated miniscrew interfaces (Reproduced with permission from Ref. [235]).

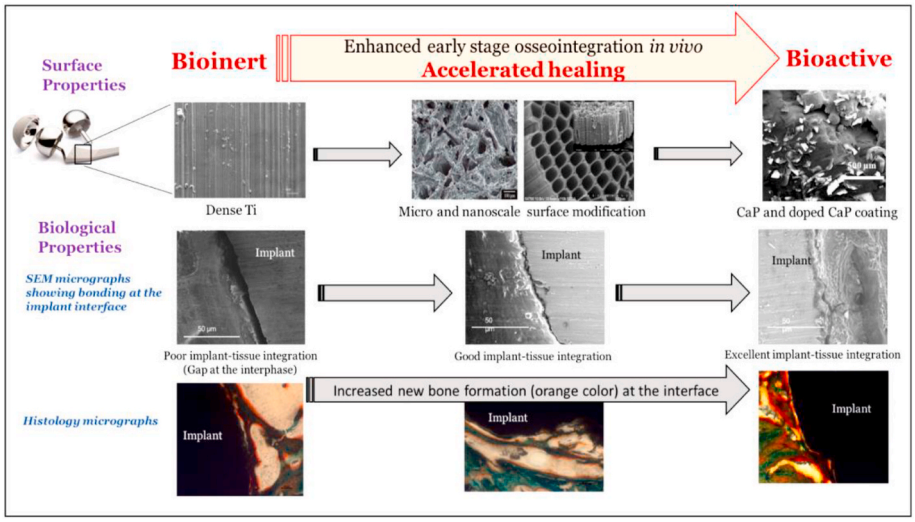

Fig. 21. The influences of linkage of nanoscale surface modification with doped calcium phosphate coating on porous commercially pure Ti on *in vivo* osseointegration in a rat distal femur model (Reproduced with permission from Ref. [43]).

overcome before the full utilization of nanotubular surface modification, especially MONs in various fields of medicine. The main contradiction is that the most favorable microstructural features and geometry of the nanotube arrays differ between different research groups. Thus, it is better to render the *in vitro* consequences into *in vivo* applications through animal models and ultimately in clinical trials. Although there are significant shreds of evidence that stem cells can be seeded into the nanotubes for their enlargement and intensification [72], such clinical studies on anodic nanotubes for implant applications are still scarce.

Nowadays, the DOTIZE® technology established by DOT America is a leading anodization process employed in the industry for the production of nanostructured implants. Benefiting from this technology allows the production of an oxide layer with a maximum thickness of 5 μm, giving rise to nanoroughness on top of the implant with improved biocompatibility, as well as corrosion and wear resistance with no substantial alterations in the dimensions [333]. Nobel Biocare® is also a marketable dental implant treated by anodization. The anodization of titanium-based alloys towards the fabrication of medical implants is composed of the following stages. First, the substances are located in a cleaner tank and thoroughly rinsed. Then, the substances are etched in a specific solution, in which the soaking period for complete etching depends on the solution. The tank anodizing stage comprises the usage of a voltage and current. The processing period of this stage can be extended with the manifestation of holes in the implants as they are less accessible, thereafter the substances are eliminated and thoroughly washed [333].

Losic et al. [346] described the recent developments on new approaches for drug release from nanotubes for the design of nanotube-based drug-releasing implants (DRI) with improved performances, such as expanded drug release and zero-order liberation kinetics and remotely activated release. Anodic nanotubes possess great potential to enhance the efficiency of Ti-based implants as a surface coating because of their biocompatibility, high surface area, and capability of promoting bone growth. Nevertheless, there are two concerns required to be clarified before more advancing anodic nanotubes technology as a drug carrier: (i) uncontrolled liberation of drug and (ii) poor mechanical behavior [347]. To overcome these issues, efforts have focused on developing a drug carrier using a composite of biodegradable polymer/anodic nanotubes [347–350]. Instances of primary medical purposes of titania nanotubes towards bone healing and medical implants, cardiovascular stents, dentistry and cancer treatment are accessible [333,351–353]. These attitudes can be further developed by using various MONs surface modifications, which can be promising strategies for improving bone-implant interaction and accelerating the healing time [124,129]. However, anodic nanotube research in orthopedic directions is still in its infancy and there is a long distance to go in clinical use. The biological interactions between cells and anodic nanotubes, especially MONs are required to expand from the cellular stage to the molecular phase and from morphological alterations to molecular changes. It is well-established that the diameter of nanotubes has direct effects on adhesion, scattering, and growth of osteoblast and mesenchymal stem cells, thus the consistency and basis of this development as well as other factors stimulating cells' performance are obliged to be further discovered [82].

7. Future directions

Despite vast global advances in orthopedic implants [354]; however, there are no standardized schemes for evaluating fracture healing, with physicians relying on X-rays that are merely helpful at later steps of healing [355]. The global orthopedic tools market is expected to drop from $52.7 billion in 2019 to $39.3 billion in 2020 at a compound annual growth rate (CAGR) of −25.6%. This decrement is predominantly due to the COVID-19 outbreak and the measures to contain it [356]. Numerous medical care services in affected countries have been entirely closed or have been merely presenting minimal treatment for emergency cases. Accordingly, orthopedic surgeries have been delayed or even canceled owing to the nation's lockdown [357–359], whereby the production of orthopedic devices and implants has been sharply decreased thanks to prolonging factory closures. The global orthopedic tools market is then expected to resume and raise at a CAGR of 5% from 2021 and overtake $63.6 billion in 2023 [356].

With the growth of the medical implants market, there is great potential for the smart implant systems, which can incorporate with current orthopedic hardware platforms to give physicians information about each patient's healing trajectory [355,360]. In this regard, Parkes [361] recently discussed how intelligent implantable materials are varying the way bone diseases and damages are treated. In general, implants can be smart in two approaches, either through additively fabricated to produce patient-specific implants (PSIs) through computed tomography (CT) or via integrating sensors that are utilized to heal fractures. In this approach, sensors can compute the strain applied to the implant, showing the extent of fracture healing. Accordingly, surgeons could recognize the best time for the patient to progress to the next step of treatment and could recognize healing difficulties much earlier. In the initial stages, internal sensors could gather detailed information about

the patient's condition, where surgeons and other healthcare professionals could administer the correct therapy to the patients. A sensor could measure the local temperature in the body, as increased temperature signals an infection before the symptoms emerge. This benefits both the patients and doctors by allowing therapy prior to the infection which could be complicated and expensive to treat [361]. Lin et al. [355] also recently introduced smart bone plates that inspector fracture healing through microscale EIS sensors fabricated to calculate electrical features of the fracture callus longitudinally for the period of healing in two dissimilar murine fracture models. They examined the capacity of these sensors to differentiate between healing and poor-healing fractures steadied by minified external fixators or bone plates and discovered that frequency spectra of impedance capacities are strongly interrelated with measured quantities of bone mineral density and volume. This suggests that the combination of surface engineering by creating the MONs layer and incorporating a biosensor could lead to a new generation of implants, where the long-term perspective is that the EIS-based sensors can be developed to boost current clinical care by scrutinizing the healing progress via regular measurements at the fracture zone, and further allow early evaluation of risk for nonunion [355, 362].

The main applications of this smart design seem to be in orthopedic implants (such as knee and hip arthroplasty, spinal fusion as well as fracture fixation) and dental implants, where physical stimuli are obtained using special technology used in implants. Osteoarthritis of the knee is one of the most widespread musculoskeletal pathologies worldwide. Smart knee implants take an important part in the properties of knee biomechanics. From the data of intelligent knee implants, the peak force such as walking after total knee arthroplasty is around 1.8–2.6 times of the body weight and occurs in the middle of the tibial tray. Wholly *in vivo* purposes for fixed intelligent knee implants are still part of applied research and not part of clinical practice. Due to the importance of bio-functionality of permanent intelligent knee implants, future applications of these implants must involve the protection of the knee from external forces which hasten the wear, implant loosening, or premature collapse of the implant [363]. Osteoarthritis is also a frequent problem found in the hip. The enthusiasm towards *in vivo* intelligent hip implants is presently associated with applied research, and not towards clinical applications for the specific care of the patient. Accordingly, records from intelligent hip implants could be used to describe the load circumstances for testing and authenticating the *in vitro* function of implants [364,365]. Besides this, intelligent implants can present some vital information about the function of posture, motion, and muscle activation in spine biomechanics, which is very essential as the spine loading takes a crucial part in the disease process and the therapeutic process for patients with lower back pain. Scrutinizing the loads on an intelligent fracture fixation device during weight-bearing is proof of the strengthening and fracture healing [363]. Despite the above description, the sensor concept may not very practical particularly at the outer surface as the cellular layer will cover that within few hours and beyond a few days, those sensors generally don't function [366].

On the other hand, smart implants probably have a better future in the field of spinal and dental implants [367–372]. In this context, a self-directed intelligent dental prosthesis has been introduced by Van Ham et al. [367] for rapid rehabilitation, wherein the device can connect wirelessly with an exterior transceiver, which enables a patient-tailored approach. A monolithic human oral motion-powered smart dental implant with suitable mechanical strength has been proposed by Park et al. [368] as an ambulatory photo-biomodulation therapy modality, wherein the system could convert human oral movements into well-regulated *in situ* light irradiances. This feature is made possible through the energy collecting from dynamic human oral movements using the developed piezoelectric dental crown, a linked circuit, and micro light emitting diodes (LEDs), as illustrated in Fig. 22. The findings of this comprehensive study not only lead to highly advanced multi-functional implants to avoid peri-implant complications and

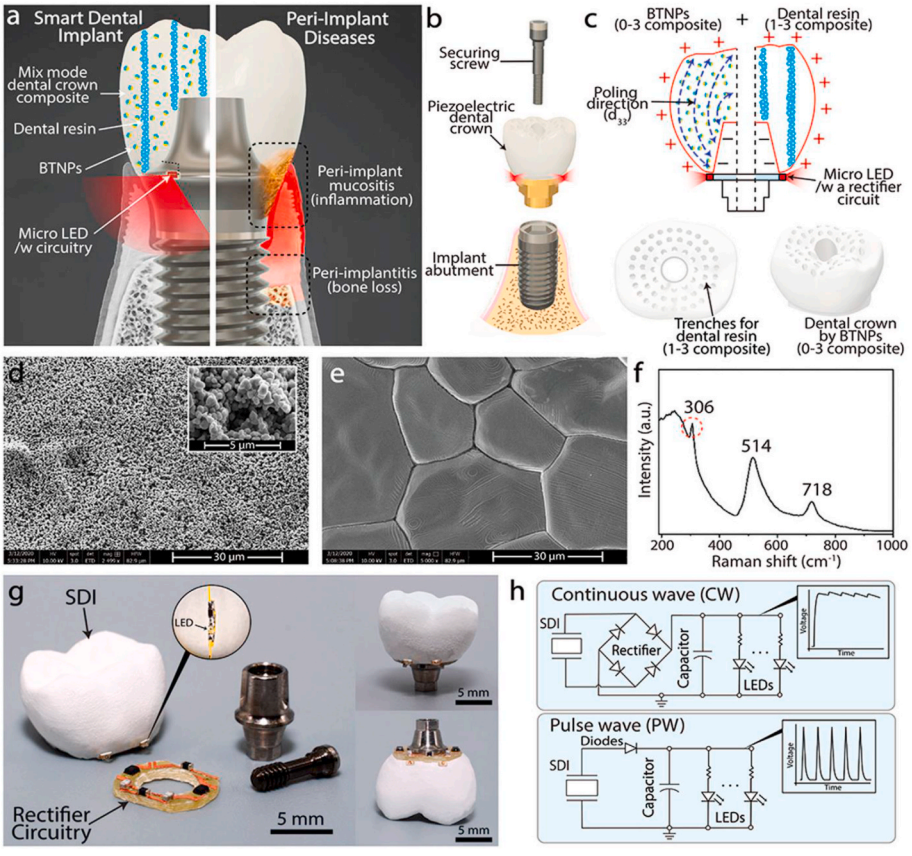

Fig. 22. Smart dental implant system, (a) ambulatory photobiomodulation therapy enabled by smart dental implant maintains overall oral health, whereas common dental implant without therapeutic function can trigger severe oral diseases, (b) the schematic vision of smart dental implant assembly on the basis of screw-retained dental implant design including (c) two-phase composite dental crown, linked electronics, and micro LEDs, (d,e) SEM micrographs of the dental material, (f) Raman spectrum of barium titanate nanoparticles, (g) prototype smart dental implant on a US penny, and (h) two dissimilar kinds of joined circuits for continuous or pulsed wave, i.e. CW or PW (Reproduced with permission from Ref. [368]).

lessen the risk of implant failure, but also could be employed to other orthopedic implants prone to continuous exposure to bacterial burdens.

Regarding the smart spinal implants, many efforts have been made to set up various sensing tactics; nevertheless, they fail to provide mechanical sensing necessities or deficiency *in vivo* translatability [373–376]. To this aim, polymeric-based sensors and Micro-electromechanical Systems (MEMS) possess desirable characteristics that correspond to the characteristics needed to measure the load in the body. However, these approaches have not yet been widely examined in orthopedics. Whereas inductive powering is favorable, wireless energy transmission and telemetry are ongoing research topics [371]. This outlook recommends a systematic consideration of the pertinent biomechanics to recognize the relevant sensing factors, simultaneous treatment of sensing and powering features, as well as exploitation of energy harvesting aimed at sensing and data transmission.

On the other hand, as described above, the anodic nanotubes have a higher surface area than the flat implant surface and can overcome the current clinical implant restrictions by creating extra spaces for cell interaction remarkably at the cell-extracellular matrix level. Furthermore, the enhanced bioactive layer of inward growth of anodic nanotubular arrays on Ti and its alloys can deliver superior adherence of the nanotubes layer to the substrate, dismissing the difficulties of infirm interfacial bonding of the present ceramic coatings. Besides that, the nanotubes may afford similar features with the natural bone topography (pore size/diameter~ 60–100 nm) that could modify the interference of bone cell response. Therefore, the combination of nanotubular surface modification and biosensor offers smart orthopedic implants that effectively advance the cell interplay with the implant materials and may improve osseointegration. This also provides some important physical data from inside the body, such as pressure, force, strain, displacement, proximity, and temperature [377]. This could significantly decrease the number of patients admitted to the hospital. Apart from the above explanations, intelligent orthopedic implantation for clinical practice is a challenging task, because the integration of the current sensor technology requires some substantial modifications of the implants [378]. Also, the physicochemical properties of anodic nanotubes, in particular, MONs for various orthopedic applications should be assessed in detail [307]. Thus, nano surface modification and biosensors for next-generation intelligent orthopedic implants should be simple, tiny, robust, and reasonably priced [363], wherein deeper insights into their biomechanical function is vital before choosing a proper sensing mode. Based on innovative medical approaches, it is conceivable that a new generation of smart orthopedic implants will eventually become available to surgeons and enable intensive medical care.

8. Conclusions

One-dimensional anodic nanotubes are promising biomaterials in a broad range of biomedical applications due to their large surface-to-volume ratio, low-cost, chemical stability, outstanding biocompatibility, and resistance to bio-corrosion. In the field of orthopedic implant manufacturing, nanosurface modifications have been widely studied in the literature for improving implant performance, however, the scientific and clinical understanding of MONs are still in the initial phase. One of the most important questions in this regard is whether the development of MONs is an effectual strategy to develop the properties of medical implants or an ineffective research approach? Based on the literature, a wide range of MONs can be formed on different binary, ternary, quaternary, and more complex Ti-based alloys by controlling the anodization conditions. However, the formation mechanism of MONs in different systems is complex and the presence of various elements in the system directly impacts the electrochemical performance, morphology, and composition of the resultant MONs. The studies included in this review showed anodizing is a convenient way of adjusting some, but not all features in MONs and should be strengthened ideally in combination with other treatments like thermal treatment. In addition to direct anodization of Ti-based alloys, there are different combined methods, e.g. PVD-assisted anodization, which could be also utilized in the fabrication of various complex multifaceted MONs for a variety of orthopedic purposes. It was proposed that the integration of nanotubular surface modification and biosensor may result in smart orthopedic implants that not only make progress the form, fit, and function of implants, but also provide important physical data from inside the body, such as strain, force, pressure, proximity, temperature and displacement, which can be effective in clinical care. However, this smart orthopedic implantation is a challenging task for clinical practice because the integration of MONs and biosensor needs more scrutiny and some optimization.

Declaration of competing interest

The authors declare that they have no known competing financial interests or personal relationships that could have appeared to influence the work reported in this paper.

Acknowledgments

The authors would like to acknowledge University of Malaya, Taylor's University and the Sharif University of Technology for supporting this research.

References

[1] V.P. Mantripragada, B. Lecka-Czernik, N.A. Ebraheim, A.C. Jayasuriya, An overview of recent advances in designing orthopedic and craniofacial implants, J. Biomed. Mater. Res. 101 (2013) 3349–3364.
[2] K. Kawagoe, M. Saito, T. Shibuya, T. Nakashima, K. Hino, H. Yoshikawa, Augmentation of cancellous screw fixation with hydroxyapatite composite resin (CAP) in vivo, J. Biomed. Mater. Res.: An Off. J. Soc. Biomater. 53 (2000) 678–684. The Japanese Society for Biomaterials, and The Australian Society for Biomaterials and the Korean Society for Biomaterials.
[3] D. Nunamaker, P. Blauner, in: C (Ed.), Textbook of Small Animal Orthopaedics, 1985.
[4] X. Liu, P.K. Chu, C. Ding, Surface modification of titanium, titanium alloys, and related materials for biomedical applications, Mater. Sci. Eng. R Rep. 47 (2004) 49–121.
[5] A. Kurella, N.B. Dahotre, Laser induced multi-scale textured zirconia coating on Ti-6Al-4V, J. Mater. Sci. Mater. Med. 17 (2006) 565–572.
[6] R. Narayanan, S. Seshadri, Phosphoric acid anodization of Ti–6Al–4V–Structural and corrosion aspects, Corrosion Sci. 49 (2007) 542–558.
[7] M. Niinomi, C.J. Boehlert, Titanium alloys for biomedical applications, advances in metallic biomaterials, Springer, 2015, pp. 179–213.
[8] H. Guleryuz, H. Cimenoglu, Surface modification of a Ti–6Al–4V alloy by thermal oxidation, Surf. Coating. Technol. 192 (2005) 164–170.
[9] W.C. Clem, S. Chowdhury, S.A. Catledge, J.J. Weimer, F.M. Shaikh, K. M. Hennessy, V.V. Konovalov, M.R. Hill, A. Waterfeld, S.L. Bellis, Mesenchymal stem cell interaction with ultra-smooth nanostructured diamond for wear-resistant orthopaedic implants, Biomaterials 29 (2008) 3461–3468.
[10] P. Fauchais, A. Vardelle, Thermal Sprayed Coatings Used against Corrosion and Corrosive Wear, Advanced Plasma Spray Applications, IntechOpen, 2012.
[11] K.C. Popat, M. Eltgroth, T.J. LaTempa, C.A. Grimes, T.A. Desai, Decreased Staphylococcus epidermis adhesion and increased osteoblast functionality on antibiotic-loaded titania nanotubes, Biomaterials 28 (2007) 4880–4888.
[12] M. Geetha, A.K. Singh, R. Asokamani, A.K. Gogia, Ti based biomaterials, the ultimate choice for orthopaedic implants–a review, Prog. Mater. Sci. 54 (2009) 397–425.
[13] D. Khang, J. Lu, C. Yao, K.M. Haberstroh, T.J. Webster, The role of nanometer and sub-micron surface features on vascular and bone cell adhesion on titanium, Biomaterials 29 (2008) 970–983.
[14] K. Das, A. Bandyopadhyay, S. Bose, Biocompatibility and in situ growth of TiO2 nanotubes on Ti using different electrolyte chemistry, J. Am. Ceram. Soc. 91 (2008) 2808–2814.
[15] K.C. Popat, L. Leoni, C.A. Grimes, T.A. Desai, Influence of engineered titania nanotubular surfaces on bone cells, Biomaterials 28 (2007) 3188–3197.
[16] A.P. Ross, T.J. Webster, Anodizing color coded anodized Ti6Al4V medical devices for increasing bone cell functions, Int. J. Nanomed. 8 (2013) 109.
[17] C. Yao, E.B. Slamovich, T.J. Webster, Enhanced osteoblast functions on anodized titanium with nanotube-like structures, J. Biomed. Mater. Res. Part A: Off. J. Soc. Biomater. 85 (2008) 157–166. The Japanese Society for Biomaterials, and The Australian Society for Biomaterials and the Korean Society for Biomaterials.
[18] C. Yao, V. Perla, J.L. McKenzie, E.B. Slamovich, T.J. Webster, Anodized Ti and Ti6Al4V possessing nanometer surface features enhances osteoblast adhesion, J. Biomed. Nanotechnol. 1 (2005) 68–73.

[19] G. Balasundaram, C. Yao, T.J. Webster, TiO2 nanotubes functionalized with regions of bone morphogenetic protein-2 increases osteoblast adhesion, J. Biomed. Mater. Res. 84 (2008) 447–453.
[20] B. Ercan, E. Taylor, E. Alpaslan, T.J. Webster, Diameter of titanium nanotubes influences anti-bacterial efficacy, Nanotechnology 22 (2011) 295102.
[21] W. Liu, P. Su, S. Chen, N. Wang, Y. Ma, Y. Liu, J. Wang, Z. Zhang, H. Li, T. J. Webster, Synthesis of TiO 2 nanotubes with ZnO nanoparticles to achieve antibacterial properties and stem cell compatibility, Nanoscale 6 (2014) 9050–9062.
[22] K.M. Kummer, E.N. Taylor, N.G. Durmas, K.M. Tarquinio, B. Ercan, T.J. Webster, Effects of different sterilization techniques and varying anodized TiO2 nanotube dimensions on bacteria growth, J. Biomed. Mater. Res. B Appl. Biomater. 101 (2013) 677–688.
[23] W. Liu, N.H. Golshan, X. Deng, D.J. Hickey, K. Zeimer, H. Li, T.J. Webster, Selenium nanoparticles incorporated into titania nanotubes inhibit bacterial growth and macrophage proliferation, Nanoscale 8 (2016) 15783–15794.
[24] W. Liu, P. Su, S. Chen, N. Wang, J. Wang, Y. Liu, Y. Ma, H. Li, Z. Zhang, T.J.J. N. Webster, Antibacterial and osteogenic stem cell differentiation properties of photoinduced TiO2 nanoparticle-decorated TiO2 nanotubes 10 (2015) 713–723.
[25] W. Liu, P. Su, A. Gonzales III, S. Chen, N. Wang, J. Wang, H. Li, Z. Zhang, T. J. Webster, Optimizing stem cell functions and antibacterial properties of TiO2 nanotubes incorporated with ZnO nanoparticles: experiments and modeling, Int. J. Nanomed. 10 (2015) 1997.
[26] T. Webster, C. Yao, Anodization: A Promising Nano Modification Technique of Titanium-Based Implants for Orthopedic Applications, Surgical Tools and Medical Devices, Springer, 2016, pp. 55–79.
[27] C. Yao, T.J. Webster, Anodization: a promising nano-modification technique of titanium implants for orthopedic applications, J. Nanosci. Nanotechnol. 6 (2006) 2682–2692.
[28] G.E. Aninwene, C.Y. II, T.J. Webster, Enhanced osteoblast adhesion to drug-coated anodized nanotubular titanium surfaces, Int. J. Nanomed. 3 (2008) 257.
[29] C. Yao, T.J. Webster, Prolonged antibiotic delivery from anodized nanotubular titanium using a co-precipitation drug loading method, J. Biomed. Mater. Res. Part B: Applied Biomaterials: An Official Journal of The Society for Biomaterials, The Japanese Society for Biomaterials, and The Australian Society for Biomaterials, and the Korean Society for Biomaterials 91 (2009) 587–595.
[30] B. Ercan, K.M. Kummer, K.M. Tarquinio, T.J.J.A.b. Webster, Decreased Staphylococcus aureus Biofilm Growth on Anodized Nanotubular Titanium and the Effect of Electrical Stimulation, 7, 2011, pp. 3003–3012.
[31] S. Sirivisoot, C. Yao, X. Xiao, B.W. Sheldon, T.J. Webster, Greater osteoblast functions on multiwalled carbon nanotubes grown from anodized nanotubular titanium for orthopedic applications, Nanotechnology 18 (2007) 365102.
[32] B. Ercan, T.J.J.B. Webster, The effect of biphasic electrical stimulation on osteoblast function at anodized, nanotubular titanium surfaces 31 (2010) 3684–3693.
[33] B. Ercan, T.J. Webster, Greater osteoblast proliferation on anodized nanotubular titanium upon electrical stimulation, Int. J. Nanomed. 3 (2008) 477.
[34] K. Burns, C. Yao, T.J. Webster, Increased chondrocyte adhesion on nanotubular anodized titanium, J. Biomed. Mater. Res. Part A: An Official Journal of The Society for Biomaterials, The Japanese Society for Biomaterials, and The Australian Society for Biomaterials, and the Korean Society for Biomaterials 88 (2009) 561–568.
[35] A. Rajyalakshmi, B. Ercan, K. Balasubramanian, T.J. Webster, Reduced adhesion of macrophages on anodized titanium with select nanotube surface features, Int. J. Nanomed. 6 (2011) 1765.
[36] K.M. Kummer, E. Taylor, T.J. Webster, Biological applications of anodized TiO2 nanostructures: a review from orthopedic to stent applications, Nanosci. Nanotechnol. Lett. 4 (2012) 483–493.
[37] E. Alpaslan, B. Ercan, T.J. Webster, Anodized 20 nm diameter nanotubular titanium for improved bladder stent applications, Int. J. Nanomed. 6 (2011) 219.
[38] G. Balasundaram, T.M. Shimpi, W.R. Sanow, D.M. Storey, B.S. Kitchell, T. J. Webster, Molecular plasma deposited peptides on anodized nanotubular titanium: an osteoblast density study, J. Biomed. Mater. Res. 98 (2011) 192–200.
[39] C. Yao, E.B. Slamovich, T.J. Webster, Titanium nanosurface modification by anodization for orthopedic applications, MRS Online Proceedings Library Archive, 2004, p. 845.
[40] K. Kummer, E. Taylor, T. Webster, Anodized Nanotubular TiO2 Structures Significantly Improve Titanium Implant Materials, Vitro, 2012.
[41] K. Das, S. Bose, A. Bandyopadhyay, TiO2 nanotubes on Ti: influence of nanoscale morphology on bone cell–materials interaction, J. Biomed. Mater. Res. Part A: An Official Journal of The Society for Biomaterials, The Japanese Society for Biomaterials, and The Australian Society for Biomaterials and the Korean Society for Biomaterials 90 (2009) 225–237.
[42] M. Mour, D. Das, T. Winkler, E. Hoenig, G. Mielke, M.M. Morlock, A.F. Schilling, Advances in porous biomaterials for dental and orthopaedic applications, Materials 3 (2010) 2947–2974.
[43] S. Bose, D. Banerjee, A. Shivaram, S. Tarafder, A. Bandyopadhyay, Calcium phosphate coated 3D printed porous titanium with nanoscale surface modification for orthopedic and dental applications, Mater. Des. 151 (2018) 102–112.
[44] A. Bandyopadhyay, A. Shivaram, S. Tarafder, H. Sahasrabudhe, D. Banerjee, S. Bose, In vivo response of laser processed porous titanium implants for load-bearing implants, Ann. Biomed. Eng. 45 (2017) 249–260.
[45] K.S. Brammer, S. Oh, J.O. Gallagher, S. Jin, Enhanced cellular mobility guided by TiO2 nanotube surfaces, Nano Lett. 8 (2008) 786–793.
[46] S.F. Lamolle, M. Monjo, M. Rubert, H.J. Haugen, S.P. Lyngstadaas, J.E. Ellingsen, The effect of hydrofluoric acid treatment of titanium surface on nanostructural and chemical changes and the growth of MC3T3-E1 cells, Biomaterials 30 (2009) 736–742.
[47] S. Oh, C. Daraio, L.H. Chen, T.R. Pisanic, R.R. Finones, S. Jin, Significantly accelerated osteoblast cell growth on aligned TiO2 nanotubes, J. Biomed. Mater. Res. Part A: An Official Journal of The Society for Biomaterials, The Japanese Society for Biomaterials, and The Australian Society for Biomaterials and the Korean Society for Biomaterials 78 (2006) 97–103.
[48] A. Gao, R. Hang, X. Huang, L. Zhao, X. Zhang, L. Wang, B. Tang, S. Ma, P.K. Chu, The effects of titania nanotubes with embedded silver oxide nanoparticles on bacteria and osteoblasts, Biomaterials 35 (2014) 4223–4235.
[49] L. Zhao, P.K. Chu, Y. Zhang, Z. Wu, Antibacterial coatings on titanium implants, J. Biomed. Mater. Res. B Appl. Biomater. 91 (2009) 470–480.
[50] K. Das, S. Bose, A. Bandyopadhyay, B. Karandikar, B.L. Gibbins, Influence of silver on antibacterial activities of surface modified Ti, J. Biomed. Mater. Res. B 87 (2008) 455–460.
[51] S. Mei, H. Wang, W. Wang, L. Tong, H. Pan, C. Ruan, Q. Ma, M. Liu, H. Yang, L. Zhang, Antibacterial effects and biocompatibility of titanium surfaces with graded silver incorporation in titania nanotubes, Biomaterials 35 (2014) 4255–4265.
[52] M. Hartman, Design and fabrication of a fixed implant-supported interim restoration from a dynamic navigation virtual plan, J. Prosthet. Dent (2020).
[53] K. Kumar, R. Gill, U. Batra, Challenges and opportunities for biodegradable magnesium alloy implants, Mater. Technol. 33 (2018) 153–172.
[54] F.A. Cotton, G. Wilkinson, C.A. Murillo, M. Bochmann, R. Grimes, Advanced Inorganic Chemistry, Wiley, New, 1988.
[55] H. Ogihara, M. Sadakane, W. Ueda, Synthesis and Applications of Mixed Oxide Nanotubes, Inorganic and Metallic Nanotubular Materials, Springer, 2010, pp. 147–158.
[56] T. Kijima, Inorganic and Metallic Nanotubular Materials: Recent Technologies and Applications, Springer Berlin Heidelberg, 2010.
[57] M. Khosravi, H. Feizi, B. Haghighi, S.I. Allakhverdiev, M.M. Najafpour, Photoelectrochemistry of manganese oxide/mixed phase titanium oxide heterojunction, New J. Chem. 44 (2020) 3514–3523.
[58] S. Palit, Recent Advances in the Application of Nanotechnology in Food Industry and the Vast Vision for the Future, Nanoengineering in the Beverage Industry, Elsevier, 2020, pp. 1–34.
[59] J. Huang, J. Liu, J. Wang, Optical properties of biomass-derived nanomaterials for sensing, catalytic, biomedical and environmental applications, Trac. Trends Anal. Chem. (2020), 115800.
[60] L. Filipponi, D. Sutherland, I.N. Center, Introduction to nanoscience and nanotechnologies, NANOYOU Teachers Training Kit in Nanoscience and Nanotechnologies (2010) 1–29.
[61] A. Ghicov, S. Aldabergenova, H. Tsuchyia, P. Schmuki, TiO2–Nb2O5 nanotubes with electrochemically tunable morphologies, Angew. Chem. Int. Ed. 45 (2006) 6993–6996.
[62] L.-N. Wang, M. Jin, Y. Zheng, Y. Guan, X. Lu, J.-L. Luo, Nanotubular surface modification of metallic implants via electrochemical anodization technique, Int. J. Nanomed. 9 (2014) 4421.
[63] K. Rezwan, Q. Chen, J. Blaker, A.R. Boccaccini, Biodegradable and bioactive porous polymer/inorganic composite scaffolds for bone tissue engineering, Biomaterials 27 (2006) 3413–3431.
[64] R.Z. LeGeros, Calcium phosphate-based osteoinductive materials, Chem. Rev. 108 (2008) 4742–4753.
[65] S. Minagar, J. Wang, C.C. Berndt, E.P. Ivanova, C. Wen, Cell response of anodized nanotubes on titanium and titanium alloys, J. Biomed. Mater. Res. 101 (2013) 2726–2739.
[66] K. Lee, H.-C. Choe, B.-H. Kim, Y.-M. Ko, The biocompatibility of HA thin films deposition on anodized titanium alloys, Surf. Coating. Technol. 205 (2010) S267–S270.
[67] M. Kulkarni, A. Mazare, P. Schmuki, A. Iglič, Biomaterial surface modification of titanium and titanium alloys for medical applications, Nanomedicine 111 (2014) 111.
[68] Z.U. Rahman, W. Haider, L. Pompa, K. Deen, Electrochemical & osteoblast adhesion study of engineered TiO2 nanotubular surfaces on titanium alloys, Mater. Sci. Eng. C 58 (2016) 160–168.
[69] M. İzmir, B. Ercan, Anodization of titanium alloys for orthopedic applications, Front. Chem. Sci. Eng. 13 (2019) 28–45.
[70] L. Mohan, C. Dennis, N. Padmapriya, C. Anandan, N. Rajendran, Effect of electrolyte temperature and anodization time on formation of TiO2 nanotubes for biomedical applications, Materials Today Communications (2020) 101103.
[71] S. Minagar, C.C. Berndt, J. Wang, E. Ivanova, C. Wen, A review of the application of anodization for the fabrication of nanotubes on metal implant surfaces, Acta Biomater. 8 (2012) 2875–2888.
[72] Lu-Ning Wang, M. Jin, Y. Zheng, Y. Guan, X. Lu, J.-L. Luo, Nanotubular surface modification of metallic implants via electrochemical anodization technique, Int. J. Nanomed. 9 (2014) 4421.
[73] H. Masuda, K. Fukuda, Ordered metal nanohole arrays made by a two-step replication of honeycomb structures of anodic alumina, Science 268 (1995) 1466–1468.
[74] M. Sarraf, A. Dabbagh, B.A. Razak, B. Nasiri-Tabrizi, H.R.M. Hosseini, S. Saber-Samandari, N.H.A. Kasim, L.K. Yean, N.L. Sukiman, Silver oxide nanoparticles-decorated tantala nanotubes for enhanced antibacterial activity and osseointegration of Ti6Al4V, Mater. Des. 154 (2018) 28–40.

[75] K. Yasuda, P. Schmuki, Electrochemical formation of self-organized zirconium titanate nanotube multilayers, Electrochem. Commun. 9 (2007) 615–619.
[76] Q. Lu, T. Hashimoto, P. Skeldon, G. Thompson, H. Habazaki, K. Shimizu, Nanoporous anodic niobium oxide formed in phosphate/glycerol electrolyte, Electrochem. Solid State Lett. 8 (2005) B17–B20.
[77] I. Sieber, H. Hildebrand, A. Friedrich, P. Schmuki, Formation of self-organized niobium porous oxide on niobium, Electrochem. Commun. 7 (2005) 97–100.
[78] J. Choi, J.H. Lim, S.C. Lee, J.H. Chang, K.J. Kim, M.A. Cho, Porous niobium oxide films prepared by anodization in HF/H3PO4, Electrochim. Acta 51 (2006) 5502–5507.
[79] S.P. Albu, A. Ghicov, P. Schmuki, High aspect ratio, self-ordered iron oxide nanopores formed by anodization of Fe in ethylene glycol/NH4F electrolytes, Phys. Status Solidi Rapid Res. Lett. 3 (2009) 64–66.
[80] T. Burleigh, P. Schmuki, S. Virtanen, Properties of the nanoporous anodic oxide electrochemically grown on steel in hot 50% NaOH, J. Electrochem. Soc. 156 (2009) C45–C53.
[81] K. Indira, U.K. Mudali, T. Nishimura, N. Rajendran, A review on TiO2 nanotubes: influence of anodization parameters, formation mechanism, properties, corrosion behavior, and biomedical applications, Journal of Bio- and Tribo-Corrosion 1 (2015) 28.
[82] Y. Fu, A. Mo, A review on the electrochemically self-organized titania nanotube Arrays: synthesis, modifications, and biomedical applications, Nanoscale Research Letters 13 (2018) 187.
[83] A. Matsuda, S. Sreekantan, W. Krengvirat, Well-aligned TiO2 nanotube arrays for energy-related applications under solar irradiation, Journal of Asian Ceramic Societies 1 (2013) 203–219.
[84] A. El Ruby Mohamed, S. Rohani, Modified TiO2 nanotube arrays (TNTAs): progressive strategies towards visible light responsive photoanode, a review, Energy Environ. Sci. 4 (2011) 1065–1086.
[85] G.D. Sulka, Nanostructured Anodic Metal Oxides: Synthesis and Applications, Elsevier Science, 2020.
[86] J.-Y. Huang, K.-Q. Zhang, Y.-K. Lai, Fabrication, modification, and emerging applications of TiO2 nanotube arrays by electrochemical synthesis: a review, Int. J. Photoenergy (2013) 2013.
[87] Q. Cai, M. Paulose, O.K. Varghese, C.A. Grimes, The effect of electrolyte composition on the fabrication of self-organized titanium oxide nanotube arrays by anodic oxidation, J. Mater. Res. 20 (2005) 230–236.
[88] M. Paulose, K. Shankar, S. Yoriya, H.E. Prakasam, O.K. Varghese, G.K. Mor, T. A. Latempa, A. Fitzgerald, C.A. Grimes, Anodic growth of highly ordered TiO2 nanotube arrays to 134 μm in length, J. Phys. Chem. B 110 (2006) 16179–16184.
[89] H.E. Prakasam, K. Shankar, M. Paulose, O.K. Varghese, C.A. Grimes, A new benchmark for TiO2 nanotube array growth by anodization, J. Phys. Chem. C 111 (2007) 7235–7241.
[90] K. Shankar, G.K. Mor, A. Fitzgerald, C.A. Grimes, Cation effect on the electrochemical formation of very high aspect ratio TiO2 nanotube arrays in formamide− water mixtures, J. Phys. Chem. C 111 (2007) 21–26.
[91] K. Shankar, G.K. Mor, H.E. Prakasam, S. Yoriya, M. Paulose, O.K. Varghese, C. A. Grimes, Highly-ordered TiO2 nanotube arrays up to 220 μm in length: use in water photoelectrolysis and dye-sensitized solar cells, Nanotechnology 18 (2007), 065707.
[92] S. Yoriya, M. Paulose, O.K. Varghese, G.K. Mor, C.A. Grimes, Fabrication of vertically oriented TiO2 nanotube arrays using dimethyl sulfoxide electrolytes, J. Phys. Chem. C 111 (2007) 13770–13776.
[93] N.K. Allam, C.A. Grimes, Formation of vertically oriented TiO2 nanotube arrays using a fluoride free HCl aqueous electrolyte, J. Phys. Chem. C 111 (2007) 13028–13032.
[94] L. Wang, Surface Modification of Zirconium Implants via Electrochemical Anodization and Wet Chemical Techniques, 2011.
[95] H. Tsuchiya, J.M. Macak, L. Taveira, P. Schmuki, Fabrication and characterization of smooth high aspect ratio zirconia nanotubes, Chem. Phys. Lett. 410 (2005) 188–191.
[96] S. Berger, J. Faltenbacher, S. Bauer, P. Schmuki, Enhanced self-ordering of anodic ZrO2 nanotubes in inorganic and organic electrolytes using two-step anodization, Phys. Status Solidi Rapid Res. Lett. 2 (2008) 102–104.
[97] Y. Shin, S. Lee, A freestanding membrane of highly ordered anodic ZrO2 nanotube arrays, Nanotechnology 20 (2009) 105301.
[98] W.-J. Lee, W.H. Smyrl, Zirconium oxide nanotubes synthesized via direct electrochemical anodization, Electrochem. Solid State Lett. 8 (2005) B7–B9.
[99] H. Tsuchiya, P. Schmuki, Self-organized high aspect ratio porous hafnium oxide prepared by electrochemical anodization, Electrochem. Commun. 7 (2005) 49–52.
[100] N.K. Allam, X.J. Feng, C.A. Grimes, Self-assembled fabrication of vertically oriented Ta2O5 nanotube arrays, and membranes thereof, by one-step tantalum anodization, Chem. Mater. 20 (2008) 6477–6481.
[101] H.A. El-Sayed, V.I. Birss, Controlled interconversion of nanoarray of Ta dimples and high aspect ratio Ta oxide nanotubes, Nano Lett. 9 (2009) 1350–1355.
[102] I. Sieber, B. Kannan, P. Schmuki, Self-assembled porous tantalum oxide prepared in H 2 SO 4/HF electrolytes, Electrochem. Solid State Lett. 8 (2005) J10–J12.
[103] I. Sieber, H. Hildebrand, A. Friedrich, P. Schmuki, Initiation of tantalum oxide pores grown on tantalum by potentiodynamic anodic oxidation, J. Electroceram. 16 (2006) 35–39.
[104] C. Arnould, J. Delhalle, Z. Mekhalif, Electrodeposition from ionic liquid of 2D ordered Ta2O5 on titanium substrate through a polystyrene template, J. Electrochem. Soc. 156 (2009) K186–K190.
[105] Q. Lu, S. Mato, P. Skeldon, G.E. Thompson, D. Masheder, H. Habazaki, K. Shimizu, Anodic film growth on tantalum in dilute phosphoric acid solution at 20 and 85°C, Electrochim. Acta 47 (2002) 2761–2767.
[106] I.V. Sieber, P. Schmuki, Porous tantalum oxide prepared by electrochemical anodic oxidation, J. Electrochem. Soc. 152 (2005) C639–C644.
[107] W. Wei, J.M. Macak, N.K. Shrestha, P. Schmuki, Thick self-ordered nanoporous Ta2O5 films with long-range lateral order, J. Electrochem. Soc. 156 (2009) K104–K109.
[108] W. Wei, J.M. Macak, P. Schmuki, High aspect ratio ordered nanoporous Ta2O5 films by anodization of Ta, Electrochem. Commun. 10 (2008) 428–432.
[109] C.W. Lai, S.B. Abd Hamid, S. Sreekantan, A novel solar driven photocatalyst: well-aligned anodic WO_3 nanotubes, Int. J. Photoenergy 2013 (2013) 745301.
[110] W. Wei, K. Lee, S. Shaw, P. Schmuki, Anodic formation of high aspect ratio, self-ordered Nb 2 O 5 nanotubes, Chem. Commun. 48 (2012) 4244–4246.
[111] P. Roy, S. Berger, P. Schmuki, TiO2 nanotubes: synthesis and applications, Angew. Chem. Int. Ed. 50 (2011) 2904–2939.
[112] H. Tsuchiya, J. Nakata, S. Fujimoto, S. Berger, P. Schmuki, Anodic porous and tubular oxide layers on Ti alloys, ECS Transactions 16 (2008) 359.
[113] S. Sado, T. Ueda, K. Ueda, T. Narushima, Formation of TiO2 layers on commercially pure Ti and Ti–Mo and Ti–Nb alloys by two-step thermal oxidation and their photocatalytic activity, Appl. Surf. Sci. 357 (2015) 2198–2205.
[114] N.T.C. Oliveira, J.F. Verdério, C. Bolfarini, Obtaining self-organized nanotubes on biomedical Ti–Mo alloys, Electrochem. Commun. 35 (2013) 139–141.
[115] S. Sado, T. Ueda, Y. Tokuda, N. Sato, K. Ueda, T. Narushima, formation of photocatalytically active TiO2 layers on Ti–Nb alloys by two-step thermal oxidation, Mater. Trans. 60 (2019) 1814–1820.
[116] H. Jha, R. Hahn, P. Schmuki, Ultrafast oxide nanotube formation on TiNb, TiZr and TiTa alloys by rapid breakdown anodization, Electrochim. Acta 55 (2010) 8883–8887.
[117] A.R. Luz, C.M. Lepienski, S.L. Henke, C.R. Grandini, N.K. Kuromoto, Effect of microstructure on the nanotube growth by anodic oxidation on Ti-10Nb alloy, Mater. Res. Express 4 (2017), 076408.
[118] H. Tsuchiya, T. Akaki, J. Nakata, D. Terada, N. Tsuji, Y. Koizumi, Y. Minamino, P. Schmuki, S. Fujimoto, Anodic oxide nanotube layers on Ti–Ta alloys: substrate composition, microstructure and self-organization on two-size scales, Corrosion Sci. 51 (2009) 1528–1533.
[119] K. Lee, H.-C. Choe, Y.-M. Ko, W. Brentley, Nanotubular structure formation on Ti–6Al–4V and Ti–Ta alloy surfaces by electrochemical methods, Korean J. Met. Mater 50 (2012) 164–170.
[120] K. Yasuda, P. Schmuki, formation of self-organized zirconium titanate nanotube layers by alloy anodization, Adv. Mater. 19 (2007) 1757–1760.
[121] H. Tsuchiya, T. Akaki, J. Nakata, D. Terada, N. Tsuji, Y. Koizumi, Y. Minamino, P. Schmuki, S. Fujimoto, Metallurgical aspects on the formation of self-organized anodic oxide nanotube layers, Electrochim. Acta 54 (2009) 5155–5162.
[122] K. Yasuda, P. Schmuki, Control of morphology and composition of self-organized zirconium titanate nanotubes formed in (NH4)2SO4/NH4F electrolytes, Electrochim. Acta 52 (2007) 4053–4061.
[123] S.K. Mohapatra, K.S. Raja, M. Misra, V.K. Mahajan, M. Ahmadian, Synthesis of self-organized mixed oxide nanotubes by sonoelectrochemical anodization of Ti–8Mn alloy, Electrochim. Acta 53 (2007) 590–597.
[124] A.R. Rafieerad, A.R. Bushroa, B. Nasiri-Tabrizi, S. Baradaran, A. Amiri, S. Saber-Samandari, S. Khanahmadi, E. Zeimaran, W.J. Basirun, K. Kalaiselvam, K. M. Vellasamy, J. Vadivelu, Simultaneous enhanced antibacterial and osteoblast cytocompatibility performance of Ti6Al7Nb implant by nano-silver/graphene oxide decorated mixed oxide nanotube composite, Surf. Coating. Technol. 360 (2019) 181–195.
[125] A.R. Rafieerad, A.R. Bushroa, A. Amiri, V. Gopinath, M. Sookhakian, S. Baradaran, M. Rafieerad, S. Saber-Samandari, J. Vadivelu, Large-scale hybrid silver nanowall-reduced graphene oxide biofilm: a novel morphology by facile electrochemical deposition, Surf. Coating. Technol. 347 (2018) 297–303.
[126] A.R. Rafieerad, A.R. Bushroa, S.M. Banihashemian, A. Amiri, Not-yet-designed multilayer Nb/HA/MWCNT-Au/Se/AuNPs and NbO2/HA/GO/Se biocomposites coated Ti6Al7Nb implant, Materials Today Communications 15 (2018) 294–308.
[127] A.R. Rafieerad, A.R. Bushroa, B. Nasiri-Tabrizi, R. Crum, C. Gámez, J. Vadivelu, V. Gupta, Vertically oriented ZrO2TiO2Nb2O5Al2O3 mixed nanopatterned bioceramics on Ti6Al7Nb implant assessed by laser spallation technique, J. Alloys Compd. 721 (2017) 456–475.
[128] A.R. Rafieerad, A.R. Bushroa, B. Nasiri-Tabrizi, J. Vadivelu, F. Yusof, S. Baradaran, Graphene oxide modified anodic ternary nanobioceramics on Ti6Al7Nb alloy for orthopedic and dental applications, Procedia Engineering 184 (2017) 409–417.
[129] A.R. Rafieerad, A.R. Bushroa, B. Nasiri-Tabrizi, S.H.A. Kaboli, S. Khanahmadi, A. Amiri, J. Vadivelu, F. Yusof, W.J. Basirun, K. Wasa, Toward improved mechanical, tribological, corrosion and in-vitro bioactivity properties of mixed oxide nanotubes on Ti–6Al–7Nb implant using multi-objective PSO, Journal of the Mechanical Behavior of Biomedical Materials 69 (2017) 1–18.
[130] A.R. Rafieerad, A.R. Bushroa, E. Zalnezhad, M. Sarraf, W.J. Basirun, S. Baradaran, B. Nasiri-Tabrizi, Microstructural development and corrosion behavior of self-organized TiO2 nanotubes coated on Ti–6Al–7Nb, Ceram. Int. 41 (2015) 10844–10855.
[131] A.R. Rafieerad, E. Zalnezhad, A.R. Bushroa, A.M.S. Hamouda, M. Sarraf, B. Nasiri-Tabrizi, Self-organized TiO2 nanotube layer on Ti–6Al–7Nb for biomedical application, Surf. Coating. Technol. 265 (2015) 24–31.
[132] J.M. Macak, H. Tsuchiya, L. Taveira, A. Ghicov, P. Schmuki, Self-organized nanotubular oxide layers on Ti-6Al-7Nb and Ti-6Al-4V formed by anodization in NH4F solutions, J. Biomed. Mater. Res. Part A: An Official Journal of The Society

for Biomaterials, The Japanese Society for Biomaterials, and The Australian Society for Biomaterials and the Korean Society for Biomaterials 75 (2005) 928–933.
[133] M. Sarraf, E. Zalnezhad, A.R. Bushroa, A.M.S. Hamouda, A.R. Rafieerad, B. Nasiri-Tabrizi, Effect of microstructural evolution on wettability and tribological behavior of TiO2 nanotubular arrays coated on Ti–6Al–4V, Ceram. Int. 41 (2015) 7952–7962.
[134] M. Sarraf, A. Dabbagh, B. Abdul Razak, B. Nasiri-Tabrizi, H.R.M. Hosseini, S. Saber-Samandari, N.H. Abu Kasim, L.K. Yean, N.L. Sukiman, Silver oxide nanoparticles-decorated tantala nanotubes for enhanced antibacterial activity and osseointegration of Ti6Al4V, Mater. Des. 154 (2018) 28–40.
[135] M. Sarraf, A. Dabbagh, B. Abdul Razak, R. Mahmoodian, B. Nasiri-Tabrizi, H.R. M. Hosseini, S. Saber-Samandari, N.H. Abu Kasim, H. Abdullah, N.L. Sukiman, Highly-ordered TiO2 nanotubes decorated with Ag2O nanoparticles for improved biofunctionality of Ti6Al4V, Surf. Coating. Technol. 349 (2018) 1008–1017.
[136] M. Sarraf, B.A. Razak, B. Nasiri-Tabrizi, A. Dabbagh, N.H.A. Kasim, W.J. Basirun, E. Bin Sulaiman, Nanomechanical properties, wear resistance and in-vitro characterization of Ta2O5 nanotubes coating on biomedical grade Ti–6Al–4V, Journal of the Mechanical Behavior of Biomedical Materials 66 (2017) 159–171.
[137] A. Hamlekhan, A. Butt, S. Patel, D. Royhman, C. Takoudis, C. Sukotjo, J. Yuan, G. Jursich, M.T. Mathew, W. Hendrickson, Fabrication of anti-aging TiO2 nanotubes on biomedical Ti alloys, PloS One 9 (2014).
[138] H.-J. Kim, Y.-H. Jeong, H.-C. Choe, Nanotube nucleation phenomena of titanium dioxide on the Ti–6Al–4V alloy using anodic titanium oxide technique, J. Nanosci. Nanotechnol. 15 (2015) 467–470.
[139] M. Sarraf, A.B. Razak, R. Crum, C. Gámez, B. Ramirez, N.H.B.A. Kasim, B. Nasiri-Tabrizi, V. Gupta, N.L. Sukiman, W.J. Basirun, Adhesion measurement of highly-ordered TiO2 nanotubes on Ti-6Al-4V alloy, Processing and Application of Ceramics 11 (2017) 311–321.
[140] I.M. Ulfah, B.M. Bachtiar, A.R. Murnandityas, Slamet, Synthesis and characterization of Ag-doped TiO2 nanotubes on Ti-6Al-4V and Ti-6Al-7Nb alloy, in: AIP Conference Proceedings, AIP Publishing LLC, 2018, 020008.
[141] M. Losertová, O. Štefek, M. Galajda, K. Konečná, G.S. Martynková, K.Č. Barabaszová, Microstructure and electrochemical behavior of TiO2 nanotubes coated on titanium-based substrate before and after thermal treatment, J. Nanosci. Nanotechnol. 19 (2019) 2989–2996.
[142] S.-J. Kim, J.-M. Park, T.-S. Bae, E.-J. Park, Precalcification treatment of TiO2 nanotube on Ti-6Al-4V alloy, J Korean Acad Prosthodont 47 (2009) 39–45.
[143] S. Bai, D. Ding, C. Ning, R. Qin, L. Huang, M. Li, D. Mao, Anodic growth of uniform nanotube arrays on biphase Ti35Nb5Zr alloy, Electrochem. Commun. 12 (2010) 152–155.
[144] X.J. Feng, J.M. Macak, S.P. Albu, P. Schmuki, Electrochemical formation of self-organized anodic nanotube coating on Ti–28Zr–8Nb biomedical alloy surface, Acta Biomater. 4 (2008) 318–323.
[145] H. Tsuchiya, J. Macak, A. Ghicov, P. Schmuki, Anodic oxide nanotubes on Ti alloys, ECS Transactions 3 (2007) 365.
[146] H. Tsuchiya, J.M. Macak, A. Ghicov, P. Schmuki, Self-organization of anodic nanotubes on two size scales, Small 2 (2006) 888–891.
[147] H. Tsuchiya, J.M. Macak, A. Ghicov, Y.C. Tang, S. Fujimoto, M. Niinomi, T. Noda, P. Schmuki, Nanotube oxide coating on Ti–29Nb–13Ta–4.6Zr alloy prepared by self-organizing anodization, Electrochim. Acta 52 (2006) 94–101.
[148] S. Ono, N. Masuko, Evaluation of pore diameter of anodic porous films formed on aluminum, Surf. Coating. Technol. 169 (2003) 139–142.
[149] S. Bauer, S. Kleber, P. Schmuki, TiO2 nanotubes: tailoring the geometry in H3PO4/HF electrolytes, Electrochem. Commun. 8 (2006) 1321–1325.
[150] S. Berger, H. Tsuchiya, P. Schmuki, Transition from nanopores to nanotubes: self-ordered anodic oxide structures on Titanium−Aluminides, Chem. Mater. 20 (2008) 3245–3247.
[151] H. Tsuchiya, S. Berger, J.M. Macak, A. Ghicov, P. Schmuki, Self-organized porous and tubular oxide layers on TiAl alloys, Electrochem. Commun. 9 (2007) 2397–2402.
[152] H. Tsuchiya, S. Berger, J.M. Macak, A.G. Munoz, P. Schmuki, A new route for the formation of self-organized anodic porous alumina in neutral electrolytes, Electrochem. Commun. 9 (2007) 545–550.
[153] S. Kumar, T.S.N.S. Narayanan, Corrosion behaviour of Ti–15Mo alloy for dental implant applications, J. Dent. 36 (2008) 500–507.
[154] H. Wen, C. Zeng, A. Hemmasian Ettefagh, J. Gao, S. Guo, Laser surface treatment of Ti-10Mo alloy under Ar and N2 environment for biomedical application, J. Laser Appl. 31 (2019), 022012.
[155] F. Guastaldi, A. Martini, E. Rocha, E. Hochuli-Vieira, A. Guastaldi, Ti–15Mo alloy decreases the stress concentration in mandibular angle fracture internal fixation hardware, Journal of Maxillofacial and Oral Surgery (2019) 1–7.
[156] N.K. Shrestha, Y.-C. Nah, H. Tsuchiya, P. Schmuki, Self-organized nano-tubes of TiO2–MoO3 with enhanced electrochromic properties, Chem. Commun. (2009) 2008–2010.
[157] P. Agarwal, I. Paramasivam, N.K. Shrestha, P. Schmuki, MoO3 in self-organized TiO2 nanotubes for enhanced photocatalytic activity, Chemistry–An Asian Journal 5 (2010) 66–69.
[158] Y. Ji, K.-C. Lin, H. Zheng, J.-j. Zhu, A.C.S. Samia, Fabrication of double-walled TiO2 nanotubes with bamboo morphology via one-step alternating voltage anodization, Electrochem. Commun. 13 (2011) 1013–1015.
[159] N.T. Oliveira, G. Aleixo, R. Caram, A.C. Guastaldi, Development of Ti–Mo alloys for biomedical applications: microstructure and electrochemical characterization, Mater. Sci. Eng., A 452 (2007) 727–731.
[160] J. Hieda, M. Niinomi, M. Nakai, K. Cho, Mechanical properties of biomedical ß-type titanium alloy with rare-earth metal oxide particles formed by rare-earth metal addition. TMS 2014: 143rd Annual Meeting & Exhibition, Springer, 2014, pp. 129–135.
[161] G.L.G.S.B. Srinivas Kumar, S. Chinara, S. Das, C. Tiwari, Prakash, G.V.S.N. Rao, Studies on Ti-29Nb-13Ta-4.6Zr alloy for use as a prospective biomaterial, Mater. Today: Proceedings 15 (2019) 11–20.
[162] A.R. Luz, L.S. Santos, C.M. Lepienski, P.B. Kuroda, N.K. Kuromoto, Characterization of the morphology, structure and wettability of phase dependent lamellar and nanotube oxides on anodized Ti-10Nb alloy, Appl. Surf. Sci. 448 (2018) 30–40.
[163] J. Yan, G. Wu, N. Guan, L. Li, Nb2O5/TiO2 heterojunctions: synthesis strategy and photocatalytic activity, Appl. Catal. B Environ. 152 (2014) 280–288.
[164] Y. Furubayashi, T. Hitosugi, Y. Yamamoto, K. Inaba, G. Kinoda, Y. Hirose, T. Shimada, T. Hasegawa, A transparent metal: Nb-doped anatase Ti O 2, Appl. Phys. Lett. 86 (2005) 252101.
[165] N. Eliaz, Corrosion of metallic biomaterials: a review, Materials 12 (2019) 407.
[166] A.R. Rafieerad, A.R. Bushroa, B. Nasiri-Tabrizi, J. Vadivelu, S. Baradaran, E. Zalnezhad, A. Amiri, Optimized fabrication and characterization of TiO2–Nb2O5–Al2O3 mixed oxide nanotube arrays on Ti–6Al–7Nb, RSC Adv. 6 (2016) 10527–10540.
[167] J.M. Macak, H. Tsuchiya, P. Schmuki, High-aspect-ratio TiO2 nanotubes by anodization of titanium, Angew. Chem. Int. Ed. 44 (2005) 2100–2102.
[168] P. Bhattacharya, S. Neogi, Techniques for deposition of coatings with enhanced adhesion to bio-implants, adhesion in pharmaceutical, Biomedical and Dental Fields (2017) 235–255.
[169] S.-H. Jang, H.-C. Choe, Y.-M. Ko, W.A. Brantley, Electrochemical characteristics of nanotubes formed on Ti–Nb alloys, Thin Solid Films 517 (2009) 5038–5043.
[170] H. Tsuchiya, J.M. Macak, A. Ghicov, Y.C. Tang, S. Fujimoto, M. Niinomi, T. Noda, P. Schmuki, Nanotube oxide coating on Ti–29Nb–13Ta–4.6 Zr alloy prepared by self-organizing anodization, Electrochim. Acta 52 (2006) 94–101.
[171] W.-G. Kim, H.-C. Choe, Nanostructure and corrosion behaviors of nanotube formed Ti-Zr alloy, Trans. Nonferrous Metals Soc. China 19 (2009) 1005–1008.
[172] H. Ikawa, T. Yamada, K. Kojima, S. Matsumoto, X-ray photoelectron spectroscopy study of high-and low-temperature forms of zirconium titanate, J. Am. Ceram. Soc. 74 (1991) 1459–1462.
[173] C. Wagner, A. Naumkin, A. Kraut-Vass, J. Allison, C. Powell, J. Rumble Jr., NIST X-Ray Photoelectron Spectroscopy Database, NIST Standard Reference Database 20, Version 3.4 (Web Version), U. S. Department of Commerce., 2003.
[174] R. Beranek, H. Hildebrand, P. Schmuki, Self-organized porous titanium oxide prepared in H 2 SO 4/HF electrolytes, Electrochem. Solid State Lett. 6 (2003) B12.
[175] N. Hu, Y. Wu, L. Xie, S.M. Yusuf, N. Gao, M.J. Starink, L. Tong, P.K. Chu, H. Wang, Enhanced interfacial adhesion and osseointegration of anodic TiO2 nanotube arrays on ultra-fine-grained titanium and underlying mechanisms, Acta Biomater. 106 (2020) 360–375.
[176] M.C. Alves-Rezende, L.C. Capalbo, J.P.D.O. Limírio, B.C. Capalbo, P.H. Limírio, J. L. Rosa, The role of TiO2 nanotube surface on osseointegration of titanium implants: Biomechanical and histological study in rats, Microsc. Res. Tech. (2020).
[177] H. Tsuchiya, P. Schmuki, Thick self-organized porous zirconium oxide formed in H2SO4/NH4F electrolytes, Electrochem. Commun. 6 (2004) 1131–1134.
[178] H. Tsuchiya, J.M. Macak, L. Taveira, P. Schmuki, Fabrication and characterization of smooth high aspect ratio zirconia nanotubes, Chem. Phys. Lett. 410 (2005) 188–191.
[179] H. Habazaki, M. Uozumi, H. Konno, K. Shimizu, S. Nagata, K. Asami, K. Matsumoto, K. Takayama, Y. Oda, P. Skeldon, Influences of structure and composition on growth of anodic oxide films on Ti-Zr alloys, Electrochim. Acta 48 (2003) 3257–3266.
[180] M. Misra, K.S. Raja, K. Zhong, V.K. Mahajan, Self-ordered Nanotubes of Titanium Oxides and Titanium Alloy Oxides for Energy Storage and Battery Applications, Google Patents, 2010.
[181] M.M. Najafpour, I. Zaharieva, Z. Zand, S.M. Hosseini, M. Kouzmanova, M. Hołyńska, I. Tranca, A.W. Larkum, J.-R. Shen, S.I. Allakhverdiev, Water-oxidizing complex in Photosystem II: its structure and relation to manganese-oxide based catalysts, Coord. Chem. Rev. 409 (2020) 213183.
[182] K.S. Raja, M. Misra, Ordered Arrays of Ti-Mn Oxide Nanotubes for High Capacity Li-Ion Battery, ECS, 2011.
[183] P.F. Santos, M. Niinomi, K. Cho, M. Nakai, H. Liu, N. Ohtsu, M. Hirano, M. Ikeda, T. Narushima, Microstructures, mechanical properties and cytotoxicity of low cost beta Ti–Mn alloys for biomedical applications, Acta Biomater. 26 (2015) 366–376.
[184] J.-W. Park, Y.-J. Kim, J.-H. Jang, Surface characteristics and in vitro biocompatibility of a manganese-containing titanium oxide surface, Appl. Surf. Sci. 258 (2011) 977–985.
[185] X. Ning, X. Wang, X. Yu, J. Zhao, M. Wang, H. Li, Y. Yang, Outstanding supercapacitive properties of Mn-doped TiO2 micro/nanostructure porous film prepared by anodization method, Sci. Rep. 6 (2016) 22634.
[186] X. Ning, X. Wang, X. Yu, J. Li, J. Zhao, Preparation and capacitance properties of Mn-doped TiO2 nanotube arrays by anodisation of Ti–Mn alloy, J. Alloys Compd. 658 (2016) 177–182.
[187] M.C. Nevárez-Martínez, M.P. Kobylański, P. Mazierski, J. Wółkiewicz, G. Trykowski, A. Malankowska, M. Kozak, P.J. Espinoza-Montero, A. Zaleska-Medynska, Self-organized TiO2–MnO2 nanotube arrays for efficient photocatalytic degradation of toluene, Molecules 22 (2017) 564.
[188] B. Sarkar, Biological Aspects of Metals and Metal-Related Diseases, Raven Press, 1983.
[189] M. Niinomi, Recent metallic materials for biomedical applications, Metall. Mater. Trans. 33 (2002) 477.

[190] Y.-H. Jeong, H.-C. Choe, W.A. Brantley, Corrosion characteristics of anodized Ti–(10–40wt%)Hf alloys for metallic biomaterials use, J. Mater. Sci. Mater. Med. 22 (2011) 41–50.
[191] Z. Cai, M. Koike, H. Sato, M. Brezner, Q. Guo, M. Komatsu, O. Okuno, T. Okabe, Electrochemical characterization of cast Ti–Hf binary alloys, Acta Biomater. 1 (2005) 353–356.
[192] Y.-H. Jeong, K. Lee, H.-C. Choe, Y.-M. Ko, W.A. Brantley, Nanotube formation and morphology change of Ti alloys containing Hf for dental materials use, Thin Solid Films 517 (2009) 5365–5369.
[193] Y.-H. Jeong, W.-G. Kim, G.-H. Park, H.-C. Choe, Y.-M. Ko, Surface characteristics of HA coated Ti-Hf binary alloys after nanotube formation, Trans. Nonferrous Metals Soc. China 19 (2009) 852–856.
[194] Y. Fan, N. Zhang, L. Zhang, H. Shao, J. Wang, J. Zhang, C. Cao, Co3O4-coated TiO2 nanotube composites synthesized through photo-deposition strategy with enhanced performance for lithium-ion batteries, Electrochim. Acta 94 (2013) 285–293.
[195] C. Yu, Y. Wang, H. Zheng, J. Zhang, W. Yang, X. Shu, Y. Qin, J. Cui, Y. Zhang, Y. Wu, Supercapacitive performance of homogeneous Co 3 O 4/TiO 2 nanotube arrays enhanced by carbon layer and oxygen vacancies, J. Solid State Electrochem. 21 (2017) 1069–1078.
[196] Y. Yang, L.C. Kao, Y. Liu, K. Sun, H. Yu, J. Guo, S.Y.H. Liou, M.R. Hoffmann, Cobalt-doped black TiO2 nanotube array as a stable anode for oxygen evolution and electrochemical wastewater treatment, ACS Catal. 8 (2018) 4278–4287.
[197] B. Huang, W. Yang, Y. Wen, B. Shan, R. Chen, Co3O4-modified TiO2 nanotube arrays via atomic layer deposition for improved visible-light photoelectrochemical performance, ACS Appl. Mater. Interfaces 7 (2015) 422–431.
[198] I. Mutlu, Synthesis and characterization of Ti–Co alloy foam for biomedical applications, Trans. Nonferrous Metals Soc. China 26 (2016) 126–137.
[199] M. Guo, J. Zhao, X. Xu, W. Yu, X. Wang, Preparation of Fe-doped ZrO2 nanotube arrays by anodization of Zr–Fe alloy and their magnetic properties, Mater. Lett. 111 (2013) 93–96.
[200] M. Wang, X. Wang, J. Lin, X. Ning, X. Yang, X. Zhang, J. Zhao, Preparation and photoluminescence properties of Eu3+-doped ZrO2 nanotube arrays, Ceram. Int. 41 (2015) 8444–8450.
[201] X. Wang, J. Zhao, T. Xiao, Z. Li, X. Wang, Preparation and properties of Co 3 O 4-doped TiO 2 nanotube array electrodes, J. Appl. Electrochem. 49 (2019) 305–314.
[202] M.P. Kobylański, P. Mazierski, A. Malankowska, M. Kozak, M. Diak, M. J. Winiarski, T. Klimczuk, W. Lisowski, G. Nowaczyk, A. Zaleska-Medynska, TiO2CoxOy composite nanotube arrays via one step electrochemical anodization for visible light–induced photocatalytic reaction, Surfaces and Interfaces 12 (2018) 179–189.
[203] J.C. Pessoa, S. Etcheverry, D. Gambino, Vanadium compounds in medicine, Coord. Chem. Rev. 301–302 (2015) 24–48.
[204] S. Engelhart, R.J. Segal, Allergic reaction to vanadium causes a diffuse eczematous eruption and titanium alloy orthopedic implant failure, Cutis 99 (2017) 245–249.
[205] S.-M. Lee, Y.-J. Park, J.-H. Kim, K. Lee, Effects of annealing on electrochemical performance in graphene/V2O5 supercapacitor, Appl. Surf. Sci. 512 (2020) 145626.
[206] Y. Yang, D. Kim, P. Schmuki, Electrochromic properties of anodically grown mixed V2O5–TiO2 nanotubes, Electrochem. Commun. 13 (2011) 1021–1025.
[207] Y. Yang, D. Kim, M. Yang, P. Schmuki, Vertically aligned mixed V 2 O 5–TiO 2 nanotube arrays for supercapacitor applications, Chem. Commun. 47 (2011) 7746–7748.
[208] M.C. Nevarez-Martinez, P. Mazierski, M.P. Kobylański, G. Szczepańska, G. Trykowski, A. Malankowska, M. Kozak, P.J. Espinoza-Montero, A. Zaleska-Medynska, Growth, structure, and photocatalytic properties of hierarchical V2O5–TiO2 nanotube arrays obtained from the one-step anodic oxidation of Ti–V alloys, Molecules 22 (2017) 580.
[209] B. Han, E. Zal Nezhad, F. Musharavati, F. Jaber, S. Bae, Tribo-mechanical properties and corrosion behavior investigation of anodized Ti–V alloy, Coatings 8 (2018) 459.
[210] Q. Liu, D. Ding, C. Ning, Anodic fabrication of Ti-Ni-O nanotube arrays on shape memory alloy, Materials 7 (2014) 3262–3273.
[211] Y.-n. Zhang, W. Huang, Y. Zhang, B. Tang, H. Xiao, G. Zhao, Fabrication and enhanced visible-light photoelectrochemical performance of periodic hierarchical 3D Ti–Fe–O structure, Mater. Lett. 168 (2016) 24–27.
[212] N.K. Allam, A.J. Poncheri, M.A. El-Sayed, Vertically oriented Ti–Pd mixed oxynitride nanotube arrays for enhanced photoelectrochemical water splitting, ACS Nano 5 (2011) 5056–5066.
[213] S.N. Basahel, K. Lee, R. Hahn, P. Schmuki, S.M. Bawaked, S.A. Al-Thabaiti, Self-decoration of Pt metal particles on TiO2 nanotubes used for highly efficient photocatalytic H2 production, Chem. Commun. 50 (2014) 6123–6125.
[214] C. Elias, J. Lima, R. Valiev, M. Meyers, Biomedical applications of titanium and its alloys, JOM (J. Occup. Med.) 60 (2008) 46–49.
[215] V. Sansone, D. Pagani, M. Melato, The effects on bone cells of metal ions released from orthopaedic implants. A review, Clinical cases in mineral and bone metabolism 10 (2013) 34.
[216] N. Hu, T. Hu, A. Gao, N. Gao, M.J. Starink, Y. Chen, W. Sun, Q. Liao, L. Tong, X. Xu, P.K. Chu, H. Wang, Homogeneous anodic TiO2 nanotube layers on Ti–6Al–4V alloy with improved adhesion strength and corrosion resistance, Advanced Materials Interfaces 6 (2019) 1801964.
[217] P. Vizureanu, M.S. Bălţatu, Titanium-Based Alloys for Biomedical Applications, Materials Research Forum LLC, 2020.
[218] Titanium and titanium alloy applications in medicine, in: M.J. Jackson, W. Ahmed (Eds.), Surface Engineered Surgical Tools and Medical Devices, Springer US, Boston, MA, 2007, pp. 533–576.
[219] G. He, M. Hagiwara, Ti alloy design strategy for biomedical applications, Mater. Sci. Eng. C 26 (2006) 14–19.
[220] K.H. Cheung, M.B. Pabbruwe, W.-F. Chen, P. Koshy, C.C. Sorrell, Thermodynamic and microstructural analyses of photocatalytic TiO2 from the anodization of biomedical-grade Ti6Al4V in phosphoric acid or sulfuric acid, Ceram. Int. (2020).
[221] D. Dunn, S. Raghavan, R. Volz, Gentamicin sulfate attachment and release from anodized Ti-6Al-4V orthopedic materials, J. Biomed. Mater. Res. 27 (1993) 895–900.
[222] D. Dunn, S. Raghavan, Formation and characterization of anodized layers on CP Ti and Ti-6Al-4V biomaterials, Surf. Coating. Technol. 50 (1992) 223–232.
[223] V. Zwilling, E. Darque-Ceretti, A. Boutry-Forveille, D. David, M.-Y. Perrin, M. Aucouturier, Structure and physicochemistry of anodic oxide films on titanium and TA6V alloy, Surf. Interface Anal. 27 (1999) 629–637.
[224] A. Ahmad, E.U. Haq, W. Akhtar, M. Arshad, Z. Ahmad, Synthesis and characterization of titania nanotubes by anodizing of titanium in fluoride containing electrolytes, Appl. Nanosci. 7 (2017) 701–710.
[225] S.B. Patel, A. Hamlekhan, D. Royhman, A. Butt, J. Yuan, T. Shokuhfar, C. Sukotjo, M.T. Mathew, G. Jursich, C.G. Takoudis, Enhancing surface characteristics of Ti–6Al–4V for bio-implants using integrated anodization and thermal oxidation, J. Mater. Chem. B 2 (2014) 3597–3608.
[226] B. Luo, H. Yang, S. Liu, W. Fu, P. Sun, M. Yuan, Y. Zhang, Z. Liu, Fabrication and characterization of self-organized mixed oxide nanotube arrays by electrochemical anodization of Ti–6Al–4V alloy, Mater. Lett. 62 (2008) 4512–4515.
[227] R. Roest, B.A. Latella, G. Heness, B. Ben-Nissan, Adhesion of sol–gel derived hydroxyapatite nanocoatings on anodised pure titanium and titanium (Ti6Al4V) alloy substrates, Surf. Coating. Technol. 205 (2011) 3520–3529.
[228] P. He, K. Chen, B. Yu, C.Y. Yue, J. Yang, Surface microstructures and epoxy bonded shear strength of Ti6Al4V alloy anodized at various temperatures, Compos. Sci. Technol. 82 (2013) 15–22.
[229] E. Matykina, J.M. Hernandez-López, A. Conde, C. Domingo, J.J. de Damborenea, M.A. Arenas, Morphologies of nanostructured TiO2 doped with F on Ti–6Al–4V alloy, Electrochim. Acta 56 (2011) 2221–2229.
[230] Y. Sun, L. Wang, Y. Gao, D. Guo, Preparation of stable superamphiphobic surfaces on Ti-6Al-4V substrates by one-step anodization, Appl. Surf. Sci. 324 (2015) 825–830.
[231] Y. Gao, Y. Sun, D. Guo, Facile fabrication of superhydrophobic surfaces with low roughness on Ti–6Al–4V substrates via anodization, Appl. Surf. Sci. 314 (2014) 754–759.
[232] Y.M. Lee, E.J. Lee, S.T. Yee, B.I. Kim, E.S. Choe, H.W. Cho, In vivo and in vitro response to electrochemically anodized Ti-6Al-4V alloy, J. Mater. Sci. Mater. Med. 19 (2008) 1851–1859.
[233] L. Wang, T.-T. Zhao, Z. Zhang, G. Li, Fabrication of highly ordered TiO2 nanotube arrays via anodization of Ti–6Al–4V alloy sheet, J. Nanosci. Nanotechnol. 10 (2010) 8312–8321.
[234] L. Mohan, C. Anandan, N. Rajendran, Electrochemical behaviour and bioactivity of self-organized TiO2 nanotube arrays on Ti-6Al-4V in Hanks' solution for biomedical applications, Electrochim. Acta 155 (2015) 411–420.
[235] E.-J. Oh, T.-D.T. Nguyen, S.-Y. Lee, Y.-M. Jeon, T.-S. Bae, J.-G. Kim, Enhanced compatibility and initial stability of Ti6Al4V alloy orthodontic miniscrews subjected to anodization, cyclic precalcification, and heat treatment, Korean J Orthod 44 (2014) 246–253.
[236] E. Beltrán-Partida, A. Moreno-Ulloa, B. Valdez-Salas, C. Velasquillo, M. Carrillo, A. Escamilla, E. Valdez, F. Villarreal, Improved osteoblast and chondrocyte adhesion and viability by surface-modified Ti6Al4V alloy with anodized TiO2 nanotubes using a super-oxidative solution, Materials 8 (2015) 867–883.
[237] K. Nune, R. Misra, X. Gai, S. Li, Y. Hao, Surface nanotopography-induced favorable modulation of bioactivity and osteoconductive potential of anodized 3D printed Ti-6Al-4V alloy mesh structure, J. Biomater. Appl. 32 (2018) 1032–1048.
[238] K.A. Saharudin, S. Sreekantan, S.N.Q.A.A. Aziz, R. Hazan, C.W. Lai, R.B.S. Mydin, I. Mat, Surface modification and bioactivity of anodic Ti6Al4V alloy, J. Nanosci. Nanotechnol. 13 (2013) 1696–1705.
[239] A. Ketabchi, A. Weck, F. Variola, Influence of oxidative nanopatterning and anodization on the fatigue resistance of commercially pure titanium and Ti–6Al–4V, J. Biomed. Mater. Res. B Appl. Biomater. 103 (2015) 563–571.
[240] F. Vacandio, H. Fraoucene, V.A. Sugiawati, M. Eyraud, D. Hatem, M.S. Belkaid, M. Pasquinelli, T. Djenizian, Optical and electrochemical properties of self-organized TiO2 nanotube Arrays from anodized Ti–6Al–4V alloy, Frontiers in chemistry 7 (2019) 66.
[241] A. Radtke, A. Topolski, T. Jędrzejewski, W. Kozak, B. Sadowska, M. Więckowska-Szakiel, M. Szubka, E. Talik, L. Pleth Nielsen, P. Piszczek, The bioactivity and photocatalytic properties of titania nanotube coatings produced with the use of the low-potential anodization of Ti6Al4V alloy surface, Nanomaterials 7 (2017) 197.
[242] K. Gibran, M. Ibadurrahman, Slamet, Effect of electrolyte type on the morphology and crystallinity of TiO2nanotubes from Ti-6Al-4V anodization, IOP Conf. Ser. Earth Environ. Sci. 105 (2018), 012038.
[243] L. Benea, E. Mardare-Danaila, M. Mardare, J.-P. Celis, Preparation of titanium oxide and hydroxyapatite on Ti–6Al–4V alloy surface and electrochemical behaviour in bio-simulated fluid solution, Corrosion Sci. 80 (2014) 331–338.
[244] E. Beltrán-Partida, B. Valdéz-Salas, A. Moreno-Ulloa, A. Escamilla, M.A. Curiel, R. Rosales-Ibáñez, F. Villarreal, D.M. Bastidas, J.M. Bastidas, Improved in vitro

angiogenic behavior on anodized titanium dioxide nanotubes, J. Nanobiotechnol. 15 (2017) 10.
[245] C.P.-J. Peremarch, R.P. Tanoira, M.A. Arenas, E. Matykina, A. Conde, J.J. De Damborenea, E.G. Barrena, J. Esteban, Bacterial adherence to anodized titanium alloy, J. Phys. Conf. 252 (2010), 012011.
[246] E. Matykina, A. Conde, J. de Damborenea, D.M.y. Marero, M.A. Arenas, Growth of TiO2-based nanotubes on Ti–6Al–4V alloy, Electrochim. Acta 56 (2011) 9209–9218.
[247] M. Mansoorianfar, M. Tavoosi, R. Mozafarinia, A. Ghasemi, A. Doostmohammadi, Preparation and characterization of TiO2 nanotube arrays on Ti6Al4V surface for enhancement of cell treatment, Surf. Coating. Technol. 321 (2017) 409–415.
[248] C.-I. Jo, Y.-H. Jeong, H.-C. Choe, W.A. Brantley, Hydroxyapatite precipitation on nanotubular films formed on Ti-6Al-4V alloy for biomedical applications, Thin Solid Films 549 (2013) 135–140.
[249] A. Kaczmarek-Pawelska, E. Krasicka-Cydzik, Morphological and chemical relationships in nanotubes formed by anodizing of Ti6Al4V alloy, Adv. Mater. Sci. 14 (2014) 12–20.
[250] J. Wang, H. Li, Y. Sun, B. Bai, Y. Zhang, Y. Fan, Anodization of highly ordered TiO2 nanotube arrays using orthogonal design and its wettability, Int. J. Electrochem. Sci 11 (2016) 710–723.
[251] D. Atmani, N. Saoula, A. Abdi, M. Azzaz, Y. Wang, M. Mohamedi, Structural, morphological, and electrochemical corrosion properties of TiO2 formed on Ti6Al4V alloys by anodization, Cryst. Res. Technol. 53 (2018) 1800138.
[252] T.D. Dikova, M.G. Hahm, D.P. Hashim, N.T. Narayanan, R. Vajtai, P.M. Ajayan, Mechanism of TiO2 nanotubes formation on the surface of pure Ti and Ti-6Al-4V alloy. Advanced Materials Research, Trans Tech Publ, 2014, pp. 655–662.
[253] E. Zalnezhad, S. Baradaran, A.R. Bushroa, A.A.D. Sarhan, Mechanical property enhancement of Ti-6Al-4V by multilayer thin solid film Ti/TiO2 nanotubular array coating for biomedical application, Metall. Mater. Trans. 45 (2014) 785–797.
[254] Y. Li, D. Ding, C. Ning, S. Bai, L. Huang, M. Li, D. Mao, Thermal stability andin vitrobioactivity of Ti–Al–V–O nanostructures fabricated on Ti6Al4V alloy, Nanotechnology 20 (2009), 065708.
[255] A.K.M.N. Amin, Titanium Alloys: towards Achieving Enhanced Properties for Diversified Applications, IntechOpen, 2012.
[256] G. Strnad, D. Portan, L. Jakab-Farkas, C. Petrovan, O. Russu, Morphology of nanostructured TiO2 surfaces for biomedical implants developed by electrochemical anodization, Mater. Sci. Forum 907 (2017) 91–98.
[257] E. Filova, J. Fojt, M. Kryslova, H. Moravec, L. Joska, L. Bacakova, The diameter of nanotubes formed on Ti-6Al-4V alloy controls the adhesion and differentiation of Saos-2 cells, Int. J. Nanomed. 10 (2015) 7145.
[258] C.C. Bortolan, L.C. Campanelli, C. Bolfarini, N.T.C. Oliveira, Fatigue strength of Ti-6Al-4V alloy with surface modified by TiO2 nanotubes formation, Mater. Lett. 177 (2016) 46–49.
[259] D.-H. He, P. Wang, P. Liu, X.-K. Liu, X.-H. Chen, W. Li, K. Zhang, Anodic voltage dependence of Ti-6Al-4V substrates and hydroxyapatite coating, J. Nanosci. Nanotechnol. 19 (2019) 5700–5706.
[260] G. Strnad, C. Petrovan, O. Russu, L. Jakab-Farkas, TiO2 Nanostructured Surfaces for Biomedical Applications Developed by Electrochemical Anodization, IOP Conference Series: Materials Science and Engineering, IOP Publishing, 2016, 012051.
[261] J. Hernández-López, A. Conde, J. de Damborenea, M. Arenas, Electrochemical response of TiO2 anodic layers fabricated on Ti6Al4V alloy with nanoporous, dual and nanotubular morphology, Corrosion Sci. 112 (2016) 194–203.
[262] U.F. Gunputh, H. Le, R.D. Handy, C. Tredwin, Anodised TiO2 nanotubes as a scaffold for antibacterial silver nanoparticles on titanium implants, Mater. Sci. Eng. C 91 (2018) 638–644.
[263] I.S. Park, H.J. Oh, T.S. Bae, Bioactivity and generation of anodized nanotubular TiO2 layer of Ti–6Al–4V alloy in glycerol solution, Thin Solid Films 548 (2013) 292–298.
[264] S. Poddar, A. Bit, S.K. Sinha, A study on influence of anodization on the morphology of titania nanotubes over Ti6Al4V alloy in correlation to hard tissue engineering application, Mater. Chem. Phys. 254 (2020) 123457.
[265] S. Rogers, D. Howie, S. Graves, M. Pearcy, D. Haynes, In vitro human monocyte response to wear particles of titanium alloy containing vanadium or niobium, the Journal of bone and joint surgery, British volume 79 (1997) 311–315.
[266] A. Shah, S.N.F. Ismail, M. Hassam, R. Daud, Surface modification on titanium alloy for biomedical application, beddows C. Reference Module in Materials Science and Materials Engineering, Elsevier, Amsterdam, 2018, pp. 1–9.
[267] A. Kaczmarek, T. Klekiel, E. Krasicka-Cydzik, Fluoride concentration effect on the anodic growth of self-aligned oxide nanotube array on Ti6Al7Nb alloy, Surf. Interface Anal. 42 (2010) 510–514.
[268] A. Mazare, M. Dilea, D. Ionita, I. Titorencu, V. Trusca, E. Vasile, Changing bioperformance of TiO2 amorphous nanotubes as an effect of inducing crystallinity, Bioelectrochemistry 87 (2012) 124–131.
[269] L. Mohan, C. Anandan, N. Rajendran, Electrochemical behavior and effect of heat treatment on morphology, crystalline structure of self-organized TiO2 nanotube arrays on Ti–6Al–7Nb for biomedical applications, Mater. Sci. Eng. C 50 (2015) 394–401.
[270] B. Wang, L. Li, Y. Zheng, In vitro cytotoxicity and hemocompatibility studies of Ti-Nb, Ti-Nb-Zr and Ti-Nb-Hf biomedical shape memory alloys, Biomed. Mater. 5 (2010), 044102.
[271] C. Ning, D. Ding, K. Dai, W. Zhai, L. Chen, The effect of Zr content on the microstructure, mechanical properties and cell attachment of Ti–35Nb–xZr alloys, Biomed. Mater. 5 (2010), 045006.
[272] A.L.R. Ribeiro, R.C. Junior, F.F. Cardoso, R.B. Fernandes Filho, L.G. Vaz, Mechanical, physical, and chemical characterization of Ti–35Nb–5Zr and Ti–35Nb–10Zr casting alloys, J. Mater. Sci. Mater. Med. 20 (2009) 1629–1636.
[273] A. Cremasco, A.D. Messias, A.R. Esposito, E.A.d.R. Duek, R. Caram, Effects of alloying elements on the cytotoxic response of titanium alloys, Mater. Sci. Eng. C 31 (2011) 833–839.
[274] N.K. Allam, F. Alamgir, M.A. El-Sayed, Enhanced photoassisted water electrolysis using vertically oriented anodically fabricated Ti− Nb− Zr− O mixed oxide nanotube arrays, ACS Nano 4 (2010) 5819–5826.
[275] R. Qin, D. Ding, C. Ning, H. Liu, M. Li, D. Mao, Fabrication and Hydrogen Sensing Properties of Doped Titania Nanotubes, 2010 11th International Conference on Electronic Packaging Technology & High Density Packaging, IEEE, 2010, pp. 1327–1330.
[276] Y.-H. Jeong, H.-C. Choe, W.A. Brantley, Electrochemical and surface behavior of hydyroxyapatite/Ti film on nanotubular Ti–35Nb–xZr alloys, Appl. Surf. Sci. 258 (2012) 2129–2136.
[277] Q. Liu, D. Ding, C. Ning, Anodic fabrication of Ti-Nb-Zr-O nanotube Arrays, J. Nanomater. (2014), 240346.
[278] E.-J. Kim, Y.-H. Jeong, H.-C. Choe, Surface phenomena of hydroxyapatite film on the nanopore formed Ti–29Nb–xZr alloy by anodization for bioimplants, J. Nanosci. Nanotechnol. 13 (2013) 1679–1683.
[279] J.M. Hernández-López, A. Conde, J. de Damborenea, M.A. Arenas, Correlation of the nanostructure of the anodic layers fabricated on Ti13Nb13Zr with the electrochemical impedance response, Corrosion Sci. 94 (2015) 61–69.
[280] A. Zieliński, P. Antoniuk, K. Krzysztofowicz, Nanotubular oxide layers and hydroxyapatite coatings on 'Ti–13Zr–13Nb'alloy, Surf. Eng. 30 (2014) 643–649.
[281] A.L.R. Ribeiro, P. Hammer, L.G. Vaz, L.A. Rocha, Are new TiNbZr alloys potential substitutes of the Ti6Al4V alloy for dental applications? An electrochemical corrosion study, Biomed. Mater. 8 (2013), 065005.
[282] J.-U. Kim, Y.-H. Jeong, H.-C. Choe, Morphology of hydroxyapatite coated nanotube surface of Ti–35Nb–xHf alloys for implant materials, Thin Solid Films 520 (2011) 793–799.
[283] S.-Y. Park, H.-C. Choe, Variations of nanotubes on the Ti–Nb–Hf alloys with applied voltages, Thin Solid Films 620 (2016) 119–125.
[284] S.-Y. Park, H.-C. Choe, Effects of Hf content on nanotubular structure of Ti-29Nb-xHf ternary alloys, Surf. Coating. Technol. 320 (2017) 109–117.
[285] E.-S. Kim, Y.-H. Jeong, H.-C. Choe, W.A. Brantley, Formation of titanium dioxide nanotubes on Ti–30Nb–xTa alloys by anodizing, Thin Solid Films 549 (2013) 141–146.
[286] J. Fornell, N.T.C. Oliveira, E. Pellicer, N. Van Steenberge, M.D. Baró, C. Bolfarini, J. Sort, Anodic formation of self-organized Ti(Nb,Sn) oxide nanotube arrays with tuneable aspect ratio and size distribution, Electrochem. Commun. 33 (2013) 84–87.
[287] Y.-H. Jeong, W.-G. Kim, H.-C. Choe, W.A. Brantley, Control of nanotube shape and morphology on Ti–Nb (Ta)–Zr alloys by varying anodizing potential, Thin Solid Films 572 (2014) 105–112.
[288] R. Xu, J. Zhao, J. Tao, X. Wang, Y. Li, Fabrication of Ti–Al–Zr alloy oxide nanotube arrays in organic electrolytes by anodization, J. Appl. Electrochem. 38 (2008) 1229–1232.
[289] S.K. Liu, Y.T. Li, H.B. Yang, W.J. Zou, Z.X. Li, Fabrication and Photoelectrochemical Properties of Self-Organized Mixed Oxide Nanotubes by Anodization of Ti-2Al-1.5 Mn Alloy, Advanced Materials Research, Trans Tech Publ, 2011, pp. 1333–1336.
[290] H.-C. Choe, V.S. Saji, Y.-M. Ko, Mechanical properties and corrosion resistance of low rigidity quaternary titanium alloy for biomedical applications, Trans. Nonferrous Metals Soc. China 19 (2009) 862–865.
[291] M. Long, H.J. Rack, Titanium alloys in total joint replacement—a materials science perspective, Biomaterials 19 (1998) 1621–1639.
[292] Y. Okazaki, A New Ti–15Zr–4Nb–4Ta alloy for medical applications, Curr. Opin. Solid State Mater. Sci. 5 (2001) 45–53.
[293] M. Niinomi, Fatigue performance and cyto-toxicity of low rigidity titanium alloy, Ti–29Nb–13Ta–4.6Zr, Biomaterials 24 (2003) 2673–2683.
[294] J.I. Qazi, H.J. Rack, B. Marquardt, High-strength metastable beta-titanium alloys for biomedical applications, JOM (J. Occup. Med.) 56 (2004) 49–51.
[295] Y.-H. Chiu, T.-H. Lai, C.-Y. Chen, P.-Y. Hsieh, K. Ozasa, M. Niinomi, K. Okada, T.-F.M. Chang, N. Matsushita, M. Sone, Y.-J. Hsu, Fully depleted Ti–Nb–Ta–Zr–O nanotubes: interfacial charge dynamics and solar hydrogen production, ACS Appl. Mater. Interfaces 10 (2018) 22997–23008.
[296] M. Calin, A. Gebert, A.C. Ghinea, P.F. Gostin, S. Abdi, C. Mickel, J. Eckert, Designing biocompatible Ti-based metallic glasses for implant applications, Mater. Sci. Eng. C 33 (2013) 875–883.
[297] S. Abdi, S. Oswald, P.F. Gostin, A. Helth, J. Sort, M.D. Baró, M. Calin, L. Schultz, J. Eckert, A. Gebert, Designing new biocompatible glass-forming Ti75-xZr10NbxSi15 (x = 0, 15) alloys: corrosion, passivity, and apatite formation, J. Biomed. Mater. Res. B Appl. Biomater. 104 (2016) 27–38.
[298] S. Abdi, M.S. Khoshkhoo, O. Shuleshova, M. Bönisch, M. Calin, L. Schultz, J. Eckert, M.D. Baró, J. Sort, A. Gebert, Effect of Nb addition on microstructure evolution and nanomechanical properties of a glass-forming Ti–Zr–Si alloy, Intermetallics 46 (2014) 156–163.
[299] H. Sopha, D. Pohl, C. Damm, L. Hromadko, B. Rellinghaus, A. Gebert, J.M. Macak, Self-organized double-wall oxide nanotube layers on glass-forming Ti-Zr-Si(-Nb) alloys, Mater. Sci. Eng. C 70 (2017) 258–263.
[300] J.M. Macak, M. Jarosova, A. Jäger, H. Sopha, M. Klementová, Influence of the Ti microstructure on anodic self-organized TiO2 nanotube layers produced in ethylene glycol electrolytes, Appl. Surf. Sci. 371 (2016) 607–612.

[301] M.G. Mello, M.O. Taipina, G. Rabelo, A. Cremasco, R. Caram, Production and characterization of TiO2 nanotubes on Ti-Nb-Mo-Sn system for biomedical applications, Surf. Coating. Technol. 326 (2017) 126–133.
[302] S. Zhang, J. Qin, C. Yang, X. Zhang, R. Liu, Effect of Zr addition on the microstructure and tribological property of the anodization of Ti-6Al-4V alloy, Surf. Coating. Technol. 356 (2018) 38–48.
[303] A. Majchrowicz, A. Roguska, M. Pisarek, M. Lewandowska, Nanotubular oxide layers formation on Ti–24Nb–4Zr–8Sn and Ti–13Zr–13Nb alloys in the ethylene glycol-based electrolyte: the role of alloying elements and phase composition, Thin Solid Films 692 (2019) 137635.
[304] H.-J. Kim, H.-C. Choe, Nanotube morphology changes on the Ti–xNb–Ag–Pt alloy with Nb contents, J. Nanosci. Nanotechnol. 20 (2020) 5751–5754.
[305] S. Baradaran, E. Zalnezhad, W.J. Basirun, A.M.S. Hamouda, M. Sookhakian, A.A. D. Sarhan, Y. Alias, Statistical optimization and fretting fatigue study of Zr/ZrO2 nanotubular array coating on Ti–6Al–4V, Surf. Coating. Technol. 258 (2014) 979–990.
[306] A.R. Rafieerad, A.R. Bushroa, B. Nasiri-Tabrizi, A. Amiri, F. Yusof, J. Vadivelu, W. J. Basirun, Anodic pine cone-like WO 3/MoO 3/TiO 2 film with well-defined nanoflakes on Ti–6Al–7Nb implant, Journal of the Australian Ceramic Society 54 (2018) 129–137.
[307] A. Rafieerad, A. Bushroa, B. Nasiri-Tabrizi, A. Fallahpour, J. Vadivelu, S. Musa, S. Kaboli, GEP-based method to formulate adhesion strength and hardness of Nb PVD coated on Ti–6Al–7Nb aimed at developing mixed oxide nanotubular arrays, Journal of the mechanical behavior of biomedical materials 61 (2016) 182–196.
[308] M. Sarraf, B.A. Razak, A. Dabbagh, B. Nasiri-Tabrizi, N.H.A. Kasim, W.J. Basirun, Optimizing PVD conditions for electrochemical anodization growth of well-adherent Ta 2 O 5 nanotubes on Ti–6Al–4V alloy, RSC Adv. 6 (2016) 78999–79015.
[309] A. Rafieerad, A. Bushroa, B. Nasiri-Tabrizi, J. Vadivelu, W. Basirun, Silver/silver oxide nanorod arrays from physical vapor deposition and subsequent anodization processes, Surf. Coating. Technol. 302 (2016) 275–283.
[310] L. Yin, J. Zhou, L. Gao, C. Zhao, J. Chen, X. Lu, J. Wang, J. Weng, B. Feng, Characterization and osteogenic activity of SrTiO3/TiO2 nanotube heterostructures on microporous titanium, Surf. Coating. Technol. 330 (2017) 121–130.
[311] B. Chen, J. Hou, K. Lu, Formation mechanism of TiO2 nanotubes and their applications in photoelectrochemical water splitting and supercapacitors, Langmuir 29 (2013) 5911–5919.
[312] A.M. Mohamed, A.S. Aljaber, S.Y. AlQaradawi, N.K. Allam, TiO 2 nanotubes with ultrathin walls for enhanced water splitting, Chem. Commun. 51 (2015) 12617–12620.
[313] H. Snaith, P. Docampo, Solid State Dye-Sensitized Solar Cell—Encyclopedia of Applied Electrochemistry, Springer, New York, 2014.
[314] K. Nakata, A. Fujishima, TiO2 photocatalysis: design and applications, J. Photochem. Photobiol. C Photochem. Rev. 13 (2012) 169–189.
[315] D. Khudhair, A. Bhatti, Y. Li, H.A. Hamedani, H. Garmestani, P. Hodgson, S. Nahavandi, Anodization parameters influencing the morphology and electrical properties of TiO2 nanotubes for living cell interfacing and investigations, Mater. Sci. Eng. C 59 (2016) 1125–1142.
[316] Y.-T. Sul, Electrochemical growth behavior, surface properties, and enhanced in vivo bone response of TiO2 nanotubes on microstructured surfaces of blasted, screw-shaped titanium implants, Int. J. Nanomed. 5 (2010) 87.
[317] X. Zhang, Y. Huang, B. Wang, X. Chang, H. Yang, J. Lan, S. Wang, H. Qiao, H. Lin, S. Han, Y. Guo, X. Zhang, A functionalized Sm/Sr doped TiO2 nanotube array on titanium implant enables exceptional bone-implant integration and also self-antibacterial activity, Ceram. Int. 46 (2020) 14796–14807.
[318] X. Zhang, X. Zhang, B. Wang, J. Lan, H. Yang, Z. Wang, X. Chang, S. Wang, X. Ma, H. Qiao, H. Lin, S. Han, Y. Huang, Synergistic effects of lanthanum and strontium to enhance the osteogenic activity of TiO2 nanotube biological interface, Ceram. Int. 46 (2020) 13969–13979.
[319] H. Tsuchiya, J.M. Macak, L. Müller, J. Kunze, F. Müller, P. Greil, S. Virtanen, P. Schmuki, Hydroxyapatite growth on anodic TiO2 nanotubes, J. Biomed. Mater. Res. 77A (2006) 534–541.
[320] M. Sarraf, N. Sukiman, A. Bushroa, B. Nasiri-Tabrizi, A. Dabbagh, N.A. Kasim, W. Basirun, In vitro bioactivity and corrosion resistance enhancement of Ti-6Al-4V by highly ordered TiO 2 nanotube arrays, Journal of the Australian Ceramic Society 55 (2019) 187–200.
[321] D. He, P. Wang, P. Liu, X. Liu, F. Ma, W. Li, X. Chen, J. Zhao, H. Ye, Preparation of hydroxyapatite-titanium dioxide coating on Ti6Al4V substrates using hydrothermal-electrochemical method, J. Wuhan Univ. Technol.-Materials Sci. Ed. 31 (2016) 461–467.
[322] A. Kazek-Kęsik, K. Leśniak, B.U. Orzechowska, M. Drab, A. Wiśniewska, W. Simka, Alkali treatment of anodized titanium alloys affects cytocompatibility, Metals 8 (2018) 29.
[323] L. Peng, A.J. Barczak, R.A. Barbeau, Y. Xiao, T.J. LaTempa, C.A. Grimes, T. A. Desai, Whole genome expression analysis reveals differential effects of TiO2 nanotubes on vascular cells, Nano Lett. 10 (2010) 143–148.
[324] L. Peng, M.L. Eltgroth, T.J. LaTempa, C.A. Grimes, T.A. Desai, The effect of TiO2 nanotubes on endothelial function and smooth muscle proliferation, Biomaterials 30 (2009) 1268–1272.
[325] J. Park, S. Bauer, K.A. Schlegel, F.W. Neukam, K. von der Mark, P. Schmuki, TiO2 nanotube surfaces: 15 nm—an optimal length scale of surface topography for cell adhesion and differentiation, Small 5 (2009) 666–671.
[326] K. Vasilev, Z. Poh, K. Kant, J. Chan, A. Michelmore, D. Losic, Tailoring the surface functionalities of titania nanotube arrays, Biomaterials 31 (2010) 532–540.
[327] L. Zhao, H. Wang, K. Huo, L. Cui, W. Zhang, H. Ni, Y. Zhang, Z. Wu, P.K. Chu, Antibacterial nano-structured titania coating incorporated with silver nanoparticles, Biomaterials 32 (2011) 5706–5716.
[328] M. Sarraf, A. Dabbagh, B.A. Razak, R. Mahmoodian, B. Nasiri-Tabrizi, H.R. M. Hosseini, S. Saber-Samandari, N.H.A. Kasim, H. Abdullah, N.L. Sukiman, Highly-ordered TiO2 nanotubes decorated with Ag2O nanoparticles for improved biofunctionality of Ti6Al4V, Surf. Coating. Technol. 349 (2018) 1008–1017.
[329] Y. Lai, L. Lin, F. Pan, J. Huang, R. Song, Y. Huang, C. Lin, H. Fuchs, L. Chi, Bioinspired patterning with extreme wettability contrast on TiO2 nanotube array surface: a versatile platform for biomedical applications, Small 9 (2013) 2945–2953.
[330] B.S. Smith, S. Yoriya, T. Johnson, K.C. Popat, Dermal fibroblast and epidermal keratinocyte functionality on titania nanotube arrays, Acta Biomater. 7 (2011) 2686–2696.
[331] J. Park, S. Bauer, K. von der Mark, P. Schmuki, Nanosize and vitality: TiO2 nanotube diameter directs cell fate, Nano Lett. 7 (2007) 1686–1691.
[332] K.S. Brammer, S. Oh, C.J. Cobb, L.M. Bjursten, H. van der Heyde, S. Jin, Improved bone-forming functionality on diameter-controlled TiO2 nanotube surface, Acta Biomater. 5 (2009) 3215–3223.
[333] D.R. Barjaktarević, V.R. Djokić, I.D. Damnjanović, M.P. Rakin, Nanotubular oxide layers formed on the Ti-based implants surfaces-application and possible damages: a review, J. Inst. Eng. 24 (2018).
[334] Y.-A. Yi, Y.-B. Park, H. Choi, K.-W. Lee, S.-J. Kim, K.-M. Kim, S. Oh, J.-S. Shim, The evaluation of osseointegration of dental implant surface with different size of TiO 2 nanotube in rats, J. Nanomater. (2015) 2.
[335] L. Lin, H. Wang, M. Ni, Y. Rui, T.-Y. Cheng, C.-K. Cheng, X. Pan, G. Li, C. Lin, Enhanced osteointegration of medical titanium implant with surface modifications in micro/nanoscale structures, Journal of Orthopaedic Translation 2 (2014) 35–42.
[336] H. Cheng, W. Xiong, Z. Fang, H. Guan, W. Wu, Y. Li, Y. Zhang, M.M. Alvarez, B. Gao, K. Huo, Strontium (Sr) and silver (Ag) loaded nanotubular structures with combined osteoinductive and antimicrobial activities, Acta Biomater. 31 (2016) 388–400.
[337] H. Nuhn, C.E. Blanco, T.A. Desai, Nanoengineered stent surface to reduce in-stent restenosis in vivo, ACS Appl. Mater. Interfaces 9 (2017) 19677–19686.
[338] I. Jang, S.-C. Shim, D.-S. Choi, B.-K. Cha, J.-K. Lee, B.-H. Choe, W.-Y. Choi, Effect of TiO 2 nanotubes arrays on osseointegration of orthodontic miniscrew, Biomed. Microdevices 17 (2015) 76.
[339] K. Kubo, N. Tsukimura, F. Iwasa, T. Ueno, L. Saruwatari, H. Aita, W.-A. Chiou, T. Ogawa, Cellular behavior on TiO2 nanonodular structures in a micro-to-nanoscale hierarchy model, Biomaterials 30 (2009) 5319–5329.
[340] C. von Wilmowsky, S. Bauer, R. Lutz, M. Meisel, F.W. Neukam, T. Toyoshima, P. Schmuki, E. Nkenke, K.A. Schlegel, In vivo evaluation of anodic TiO2 nanotubes: an experimental study in the pig, J. Biomed. Mater. Res. Part B: Applied Biomaterials: An Official Journal of The Society for Biomaterials, The Japanese Society for Biomaterials, and The Australian Society for Biomaterials and the Korean Society for Biomaterials 89 (2009) 165–171.
[341] L. Lv, Y. Liu, P. Zhang, X. Zhang, J. Liu, T. Chen, P. Su, H. Li, Y. Zhou, The nanoscale geometry of TiO2 nanotubes influences the osteogenic differentiation of human adipose-derived stem cells by modulating H3K4 trimethylation, Biomaterials 39 (2015) 193–205.
[342] S.H. Moon, S.J. Lee, I.S. Park, M.H. Lee, Y.J. Soh, T.S. Bae, H.S. Kim, Bioactivity of Ti-6Al-4V alloy implants treated with ibandronate after the formation of the nanotube TiO2 layer, J. Biomed. Mater. Res. B Appl. Biomater. 100 (2012) 2053–2059.
[343] K. Shemtov-Yona, D. Rittel, On the mechanical integrity of retrieved dental implants, Journal of the mechanical behavior of biomedical materials 49 (2015) 290–299.
[344] A. Shivaram, S. Bose, A. Bandyopadhyay, Mechanical degradation of TiO2 nanotubes with and without nanoparticulate silver coating, Journal of the mechanical behavior of biomedical materials 59 (2016) 508–518.
[345] M. Dadsetan, T. Guda, M.B. Runge, D. Mijares, R.Z. LeGeros, J.P. LeGeros, D. T. Silliman, L. Lu, J.C. Wenke, P.R.B. Baer, Effect of calcium phosphate coating and rhBMP-2 on bone regeneration in rabbit calvaria using poly (propylene fumarate) scaffolds, Acta Biomater. 18 (2015) 9–20.
[346] D. Losic, M.S. Aw, A. Santos, K. Gulati, M. Bariana, Titania nanotube arrays for local drug delivery: recent advances and perspectives, Expet Opin. Drug Deliv. 12 (2015) 103–127.
[347] H. Jia, Anodized TiO 2 Nanotube Film for Controllable Drug Delivery, Miami University, 2013.
[348] Q. Wang, J.-Y. Huang, H.-Q. Li, A.Z.-J. Zhao, Y. Wang, K.-Q. Zhang, H.-T. Sun, Y.-K. Lai, Recent advances on smart TiO2 nanotube platforms for sustainable drug delivery applications, Int. J. Nanomed. 12 (2017) 151.
[349] H.P. Kulkarni, Synthesis and Applications of Titania Nanotubes: Drug Delivery and Ionomer Composites, 2008.
[350] W.A. Abbas, I.H. Abdullah, B.A. Ali, N. Ahmed, A.M. Mohamed, M.Y. Rezk, N. Ismail, M.A. Mohamed, N.K. Allam, Recent advances in the use of TiO2 nanotube powder in biological, environmental, and energy applications, Nanoscale Advances 1 (2019) 2801–2816.
[351] I. Junkar, M. Kulkarni, M. Benčina, J. Kovač, K. Mrak-Poljšak, K. Lakota, S. Sodin-Šemrl, M. Mozetič, A. Iglič, Titanium dioxide nanotube Arrays for cardiovascular stent applications, ACS Omega 5 (2020) 7280–7289.
[352] A. Roguska, A. Belcarz, J. Zalewska, M. Hołdyński, M. Andrzejczuk, M. Pisarek, G. Ginalska, Metal TiO2 nanotube layers for the treatment of dental implant infections, ACS Appl. Mater. Interfaces 10 (2018) 17089–17099.

[353] C. Lee, C. Hong, H. Kim, J. Kang, H.M. Zheng, TiO2 nanotubes as a therapeutic agent for cancer thermotherapy, Photochem. Photobiol. 86 (2010) 981–989.
[354] G.-I. Im, Biomaterials in orthopaedics: the past and future with immune modulation, Biomater. Res. 24 (2020) 7.
[355] M.C. Lin, D. Hu, M. Marmor, S.T. Herfat, C.S. Bahney, M.M. Maharbiz, Smart bone plates can monitor fracture healing, Sci. Rep. 9 (2019) 1–15.
[356] O. Guirdham, Orthopedic Devices Global Market Report 2020-30: Covid 19 Impact and Recovery, The Business Research Company, 2020, p. 8396.
[357] C. Collaborative, Elective surgery cancellations due to the COVID-19 pandemic: global predictive modelling to inform surgical recovery plans, Br. J. Surg. (2020). PMID: 32395848.
[358] J. Hernigou, J. Valcarenghi, A. Safar, M.A. Ferchichi, E. Chahidi, H. Jennart, P. Hernigou, Post-COVID-19 return to elective orthopaedic surgery—is rescheduling just a reboot process? Which timing for tests? Is chest CT scan still useful? Safety of the first hundred elective cases? How to explain the “new normality health organization” to patients? International Orthopaedics, 2020.
[359] V.K. Jain, R. Vaishya, COVID-19 and orthopaedic surgeons: the Indian scenario, Trop. Doct. 50 (2020) 108–110.
[360] W. Borchani, K. Aono, N. Lajnef, S. Chakrabartty, Monitoring of postoperative bone healing using smart trauma-fixation device with integrated self-powered piezo-floating-gate sensors, IEEE (Inst. Electr. Electron. Eng.) Trans. Biomed. Eng. 63 (2015) 1463–1472.
[361] M. Parkes, Improving Patient Outcomes with Smart Implants, Renishaw, 2018.
[362] Z. Li, M.A. Mohamed, A. Vinu Mohan, Z. Zhu, V. Sharma, G.K. Mishra, R. K. Mishra, Application of electrochemical aptasensors toward clinical diagnostics, Food, and Environmental Monitoring, Sensors 19 (2019) 5435.
[363] E.H. Ledet, B. Liddle, K. Kradinova, S. Harper, Smart implants in orthopedic surgery, improving patient outcomes: a review, Innovat. Enterpren. Health 5 (2018) 41.
[364] G. Bergmann, F. Graichen, A. Rohlmann, Hip joint contact forces during stumbling, Langenbeck’s Arch. Surg. 389 (2004) 53–59.
[365] G. Bergmann, F. Graichen, A. Rohlmann, Hip joint loading during walking and running, measured in two patients, J. Biomech. 26 (1993) 969–990.
[366] I. Kolker Baravik, E. Capua, E. Ainbinder, R. Naaman, Sensing cellular metabolic activity via a molecular-controlled semiconductor resistor, ACS Omega 2 (2017) 8550–8556.
[367] J.V. Ham, M.D. Cooman, W. Claes, R. Puers, I. Naert, C.V. Lierde, J.L. Beckers, K. U. Leuven, An Autonomous Smart Dental Prosthesis for Fast Rehabilitation, International Workshop on Wearable and Implantable Body Sensor Networks, BSN’06), 2006, pp. 4–106.
[368] M. Park, S. Islam, H.E. Kim, J. Korostoff, M.B. Blatz, G. Hwang, A. Kim, Human oral motion-powered smart dental implant (SDI) for in situ ambulatory photo-biomodulation therapy, Advanced Healthcare Materials 9 (2020) 2000658.
[369] K. Zhang, S. Wang, C. Zhou, L. Cheng, X. Gao, X. Xie, J. Sun, H. Wang, M.D. Weir, M.A. Reynolds, N. Zhang, Y. Bai, H.H.K. Xu, Advanced smart biomaterials and constructs for hard tissue engineering and regeneration, Bone Research 6 (2018) 31.
[370] C.G. Moura, D. Faria, O. Carvalho, R.S.F. Pereira, M.F. Cerqueira, R. M. Nascimento, F.S. Silva, Laser printing of silver-based micro-wires in ZrO2 substrate for smart implant applications, Optic Laser. Technol. 131 (2020) 106416.
[371] V.A.S. Ramakrishna, U. Chamoli, G. Rajan, S.C. Mukhopadhyay, B.G. Prusty, A. D. Diwan, Smart orthopaedic implants: a targeted approach for continuous postoperative evaluation in the spine, J. Biomech. 104 (2020) 109690.
[372] J. Nycz, J.C. Serbousek, Spinal Implant, Google Patents, 2020.
[373] E. Al-Fakih, N.A. Abu Osman, F.R. Mahamd Adikan, The use of fiber Bragg grating sensors in biomechanics and rehabilitation applications: the state-of-the-art and ongoing research topics, Sensors 12 (2012) 12890–12926.
[374] C.M. Boutry, L. Beker, Y. Kaizawa, C. Vassos, H. Tran, A.C. Hinckley, R. Pfattner, S. Niu, J. Li, J. Claverie, Biodegradable and flexible arterial-pulse sensor for the wireless monitoring of blood flow, Nature biomedical engineering 3 (2019) 47–57.
[375] A. Güemes, A. Fernández-López, P.F. Díaz-Maroto, A. Lozano, J. Sierra-Perez, Structural health monitoring in composite structures by fiber-optic sensors, Sensors 18 (2018) 1094.
[376] A.N. Dalrymple, V.K. Mushahwar, Intelligent control of a spinal prosthesis to restore walking after neural injury: recent work and future possibilities, Journal of Medical Robotics Research (2020) 2041003.
[377] R.B.S. Mydin, R. Hazan, M.F. FaridWajidi, S. Sreekantan, Titanium Dioxide Nanotube Arrays for Biomedical Implant Materials and Nanomedicine Applications, Titanium Dioxide-Material for a Sustainable Environment, IntechOpen, 2018.
[378] D. Hodgins, A. Bertsch, N. Post, M. Frischholz, B. Volckaerts, J. Spensley, J. Wasikiewicz, H. Higgins, F. Von Stetten, L. Kenney, Healthy aims: developing new medical implants and diagnostic equipment, IEEE Pervasive Computing 7 (2008) 14–21.